Azarbaijan Shahid Madani University
ISSN-2588-5006

Communications In Catalysis

Volume, 2 Number, 2
Winter 2023 - Spring 2024

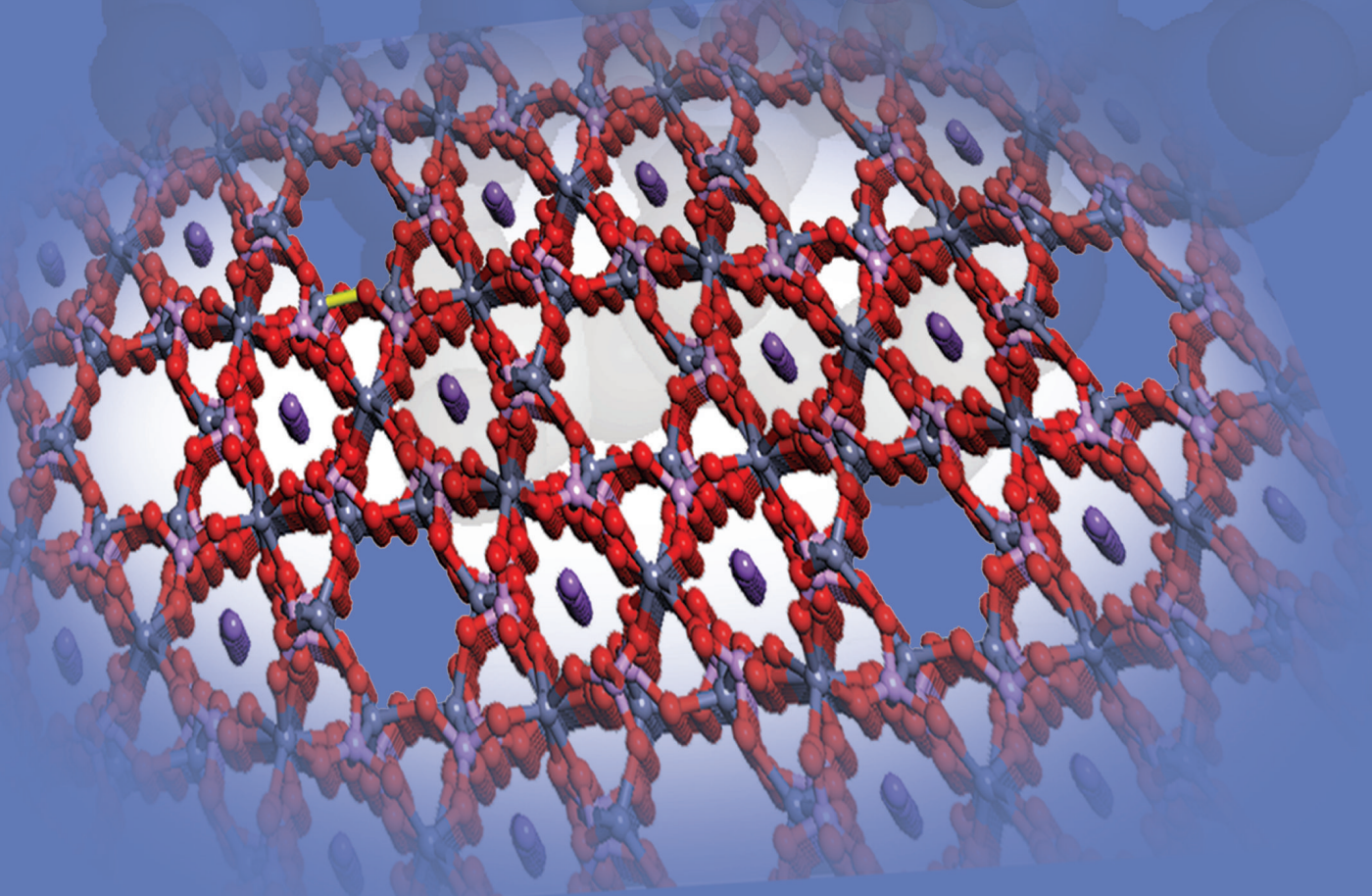

In the name of God

Communications in Catalysis (Abbreviation: CIC) is an international, open access, online/printed scholarly biannual publication issued by the Department of Chemistry, Azarbaijan Shahid Madani University, Tabriz, Iran. High quality original papers in English dealing with experimental, theoretical and applied research related to catalysis science and technology are welcomed by CIC. This journal provides a forum for publication of original research papers, short communications, and critical reviews in all branches of chemical science and technology, on catalysts and their application in several areas, such as: organic, inorganic, bioorganic, analytical, polymer, etc. Publication process of the manuscripts submitted to CIC is free of charge. All the submitted manuscripts are peer-reviewed by the editorial board and reviewers of the CIC before acceptance for publication. To submit a new manuscript, please start by reading the journal instructions for authors (http: cic.azaruniv.ac.ir).

Editorial Board:

Prof. Z. Rezvani (Editor-in-Chief)

(Chemistry Department, Faculty of Science, Azarbaijan Shahid Madani University, Tabriz,Iran.)

Prof. M. Galehassadi (Executive Manager)

(Chemistry Department, Faculty of Science, Azarbaijan Shahid Madani University, Tabriz, Iran.)

Dr. A.R. Abri

(Chemistry Department, Faculty of Science, Azarbaijan Shahid Madani University, Tabriz, Iran.)

Prof. K. Farhadi

(Department of Analytical Chemistry, Faculty of Chemistry, Urmia University, Urmia, Iran.)

Prof. B. Habibi

(Chemistry Department, Faculty of Science, Azarbaijan Shahid Madani University, Tabriz,Iran.)

Prof. M. Hosseini Sadr

(Chemistry Department, Faculty of Science, Azarbaijan Shahid Madani University, Tabriz,Iran.)

Prof. A. R. Khataee

(Applied Chemistry Department, Faculty of Chemistry, Tabriz University, Tabriz, Iran.)

Prof. M. M. Najaphpour

(Chemistry Department, Institute for Advanced Studies in Basic Science Zanjan, Zanjan, Iran.)

Prof. H. Namazi

(Organic Chemistry Department, Faculty of Chemistry, Tabriz, Iran.)

Prof. D. Nematollahi

(Chemistry Department, Faculty of Science, Buali Sina University, Hamadan, Iran.)

Prof. K. Niknam

(Chemistry Department, Faculty Science, Persian Gulf University, Bushehr, Iran.)

Prof. M. Mahkam

(Chemistry Department, Faculty of Science, Azarbaijan Shahid Madani University, Tabriz,Iran.)

Prof. H. Razmi

(Chemistry Department, Faculty of Science, Azarbaijan Shahid Madani University, Tabriz,Iran.)

Prof. A. Salimi

(Department of Chemistry, Faculty of Science, University of Kurdistan, Kurdistan, Iran.)

Prof. H. Valizadeh

(Chemistry Department, Faculty of Science, Azarbaijan Shahid Madani University, Tabriz,Iran.)

Contents

Communications In Catalysis
Vol. 2, No. 2, 2024, pp. 1-7
DOI: 10.22049/CIC.2024.29261.1034

Azarbaijan Shahid Madani University

High efficiency water oxidation using NiAlFe-layered double hydroxides

Kamellia Nejati [1], Leila Jafari Foruzin [2*]

[1] Department of Chemistry, Payame Noor University, P.O. Box 19395-3697, Tehran, Iran

[2] Inorganic Chemistry Laboratory, Department of Chemistry, Faculty of Sciences, Azarbaijan Shahid Madani University, Tabriz 53714-161, Iran.

E-mail: l.jafari @azaruniv.ac.ir , l.jafarie@gmail.com

Received: 2023-12-16, Accepted: 2024-05-03

Abstract

We report that ternary nickel-alumina-iron Layered Double Hydroxide (NiAlFe-LDH) is a highly active and stable oxygen evolution catalyst at neutral solutions. The LDHs were prepared using the co-precipitation method and were characterized by a field-emission scanning electron microscopy (FE-SEM), X-ray diffraction (XRD)**.** According to powder X-ray diffraction and field emission scanning electron microscopy, NiAlFe-LDH exhibit a nanosized plate-like morphology with a basal space (d_{003}) of 7.64 °A. Then amount of Al^{3+} at NiAlFe-LDH optimizes and the electrocatalytic activities of ternary-component were studied toward water oxidation in neutral solutions. The result compared with binary NiFe-LDH and NiAl-LDH. The obtained results show that the electrocatalytic activity of the ternary-component NiAlFe-LDH is much better than that of the binary-component NiFe-LDH and NiAl-LDH. The high electrocatalytic activity of ternary-component LDH may be attributed to the co-existence of Al and Fe active sites.

Keywords: Water Oxidation, Layered Double Hydroxide, Oxygen Evaluation, NiAlFe-LDH

Introduction

Increasing need to energy and environmental problems have motivated extensive study in several energy storage(Omer, 2009; Wang et al., 2022) .

In order to product energy by chemical fuels, water oxidation is the anodic half-reaction (in alkani: ($4OH^- \longrightarrow 2H_2O + O_2 + 4e$) and neutral or acidic solution: ($2\ H_2O \longrightarrow 4H^+ + O_2 + 4e$)) oxygen reduction reaction (ORR). The water oxidation is slow reaction (overpotential about 1.23 V need for this reaction) and various catalyst need to improve efficiency(Kubendhiran et al., 2023; Quang et al., 2022). For water electrolysis, the energy loss at the anode is significant because water oxidation requires four-electron transfer(Nai et al., 2015). Therefore, it is highly desirable to design efficient oxygen evolution reaction (OER) catalysts and ensure their assembly into practical OER electrodes. RuO_2 and IrO were active catalyst for water oxidation but scarcity and expensive cost's limited their use at water oxidation industry (Ping et al., 2016; Tang et al., 2014). So, study for achieve high yield with low cost in water oxidation is urgently required.

Layered double hydroxides (LDHs) are anionic clays, which are made of layers of trivalent and divalent metal cations connected to the OH^- anions, with interlayer anions carbonate and nitrate inserted between the layers (Guo et al., 2010; Wang & O'Hare, 2012). LDH has been used in a variety of areas, including but not limited to catalysis, energy storage, drug or gene delivery, water treatment, etc (Alcantara et al., 2010; Fan et al., 2014).

Researches have showed that the octahedral MO_6 layers in 2D metal oxides/hydroxides are suitable catalysts for Oxygen generation (Nayak et al., 2015). One of 2D metal hydroxides is the layered double hydroxides (LDHs). Their chemical formula is $[M^{2+}_{(1-x)} M^{3+}_x (OH)_2]^{q+} (A^{n-})_{q/n} \cdot yH_2O$, usual Z equal with 2 or 1 and M^{II} and M^{III} are divalent and trivalent cations (Mahjoubi et al., 2017; Song et al., 2012). In order to compensating of positive charge at interlayer anion (A^{n-}) is used and x is molar ratio M(III)/M(III)+M(II). They have the octahedral MO_6 layers, which are alike to the metal hydroxides(Khan et al., 2017).

Here in, we synthesis NiFeAl/LDHs by the co-precipitation method and thoroughly characterized via X-ray diffraction (XRD), field-emission scanning electron microscopy

(FE-SEM). Then NiFeAl/LDHs used as an improvably electrocatalyst for oxygen generation. Via the use of Al^{3+} at synthesis of ternary NiFeAl/LDHs, we can conclude that doping Al (III) ions in to NiFe-LDH ignificantly increased their electrochemical activity due to high crystallity at NiFeAl/LDHs incompared to NiAl-LDH and NiFe-LDH.

Materials and method

Nickel nitrate hexhydrate [$Ni(NO_3)_2.6H_2O$], Aluminium nitrate nonahydrate [$Al(NO_3)_2.9H_2O$] and Iron (III) nitrate nonahydrate [$Fe(NO_3)_3$ $9H_2O$], the precursors for synthesis of ternary-component layer double hydroxide, were **purchased** from Merck Company (Germany) and used as received. Other chemicals were utilized without further purification.

X-ray diffraction (XRD) patterns were achieved on a Bruker AXS model D8 Advance diffractometer with Cu-Kα radiation (λ = 1.54 Å) at 40 kV. The size and morphology of the products were studied using a field-Emission scanning electron microscope (FE-SEM)(TE-SCAN) operating at 10 kV.

Results and Discussion

Characterisation of LDHs

XRD analysis

The XRD patterns of Ni_2Al-LDH, Ni_2Fe-LDH and $Ni_2Al_{0.1}Fe_{0.9}$-LDH (Fig.1 (a, b, c)) show the hydrotalcite-like distinctive structures (Hou et al., 2023). The peaks of (003), (006), (012), (015), (018) and (110) have $R\bar{3}m$ symmetry and hexagonal lattice structure (Ray et al., 2023).

The basal spacing (d_{003}) of the LDH was calculated to be 0.803, 0.773 and 0.764 nm at $2\theta = 11.5°$ that show intercalation of CO_3^{2-} anions into the layer galleries at tree sample (Figure 1 (a, b and c)). The basal spacing (d) obtained from Braggs law, $n\lambda = 2d\sin(\theta)$ where n=1, λ is the wavelength of the incident light, and θ is the angle of incidence (Hunter et al., 2016; Xie & Liu, 2023). This show that in all three sample CO_3^{2-} ion intercalated into layers galleries between LDHs (Bhojaraj & Rajamathi, 2023; Qiu et al., 2022).

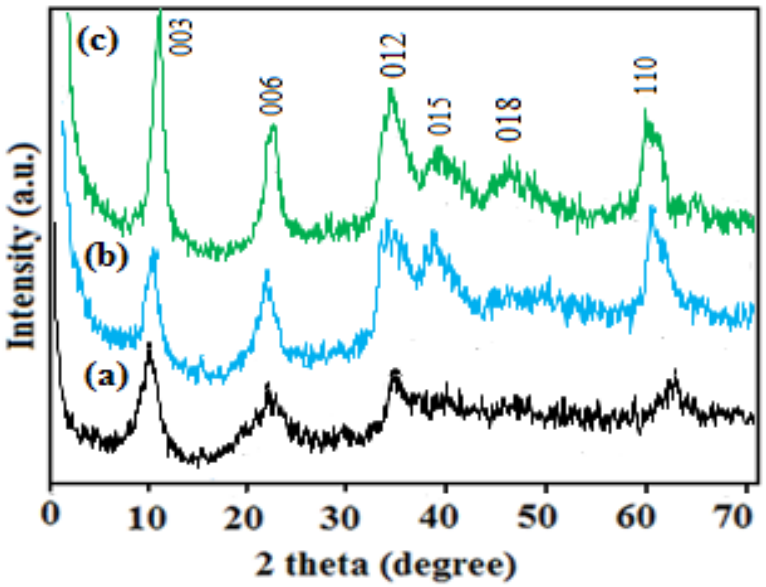

Figure 1. XRD spectra of (a) Ni_2Al-LDH, (b) Ni_2Fe-LDH and (c) $Ni_2Al_{0.1}Fe_{0.9}$-LDH

The field-emission scanning electron microscopy (FE-SEM)

The size and morphology of the resulting material were characterized by FE-SEM image. (Figure 2 (a, b and c)) show the FE-SEM images of Ni_2Al-LDH, Ni_2Fe-LDH and $Ni_2Al_{0.1}Fe_{0.9}$-LDH which display a plate-like morphology and thickness of nanosheets are 11, 13 and 16 nm. Besides, the broad peaks at XRD pattern (Figure 2 (a, b and c)) confirms the nano structures in all tree samples and increased size at $Ni_2Al_{0.1}Fe_{0.9}$-LDH.

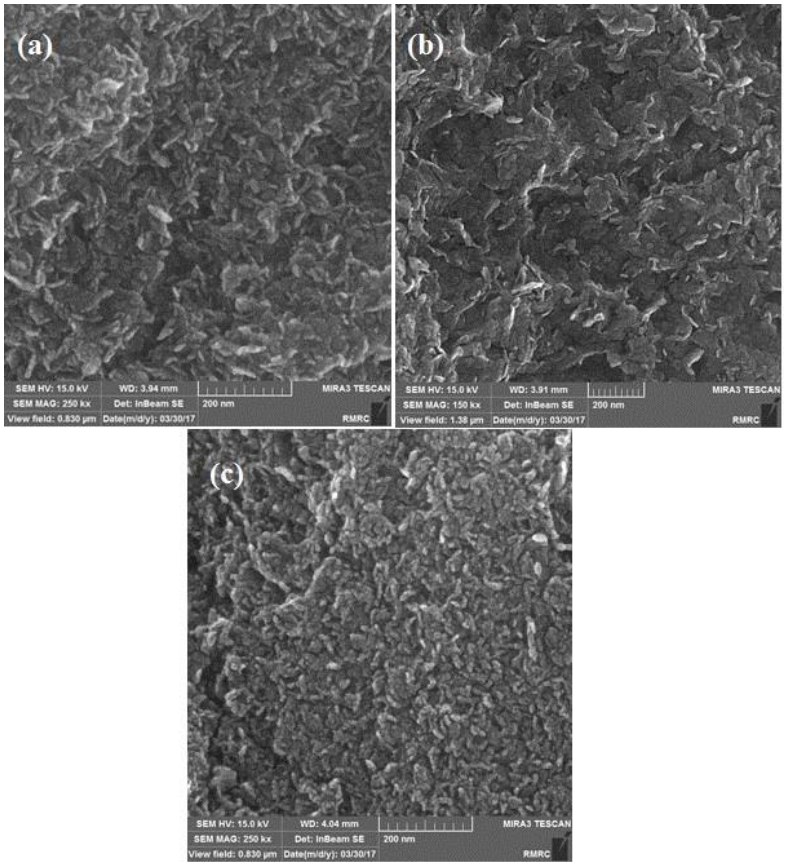

Figure 2. (a) FE-SEM images of a) Ni_2Al-LDH b) Ni_2Fe-LDH and c) $Ni_2Al_{0.1}Fe_{0.9}$-LDH

Electrochemical WOR measurements

Figure 3 (a) and (b) shows the linear sweep voltammetry (LSV) curves on a Saturated calomel electrode (SCE) scale. As show at Figure 3 (a) Bare electrode shows very poor OER activity with the need of large overpotential of 311mV to drive 0.7 $mAcm^{-2}$. Ni_2Fe-LDH exhibits excellent activity and only demands overpotential of 81 mV to approach the same current density. Ni_2Al-LDH is also active for OER but with the need of overpotential of 236 mV for 0.7 $mAcm^{-2}$. In sharp contrast, $Ni_2Al_{0.1}Fe_{0.9}$-LDH shows much superior OER activity over Ni_3Fe-LDH and only demands much smaller overpotentials of 11mV to afford geometrical catalytic current densities of 0.7 $mAcm^{-2}$. As show at Figure 3 (a) the $Ni_2Al_{0.1}Fe_{0.9}$-LDH in compared to Ni_2Al-LDH, Ni_2Fe-LDH, provided the earliest onset potential. The

onset potential for Ni_2Al-LDH and Ni_2Fe-LDH is 1.15, 1.03 which are 0.17 and 0.05 V larger than $Ni_2Al_{0.1}Fe_{0.9}$-LDH. The onset potential of $Ni_2Al_{0.1}Fe_{0.9}$-LDH is about 0.98V and indicating the start of water oxidation. Despite the similar OER overpotentials of the three catalysts, the $Ni_2Al_{0.1}Fe_{0.9}$-LDH can attain the highest current density at the same applied potential. This result underscores the importance of assembling catalytically active materials at the molecular level in designing high performing electrochemical catalysts.

Based on results obtained from Fig. 6 (b) doping 0.1 mol Al^{3+} and synthesis $Ni_2Al_{0.1}Fe_{0.9}$-LDH suggested because $Ni_2Al_{0.1}Fe_{0.9}$-LDH have lowest onset potential and highest current density. It is more favorable catalyst for OER.

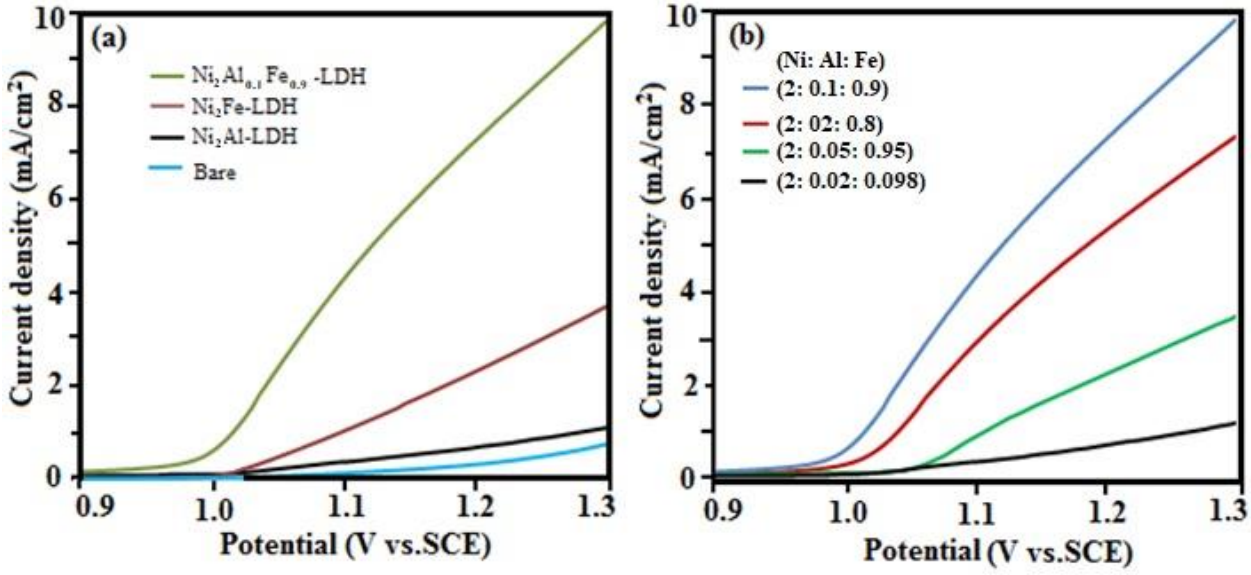

Figure 3. (a) Linear sweep voltammetric tests at neutral solution and using Ni_2Al –LDH, Ni_2Fe –LDH and $Ni_2Al_{0.1}Fe_{0.9}$-LDH as electrocatalyst and (b) the effect amount of Al^{3+} doping into Ni Al Fe-LDH at OER

Conclusions

In summary, the $Ni_2Al_{0.1}Fe_{0.9}$-LDH which synthesis by co-precipitation method is applied as a new low-overpotential catalyst for efficiently electro chemical water oxidation at neutral solutions. Electrochemical measurements have demonstrated their excellent performance as OER electrocatalysts in neutral media. Linear sweep voltammetry measurements show that the $Ni_2Al_{0.1}Fe_{0.9}$-LDH exhibited high-performance catalytic activity for electrochemical water

oxidation in neutral solution, which are superior or comparable to those of Ni_2Al-LDH and Ni_2Fe-LDH with similar structures in terms of the onset potential.

Acknowledgment

We are grateful to Azarbijan Shahid Madani University for financial supports.

References

[1] Omer, A.M.; J. Renew. Sustain. Energy. 2009, 5

[2] Wang, G.; Chang, J.; Tang, W.; Xie, W.; Ang, Y.S.; J. Phys. D Appl. Phys. 2022, 5, 293002.

[3] Quang, N.D.; Van, P.C.; Majumder, S.; Jeong, J.-R.; Kim, D.; Kim, C.; J. Colloid Interface Sci. 2022, 616,749

[4] Kubendhiran, S.; Chung, R.-J.; Yougbaré, S.; Lin, L.-Y.; Wu, Y.-F.; Int. J. Hydrogen Energy. 2023, 48, 101.

[5] Nai, J.; Yin, H.; You, T.; Zheng, L.; Zhang, J.; Wang, P.; Jin, Z.; Tian, Y.; Liu, J.; Tang, Z.; Adv. Energy Mater. 2015, 5, 1401880.

[6] Tang, D.; Han, Y.; Ji, W.; Qiao, S.; Zhou, X.; Liu, R.; Han, X.; Huang, H.; Liu, Y.; Kang, Z.; Dalton Trans. 2014, 43, 15119.

[7] Ping, J.; Wang, Y.; Lu, Q.; Chen, B.; Chen, J.; Huang, Y.; Ma, Q.; Tan, C.; Yang, J.; Cao, X.; Adv. Mater. 2016, 28, 764.

[8] Wang, Q.; O'Hare, D.; Chem. Rev. 2012, 112, 4124.

[9] Guo, X.; Zhang, F.; Evans, D.G.; Duan, X.; ChemComm. 2010, 46, 5197.

[10] Fan, G.; Li, F.; Evans, D.G.; Duan, X.; Chem. Soc. Rev. 2014, 43, 7040.

[11] Alcantara, A.; Aranda, P.; Darder, M.; Ruiz-Hitzky, E.; J. Mater. Chem. 2010, 42, 9495.

[12] Nayak, S.; Mohapatra, L.; Parida, K.; J. Mater. Chem. 2015, 3, 18622.

[13] Song, J.; Leng, M.; Fu, X.; Liu, J.; J. Alloys Compd. 2012, 543, 142.

[14] Mahjoubi, F.Z.; Khalidi, A.; Abdennouri, M.; Barka, N.; J. Taibah Univ. SCI. 2017, 11, 90.

[15] Khan, I.; Yamani, Z.H.; Qurashi, A.; Ultrason. Sonochem. 2017, 34, 484.

[16] Hou, L.; Zhou, X.; Kong, L.; Ma, Z.; Su, L.; Liu, Z.; Shao, G.; Nanomater. 2023, 13, 1192.

[17] Ray, P.K.; Mohanty, R.; Parida, K.; J. Energy Storage. 2023, 72, 108335.

[18] Xie, J.-J.; Liu, H.-W.; Appl. Math. Model. 2023, 119, 717.

[19] Hunter, B.M.; Hieringer, W.; Winkler, J.; Gray, H.; Müller, A.; Energy Environ. Sci. 2016, 6, 1734.

[20] Bhojaraj, M.; Rajamathi,; ACS. 2023, 10185.

[21] Qiu, Y.; Liu, Z.; Zhang, X.; Sun, A.; Liu, J.; Appl. Surf. Sci. 2022, 598, 153690

Communications In Catalysis
Vol. 2, No. 2, 2024, pp. 8-21
DOI: 10.22049/CIC.2024.29382.1035

Azarbaijan Shahid Madani University

Synthesis, Structural Properties and Water Oxidation Activity of Iron (III) Complexes with Salophen Ligands

Zohreh Shaghaghi[1]*, Habibeh Tajdar[2], Mehri Aligholivand[3]

[1,2,3] Coordination Chemistry Research Laboratory, Department of Chemistry, Faculty of Science, Azarbaijan Shahid Madani University,5375171379, Tabriz, Iran

E-mail: shaghaghi@azaruniv.ac.ir, zsh024@gmail.com

Received: 2024-01-25, Accepted: 2024-05-03

Abstract

In this work, Fe^{III} salophen complexes **1-3** were prepared from the reaction of $H_2L^{1\text{-}3}$ (H_2L^1=N,N'-bis(salicylidene)-4-chloro-1,2-phenylenediamine, H_2L^2=N,N'-bis(salicylidene)-4-bromo-1,2-phenylenediamine, and H_2L^3=N,N'-bis(salicylene)-4-nitro-1,2-phenylenediamine) with $FeCl_3.6H_2O$. The structure of the complexes was investigated by spectroscopic techniques, molar conductivity measurements and elemental analysis. In addition, water oxidation activity of complexes was investigated by different electrochemical methods in alkaline solution. The results showed that the compounds reveal high performance for water oxidation in terms of overpotential and Tafel slope values. Fe^{III} complex **3** displayed the best activity for the reaction with low overpotential of 485 mV at a j of 10 mA cm^{-2} and a suitable Tafel slope of 216 mV dec^{-1} among other complexes. This is due to larger electrochemically active surface area of **3**, which leads to more active catalytic sites and improved water oxidation activity. Finally, the chronoamperometry test revealed that **3** is a stable and durable electrocatalyst for water oxidation.

Keywords: Iron(III) complexes, Salophen-type ligands, Electrocatalyst, Electrochemistry, Water oxidation

Introduction

Synthesis and design of iron(III) complexes with N_2O_2 ligands has always been an interesting field of research [1-6]. These complexes can be used as synthetic models for iron-containing enzymes [7-9]. They also can be used as catalysts for various asymmetric reactions [10, 11]. In addition, many non-heme iron metalloproteins having several active sites with mononuclear iron centers are biologically important [12, 13]. Iron can take various oxidation states from -2 to +6, but the most common iron oxidation numbers are +2 and +3. The redox potential of Fe^{3+}/Fe^{2+} couple depends on the type of ligands around it and, this facilitates the catalytic role of iron in biological systems [14]. For these reasons, the coordination chemistry of Fe complexes has always been of interest to researchers. For example, Basak et al. [15] reported two mononuclear iron(III) complexes containing *N*,*N*′-bis(3-methoxysalicylidene)diethylenetriamine, *N*,*N*′-bis(3-ethoxysalicylidene)diethylenetriamine and azide ligands. They also studied the band gap and conductivity of the complexes. The results showed that the complex with methoxy substitute is a better candidate for electronic device applications. Boca and coworkers investigated magnetic properties of some pentacoordinate Fe^{III} complexes with bidentate Schiff-base N and O donor ligands [16]. They found that a distant ethoxy group to the methoxy residing at the phenyl ring of ligand influences the relaxation characteristics. Sharghi and coworkers applied the Fe^{III} salen complex as a catalyst for the synthesis of benzoaxzol derivatives from catechols, ammonium acetate and aldehydes for the first time [17]. Sonmez et al. [18] prepared some complexes with polydentate Schiff-base ligands containing phenoxy groups with Ru^{III}, Cr^{III} and Fe^{III}. Their findings that the Fe^{III} complex reveals very efficient catalytic activity in the green synthesis of vitamin K_3 from 2-methylnaphthalene. Moreover, another important application of iron(III) complexes is their valuable catalytic role in the water splitting reaction, which have received special attention in recent years. Water splitting, which leads to the production of oxygen and hydrogen, is one of the most promising ways to storage energy [19-23]. For example, some iron (III) complexes with nitrogen and oxygen donor ligands that have been used as catalysts for the oxidation of water are: cis-$[Fe(cyclam)Cl_2]Cl$ (cyclam= *1,4,8,11-tetraazacyclotetradecane)* [24], non-heme Fe^{III} complexes [25, 26], Fe(salen)-MOF composite (salen= *N,N′-bis(salicylidene)ethylenediamine*, MOF=metal-organometallic framworke) [27] , Fe-TAML (TAML=tetraamido macrocyclic ligand) [28], six coordinate Fe^{III} aqua complex, $[Fe^{III}(dpaq)(H_2O)]^{2+}$ (*dpaq= 2*-[bis(pyridine-***2***-ylmethyl*)]*amino-N-quinolin-8-yl-acetamido) [29], pentanuclear iron complexes, $[Fe_4^{II}Fe^{III}(\mu_3O)(Me\text{-}bpp)_6](PF_6)_3$([$Fe_5$-Me]$(PF_6)_3$), $[Fe_4^{II}Fe_{III}(\mu_3O)(Br\text{-}bpp)_6](PF_6)_3$([$Fe_5$-Br]$(PF_6)_3$) (4-substituted-3,5-bis(pyridyl)pyrazole) [30], $[Fe^{II}{}_4Fe^{III}(\mu\text{-}L)_6(\mu\text{-}O)]\cdot(BF_4)_3(H_2O)_n$ (LH: 2,2′-(1H-pyrazole-3,5-diyl)dipyridine] [31] and so on.

Among the Schiff-base complexes of iron with N and O donor ligands, Fe-salophen complexes have attracted a lot of attention due to their stability, ease of preparation and

excellent electrochemical behavior [32-37]. Salophens are tetradentate N_2O_2 Schiff base ligands which are produced from the condensation reaction of 1,2-phenylenediamine derivatives with two equivalents of salicylaldehyde derivatives. Although there are many reports of mononuclear and binuclear complexes of iron containing salophen type ligands, synthesis and study of properties of Fe-salophen complexes and their application in catalytic processes are still of interest to researchers.

The aim of the present study is to synthesis and investigate of important structural properties and water oxidation activity of a number of iron(III) complexes with salophen ligands containing different electron-withdrawing substituents. Thus, in our continuing research on the coordination chemistry of salophen type ligands [19, 20, 32, 37, 38], in this work we report experimental studies and water oxidation activity of iron(III)-salophen complexes with different electron-withdrawing substituents on the central phenyl ring of ligands. The results show that these compounds can catalyze the water oxidation reaction as stable and molecular electrocatalysts, and complex **3** shows the highest activity in terms of overpotential and Tafel slope values compared to complexes **1** and **2**.

Experimental

Materials and Instruments

N_2O_2 Schiff-base ligands, $H_2L^{1\text{-}3}$, N,N'-bis(salicylidene)-4-chloro-1,2-phenylendiamine, N,N'-bis(salicylidene)-4-bromo-1,2-phenylendiamine, and N,N'-bis(salicylidene)-4-nitro-1,2-phenylendiamine were prepared according to the literature [38]. FT-IR spectra of compounds were obtained by a FT-IR Spectrometer Bruker Tensor 27 with using KBr pellet. Electronic absorption spectra were recorded with T 60 UV/Vis Spectrometer PG Instruments Ltd. The elemental analyses of the complexes were obtained from an Elementar elx III. Cyclic voltammograms of complexes were recorded using an Autolab PGSTAT204.

General method for synthesis of Fe^{III} complexes

An ethanol solution (20 mL) of $FeCl_3.6H_2O$ (0.189 g, 0.700 mmol) was slowly added to the solution of Ligands, $H_2L^{1\text{-}3}$ (0.700 mmol) in dichloromethane (15 mL) at room temperature. Immediately, the color solution was changed and a precipitate was formed. The reaction was continued for 4 h (the reaction end was controlled by thin layer chromatography). Finally, the mixture reaction was filtered, the residue recrystallized by ethanol-dichloromethane solvents and dried.

Fe^{III} complex with H_2L^1 (**1**)

A dark brown powder was achieved (0.230 g, Yield: 74.91%). IR (KBr, cm^{-1}) 3446 (br), 1601 (s), 1573 (s), 1531(s), 1461 (m), 1439 (m), 1373 (s), 1319 (s), 1194 (w), 1146 (w), 1093 (m), 903 (m), 857 (m), 815 (s), 760 (s), 603 (w), 547 (w), 497 (w), 475 (w), 432 (w). Elem. Anal. Calc. for $C_{20}H_{13}FeO_2N_2Cl_2$ (M_w= 439.74 g mol^{-1}): C, 54.58; H, 2.96; N, 6.36%. Found: C, 55. 09; H, 3.23; N%, 6.69. UV-vis in DMSO (λ_{max} [nm] with ε [$M^{-1}cm^{-1}$]): 263 (9800), 303 (14700), 386 (8400), 442 (4200).

Fe^{III} complex with H_2L^2 (2)

A dark brown powder was achieved (0.285 g, Yield: 82.84 %). IR (KBr, cm^{-1}): 3449 (br), 1601 (s), 1571 (s), 1533 (s), 1487 (m), 1461 (m), 1437 (m), 1372 (s), 1311 (s), 1194 (w), 1149, 926, 858, 761 (s), 602 (w), 545 (m), 495 (w), 475 (w). Elem. Anal. Calc. for $C_{20}H_{14}FeO_{2.5}N_2ClBr$ (M_w= 492.75 g mol^{-1}): C, 48.70; H, 2.84; N, 5.68%. Found: C, 49.31; H, 2.96; N%, 5.69. UV-vis in DMSO (λ_{max} [nm] with ε [$M^{-1}cm^{-1}$]): 266 (23333), 304 (33333), 385 (20066), 440 (4200).

Fe^{III} complex with H_2L^3 (3)

A dark brown powder was achieved (0.250 g, Yield: 73.52 %). IR (KBr, cm^{-1}) 3422 (br), 1604 (s), 1573 (s), 1522 (s), 1462 (m), 1437 (m), 1377 (s), 1343 (s), 1310 (s), 1196 (w), 1150 (w), 1085 (m), 914 (m), 860 (m), 803 (m), 766 (s), 603 (w), 552 (w), 482 (w), 420 (w). Elem. Anal. Calc. for $C_{20}H_{17}FeO_6N_3Cl$ (M_w=486.25 g mol^{-1}): C, 49.35; H, 3.49; N, 8.64%. Found: C, 50. 10; H, 3.55; N%, 8.65. UV-vis in DMSO (λ_{max} [nm] with ε [$M^{-1}cm^{-1}$]): 271 (9033), 311(17433), 396 (10800), 452 (6433).

Fabrication of modified electrodes

To produce modified electrodes with Fe complexes **1-3**, graphite, paraffin, and Fe complexes **1-3** with a mass ratio of 80: 5: 15 were thoroughly mixed and homogenized for at least 2 hours. Then the obtained pastes were placed in copper wires with a radius of 1.1 mm. The surface of electrodes was washed several times with diluted water and completely smoothed before use. To prepare the unmodified electrode, paraffin and graphite were mixed with a mass ratio of 20:80 and after homogenization, they were placed in a copper wire. All electrochemical experiments were carried out in a three-electrode system containing Ag/AgCl, Pt wire, and unmodified or modified carbon past electrodes as reference, counter, and working electrodes in the presence of 25 mL of borate solution (0.5 M, pH=11).

Results and discussions

Fe^{III} complexes **1-3** were prepared from the reaction of $FeCl_3.6H_2O$ with salophen type ligands, H_2L^1-H_2L^3, in the mixture of dichloromethane-ethanol solutions at room temperature for 4 h (Scheme 1). The complexes were studied by FT-IR and UV-vis spectroscopy, molar conductivity measurements, and elemental analysis. In addition, electrochemical properties and water oxidation activity of the complexes were investigated.

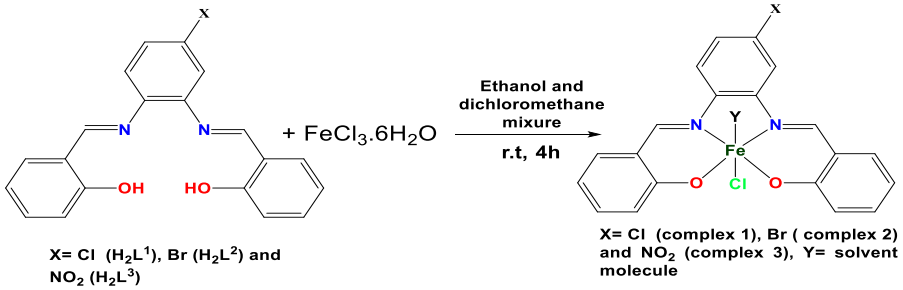

Scheme 1: The synthetic route of the Fe^{III} salophen complexes **1-3**

Structural characterizations

Some important FT-IR spectroscopy data of the complexes are given in Table 1. In the spectra of the complexes, the stretching vibration of –C=N- of imine groups appears in 1600-1604 cm^{-1} wavenumbers which shifts to the lower frequency compared to the free ligands [37]. This may be due to the bounding of the nitrogen atoms of imine groups of Schiff-base ligands to the Fe^{III} ion centers [32, 39]. The appearance of the broad peak at 3422-3449 cm^{-1} region can be assigned to the stretching vibration of coordinated water molecules. In addition, the stretching vibrations of Fe-O and Fe-N are observed as weak peaks in the range of 420-552 cm^{-1} [40]. UV-vis spectra of iron(III) complexes **1**-**3** are shown in Figure 1. In the UV-vis spectra of the complexes, the absorption bands observed at around 263-339 nm are attributed to the intra-ligand $\pi \rightarrow \pi^*$ and $n \rightarrow \pi^*$ transitions [41]. Changes in the intensity and position of $n \rightarrow \pi^*$ transition in the spectra of the complexes compared to the free ligands confirm the coordination of nitrogen atoms of imine groups to the Fe^{III} ion centers [32]. The broad absorption bands around 380-394 nm and shoulders at 441-450 nm are attributed to the charge transfer from the salophen ligand to the Fe^{III} ion center [42-44]. Also, the values of molar conductivity of Fe^{III} complexes **1**-**3** (10^{-3} M in DMSO) are 0.045, 0.049 and 0.047 $cm^2\ \Omega^{-1}mol^{-1}$ respectively, which indicate their non-electrolyte nature. This can be due to the deprotonation of salophen ligands when binding to the metal ion center [20, 22, 32, 37].

Table 1: FT-IR data for Fe^{III} complexes **1**-**3**

Compound	ν (-C= N-), (cm^{-1})	ν (H_2O) (cm^{-1})	ν (NO_2), (cm^{-1})	ν (C-Cl), (cm^{-1})	ν (C-Br), (cm^{-1})	ν (Fe-O),(Fe-N) (cm^{-1})
1	1601	3446	-	857	-	432-547
2	1601	3449	-	-	761	475-545
3	1604	3422	1343	-	-	420-552

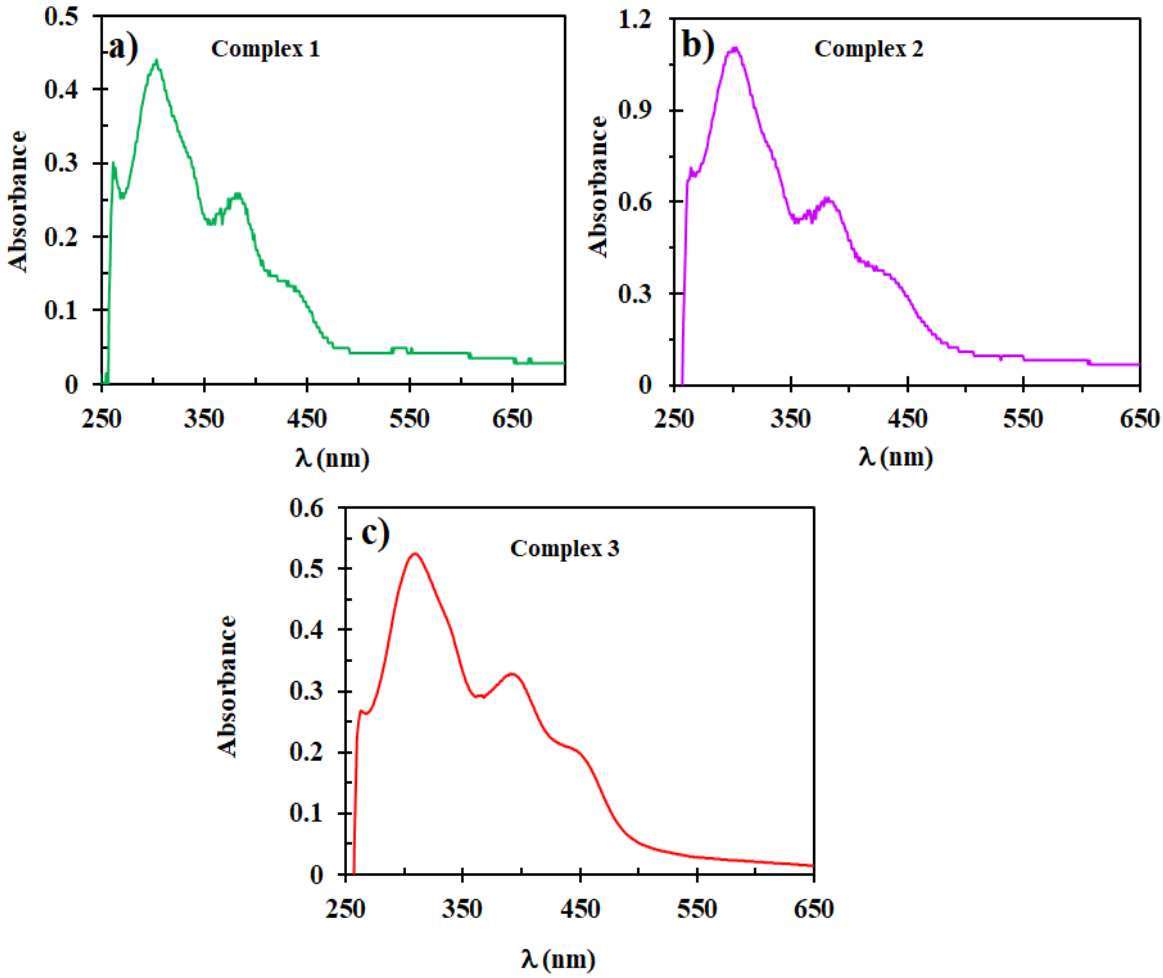

Figure 1: UV-Vis spectra of Fe^{III} complexes **1**-**3** in DMSO (3×10^{-5} M).

Electrochemical studies

Figure 2 shows cyclic voltammograms of Fe^{III} complexes **1**-**3** in DMSO solution containing 0.1 M $LiClO_4$ as a supporting electrode at room temperature and the scan rate of 50 mV s^{-1}. Fe complexes **1**-**3** display one electron reversible oxidation and reduction process. In the voltammograms of the complexes, the anodic peak at the range of -1.28 to -1.32 are assigned to the oxidation of Fe(II) to Fe(III), and the cathodic peak at the range of -1.42 to -1.46 V are attributed to the reduction of Fe(III) to Fe(II) [32]. It should be noted that the anodic peak observed at about -0.65 V and the cathodic peak observed at about -0.75 V are related to the reversible oxidation and reduction of their respective ligands [32, 37]. Finally, the anodic wave observed at the range of 0.52-0.64 V is related to the irreversible oxidation of the salophen ligands [32, 37]. The electrochemical data are summarized in Table 2.

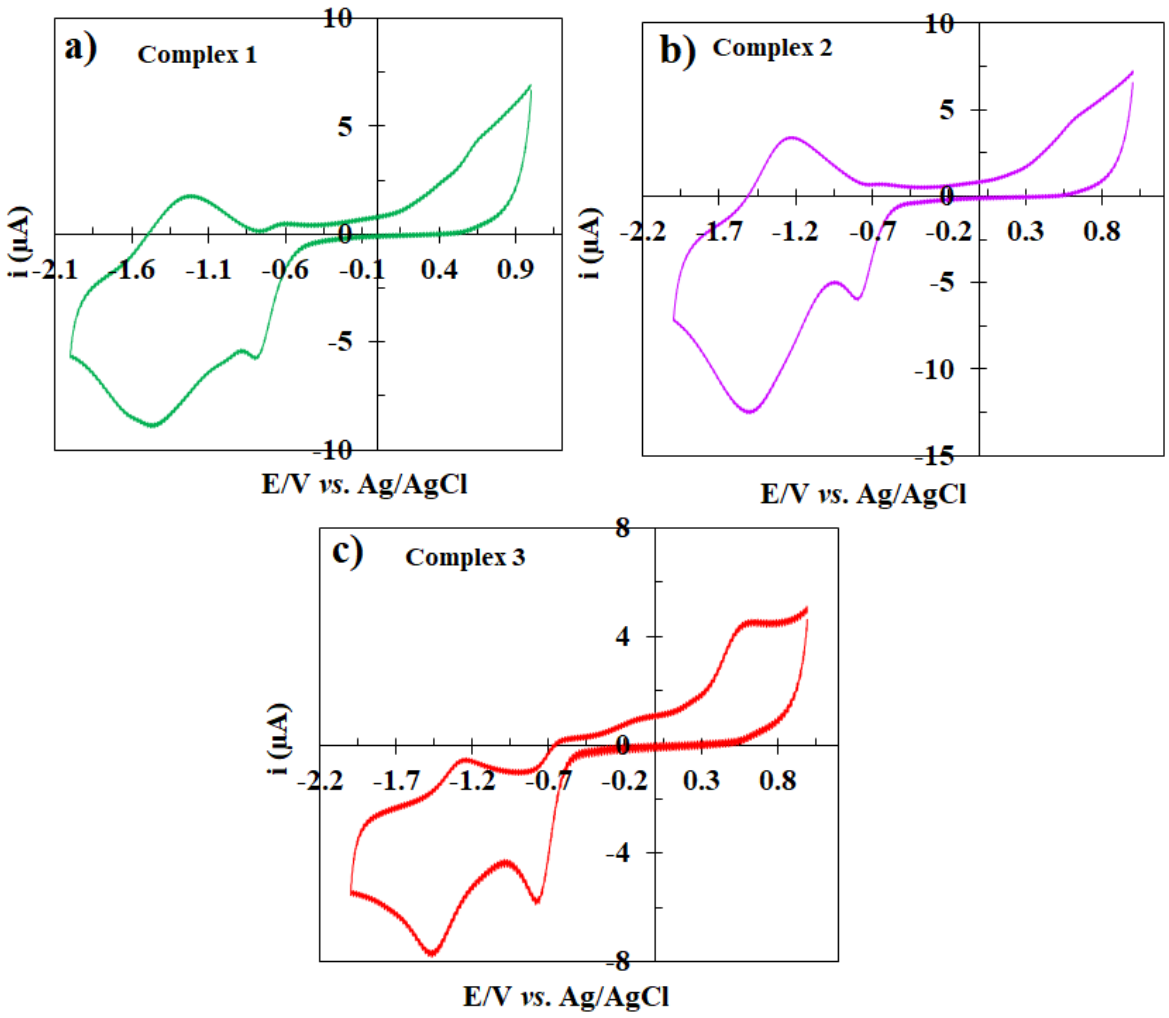

Figure 2: Cyclic voltammograms of Fe^{III} complexes **1**-**3** in DMSO solution containing 0.1 M $LiClO_4$ as a supporting electrolyte at the sweep rate of 50 mV s^{-1}.

Table 2: Electrochemical data for Fe complexes **1**-**3** in DMSO solution (10^{-3} M)

Compound	E_{pa}(V)	E_{pc}(V)	$E_{1/2}$/V (ΔEp (mV))
Complex 1	-1.28	-1.42	-1.35 (140)
	-0.650	-0.750	-0.70 (100)
	0.640		
Complex 2	-1.30	-1.46	-1.38 (160)
	-0.68	-0.76	-0.720 (80)
	0.62		
Complex 3	-1.32	-1.43	-1.375 (110)
	-0.650	-0.74	- 0.695 (90)
	0.52		

Water oxidation activity

In this section, water oxidation activity of Fe complexes **1**-**3** was investigated by Linear sweep voltammetry (LSV), cyclic voltammetry (CV), and chronoamperometry (CA) techniques in borate solution (0.5 M, pH=11). Figure 3a shows the LSV plots of the carbon paste electrode in the absence and presence of Fe salophen complexes **1**-**3** at the scan rate of 50 mV s^{-1}. As considered, bare carbon paste electrode (electrode without electrocatalysts) does not show any significant activity towards the water oxidation reaction. But, when any of the complexes are added to the carbon paste electrode, the water oxidation performance increases considerably. The onset potential for the reaction in the presence of the bare carbon paste electrode is greater than 1.5 V *vs*. Ag/AgCl at a current density of 10 mA cm^{-2}, while this value decreases to 0.98, 1.03 and 0.84 V in the presence of Fe complexes **1**-**3**, respectively under the same conditions. As can be seen, complex **3** needs the lowest onset potential to generate a current density of 10 mA cm^{-2} for water oxidation among all tested compounds. Fe complex **3** needs a relatively low overpotential of 485 mV, while complexes **1** and **2** needs an overpotential value of 625 and 675 mV under the same conditions. The overpotential values at j of 5, 10, and 20 mA cm^{-2} for all complexes are given in Figure 3b, which indicates the higher activity of complex **3** compared to complexes **1** and **2**. Cyclic voltammograms of carbon paste electrodes in the presence of electrocatalysts are shown in Figure 3c, which reveals that complex **3** has the best activity for water oxidation. Furthermore, all voltammograms shows the Fe^{III}/Fe^{II} redox couple [45], which indicates that the metal ion centers of the complexes participate in the reaction as active catalytic sites. To investigate the kinetics of the reaction in the presence of electrocatalysts, Tafel plots were obtained by plotting the potential versus the logarithm of the current density (Figure 3d). The slope value of these linear plots (Tafel slopes) is used to check the kinetics of the reaction, and a low Tafel slope indicate desirable kinetics. As shown in Figure 3d, Fe complex **3** has lower Tafel slope (216 mV dec^{-1}) than complexes **1** and **2** (227 and 313 mV dec^{-1}), and the kinetics of the oxidation of water in the presence of this complex is better. The better performance of complex **3** was proven by calculating the electrochemically active surface area (ECSA). ECSA is obtained from the equation: Cdl/C_s (C_{dl}= double layer capacitance and C_s=the specific capacitance of the electrode). C_{dl} is obtained from CVs performed at different scan rates and a plot of $\Delta j/2$ (Δj=ja-jc) versus scan rates in a non-faradaic region (Figure 4a-d). C_{dl} has a direct relationship with ECSA, and a large C_{dl} value indicates a large ECSA. Also, the higher ECSA, the number of active catalytic sites increases, and as a result, the electrocatalytic activity of the compound improves. As shown in Figure 4d, the Fe complex **3** has the largest C_{dl} value (5.21 mF cm^{-2}) compared to the other tested complexes (2.24 and 1.04 mF cm^{-2} for complexes **1** and **2**, respectively). Therefore, compound **3** has more active

catalytic sites and shows higher electrocatalytic activity for water oxidation.

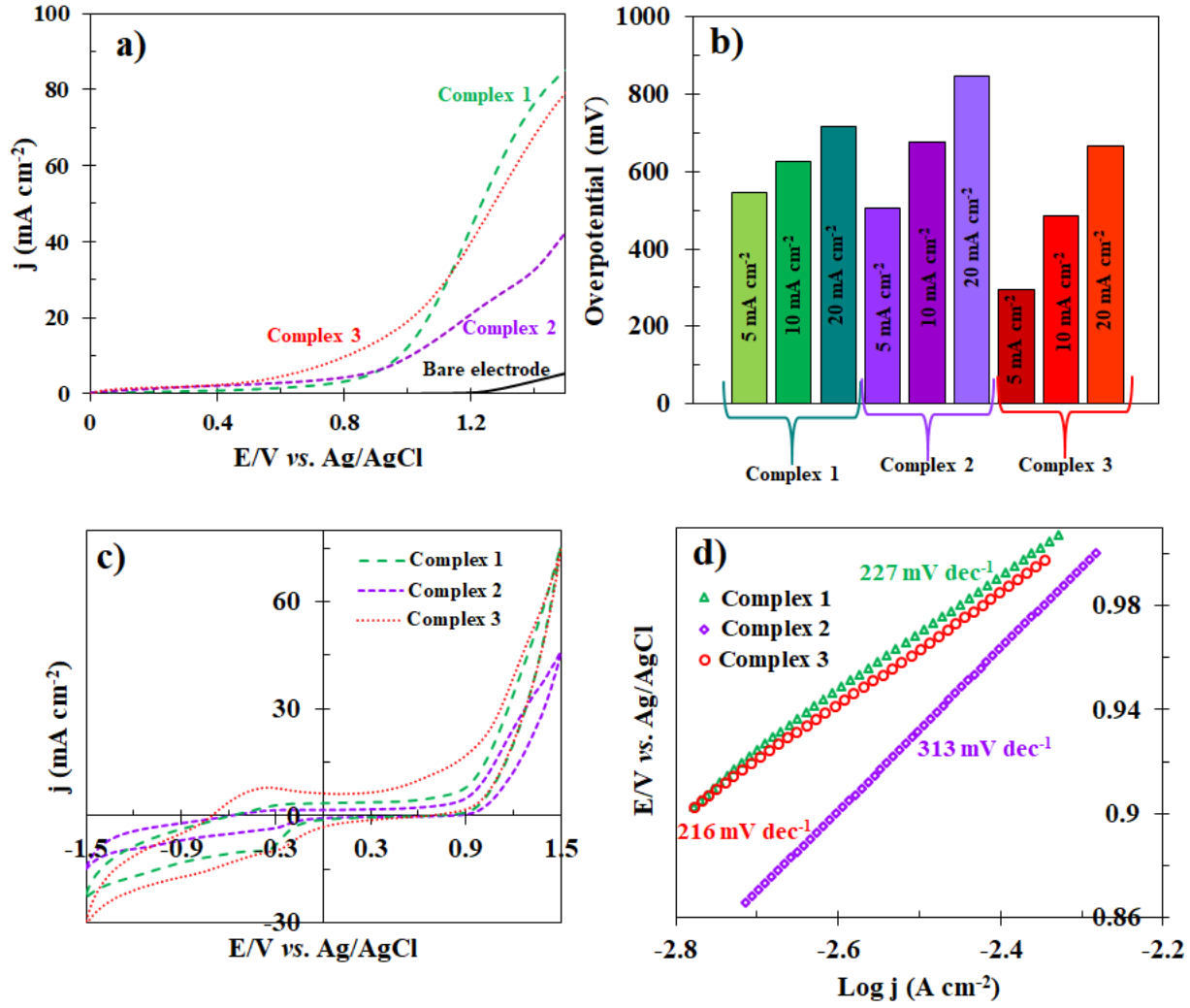

Figure 3: The LSV curves of carbon paste electrode in the absence and presence of Fe complexes **1-3** in a borate buffer solution (pH=11, 0.5 M) at a scan rate of 50 mV s^{-1}(a), the needed overpotential values at j of 5, 10, and 20 mA cm^{-2} for water oxidation in the presence of electrocatalysts (b), CVs of modified electrodes with Fe complexes **1-3** in a borate buffer solution (pH=11, 0.5 M) at a scan rate of 50 mV s^{-1}(d), and Tafel curves; obtained from CVs at a low scan speed of 5 mV s^{-1} (d).

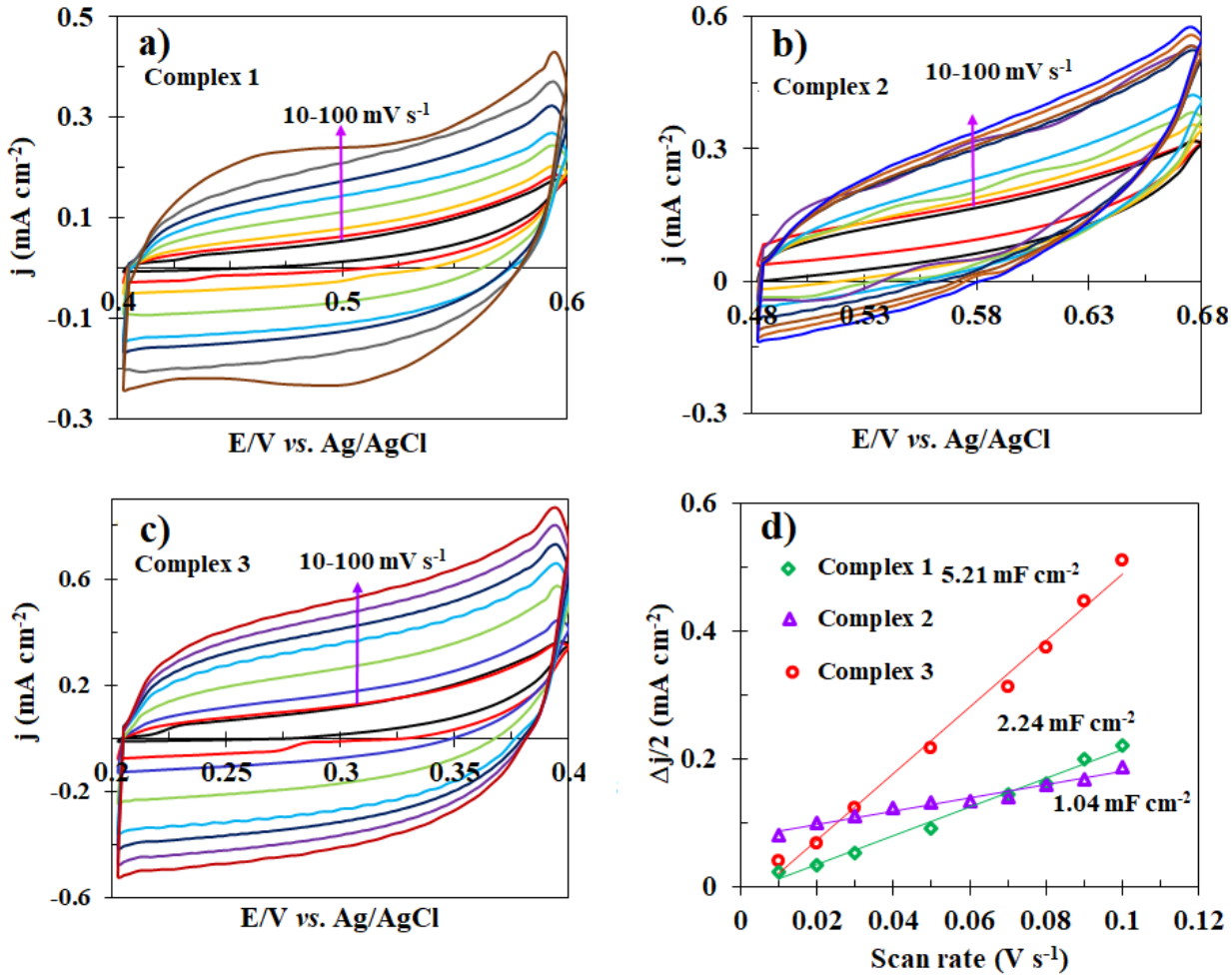

Figure 4: CVs of carbon paste electrodes modified by the Fe complexes **1-3** at different scan rates of 10-100 mV s^{-1} in a non-faradaic region (a-c) and C_{dl} curves (d).

For further investigations, continuous CVs were performed in the presence of electrocatalyst (see Figure 5). As observed, for complexes **2** and **3**, the vertex current does not change much during successive 80 cycles, while for complex **1**, the peak current density increases during the first 20 cycles and then remains almost constant. In addition, the anodic and cathodic peaks related to the oxidation and reduction of the metal ion centers in the complex structure become more intense with the increase in the number of cycles, which indicates that with the progress of the reaction, the number of Fe^{III} ions participating in the reaction as catalytic active sites increases [45]. No color change, no solid film formation on the electrode surface and no further change in the catalytic current density especially in the case of complex **3** are evidences that these complexes probably act as molecular electrocatalysts and their structure during the water oxidation reaction does not change [19]. Since, the Fe complex **3** had the best performance for water oxidation compared to the other complexes, the stability and

durability of this complex was investigated by the chronoamperometry technique at a constant potential of 0.8 V for 6 hours. The results are shown in Figure 6. As seen, a stable current density about 2 mA cm^{-2} is obtained during almost 6 h, which indicated the high stability of the complex during the reaction.

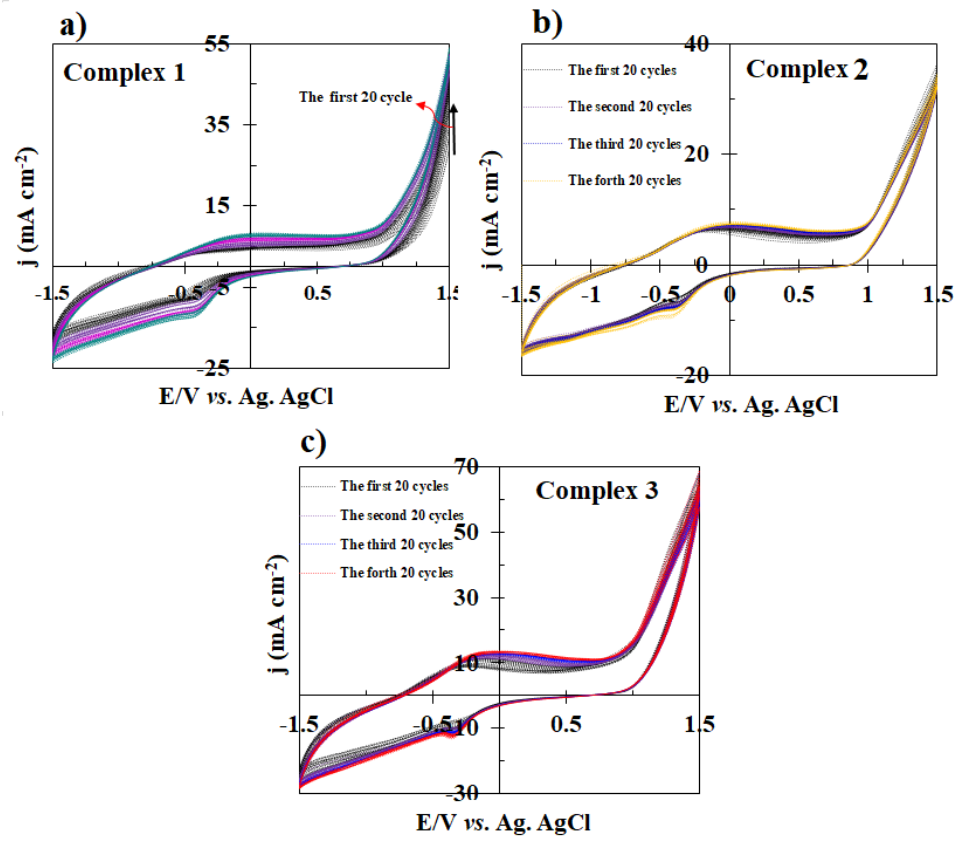

Figure 5: Continuous CVs for modified electrodes with Fe complexes **1**-3 in borate buffer solution (25 ml, 0.5 M, and pH=11) at a scan rate of 50 mV s^{-1}.

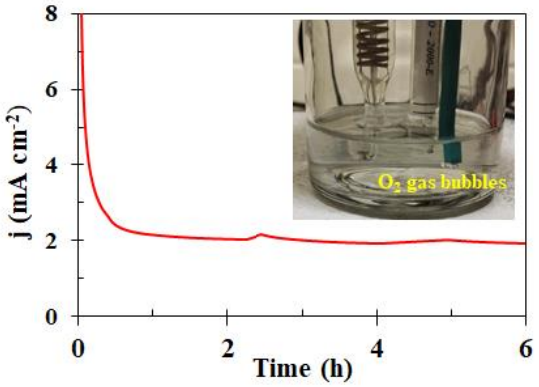

Figure 6: CA experiment for the modified electrode with complex **3** at a constant potential of 0.8 V for 6 h.

Conclusion

In the present research work, some new iron(III) complexes containing salophen ligands with different electron withdrawing substitutions (chlorine, bromine and nitro groups) were produced and characterized by conventional techniques. Then, the synthesized complexes were used as electrode materials and heterogeneous catalysts for electrochemical water oxidation in borate buffer solution. The results showed that all modified electrodes have high activity for the reaction compared to the unmodified electrode, and require relatively low overpotential to oxidize water in a constant current density. Complex **3** showed the best activity for water oxidation with overpotential values of 295 and 485 mV at j of 5 and 10 mA cm^{-2}. Calculations showed that the ECSA for complex **3** is higher than that of complexes **1** and **2**, indicating its higher active catalytic sites and improved water oxidation. This study showed that the Fe complexes with salophen ligands containing different substituents can be used as stable and molecular electrocatalysts for water oxidation.

Acknowledgment

The authors thank the financial support of Azarbaijan Shahid Madani University for this work.

References

[1] Back, D. F.; Oliveira, G. M.; Fontana, L. A.; Ramão, B. F.; Roman, D.; AlmeidaIglesias, B. J. Mol. Struct. 2015,1100, 264.

[2] Keskoğlu, E.; Gündüzalp, A. B.; Çete, S.; Hamrcu, F.; Erk, B. Spectrochim. Acta, Part A. 2008, 70, 634.

[3] Cappillino, P. J.; Miecznikowski, J. R.; Tyler, L. A.; Tarves, P. C.; McNally, J. S.; Lo, W.; Kasibhatla, B. S. T.; Krzyaniak, M. D.; McCracken, J.; Wang, F.; Armstrong, W. H.; Caradonna, J. P.; Dalton Trans. 2012, 41, 5662.

[4] Baecker, D.; Ma, B. N.; Sagasser, J.; Schultz, L.; Hörschläger, C.; Weinreich, M.; Steiner, L.; Kircher, B.; Gust, R.; Dalton Trans. 2020, 49, 6842.

[5] Guerreiro, J. F.; Gomes, M. A. G.B.; Pagliari, F.; Jansen, J.; Marafioti, M. G.; Nistico, C., Hanley, R.; Costa, R. O.; Ferreira, S. S.; Mendes, F.; Fernandes, C.; Horn, A.; Tirinato, L.; Seco, J.; RSC Adv. 2020, 10, 12699.

[6] Bouché, M.; Hognon, C.; Grandemange, S.; Monari, A.; Gros, P. C.; Dalton Trans. 2020, 49, 11451.

[7] Costas, M.; Mehn, M. P.; Jensen, M. P.; Jr, l. Q.; Chem. Rev. 2004, 104, 939.

[8] Corr, M. J.; Murphy, J. A.; Chem. Soc. Rev. 2011, 40, 2279.

[9] Kerns, S. A.; Rose, M.; J. Acc. Chem. Res. 2020, 53, 1637.

[10] Jastrzebski, R.; Weckhuysen, B. M.; Bruijnincx, P. C. A.; Chem. Commun. 2013, 49, 6912.

[11] Shaw, S.; White, J. D. Chem. Rev. 2019, 119, 9381.

[12] Bruijnincx, P. C. A.; van Koten, G.; Klein Gebbink, R. J. M.; Chem. Soc. Rev. 2008, 37, 2716.

[13] McQuilken, A. C.; Goldberg, D. P.; Dalton Trans. 2012, 41, 10883.

[14] Crichton, R. R. Biological inorganic chemistry: An Introduction, Elsevier, Amsterdam, 2008.

[15] Basak, T.; Das, D.; Ray, P. P.; Banerjee, S.; Chattopadhyay, S.; CrystEngComm. 2020, 22, 5170.

[16] Rajnák, C.; Titiš, J.; Moncol, J.; Valigura, D.; Boča, R.; Inorg. Chem. 2020, 59, 14871.

[17] Sharghi, H.; Aboonajmi, J.; Aberi, M.; J. Org. Chem, 2020, 85, 6567.

[18] Çapan, A.; Uruş, S.; Sönmez, M.; J. Saudi Chem. Soc. 2018, 2022, 757.

[19] Shaghaghi, Z.; Aligholivand, M.; Mohammad-Rezaei, R.; Int. J. Hydrog. Energy. 2021, 46, 389.

[20] Aligholivand, M.; Shaghaghi, Z.; Bikas, R.; Kozakiewicz, A.; RSC Adv. 2019, 9, 40424.

[21] Akhtar, M. N.; Bikas, R.; AlDamen, M, A.; Shaghaghi, Z.; Shahid, M.; Sokolov, A.; Dalton Trans. 2022, 51, 12686.

[22] Shaghaghi, Z.; Kouhsangini, P.S.; Mohammad-Rezaei, R.; Appl. Organomet. Chem. 2021, 35, e6103.

[23] Shaghaghi, Z.; Jafari, S.; Mohammad-Rezaei, R.; J. Electroanal. Chem. 2022, 915, 116369.

[24] Kottrup, K. G.; Hetterscheid, D. G. H.; Chem. Commun. 2016, 52, 2643.

[25] Acuña-Parés, F.; Costas, M.; Luis, J. M.; Lloret-Fillol, J.; Inorg. Chem. 2014, 53, 5474.

[26] Hong, D.; Mandal, S.; Yamada, Y.; Lee, Y.-M.; Nam, W.; Llobet, A.; Inorg. Chem. 2013, 2, 9522.

[27] Mukhopadhyay, S.; Basu, O.; Kar, A.; Das, S. K.; Inorg. Chem. 2020, 59, 472.

[28] Panda, C.; Debgupta, J.; Díaz, D. D.; Singh, K. K.; Gupta, S. S.; Dhar, B. B.; J. Am. Chem. Soc, 2014, 136, 12273.

[29] Coggins, M. K.; Zhang, M.-T.; Vannucci, A. K.; Dares, C. J.; Meyer, T. J.; J. Am. Chem. Soc, 2014, 136, 5531.

[30] Praneeth, V. K. K.; Kondo, M.; Okamura, M.; Akai, T.; Izu, H.; Masaoka , S.; Chem. Sci, 2019, 10, 4628.

[31] Mehrabani, S.; Bikas, R.; Zand, Z.; Mousazade, Y.; Allakhverdiev, S. I.; Najafpour, M. M.; Int. J. Hydrog. Energ, 2020, 45, 17434.

[32] Shaghaghi, Z.; Bikas, R.; Tajdar, H., Kozakiewicz, A.; J. Mol. Struct, 2020, 1217, 128431.

[33] Uysal, Ş.; Koç, Z. E.; J. Mol. Struct. 2018, 1165, 14.

[34] Kocyigit,O.; Guler, E.; J. Organomet. Chem. 2011, 696, 3106.

[35] Karatas, E.; Ucan, H. I.; J. Heterocycl. Chem. 2017, 54, 69.

[36] Cakmak, D.; Bulut, T.; Uzun, D.; Electroanalysis. 2020, 32,1559.

[37] Shaghaghi, Z.; Kalantari, N.; Kheyrollahpoor, M.; Haeili, M.; J. Mol. Struct. 2020, 1200, 127107.

[38] Shaghaghi, Z.; Mohammad-Rezaei, R.; Jafari, S.; J. Electroanal. Chem. 2022, 922, 116733.

[39] Gruzdev, M. S.; Vorobeva, V. E.; Zueva, E. M.; Chervonova, U. V.; Petrova, M. M.; Domracheva, N. E.; Polyhedron. 2018, 155, 415.

[40] Chervonova, U.V.; Gruzdev, M.S.; Zueva, E.M.; Vorobeva, V.E.; Ksenofontov, A. A.; Alexandrov, A. I.; Pashkova, T. V.; Kolker, A. M.; J. Mol. Struct. 2020, 1200, 127090.

[41] Pramanik, H. A. R.; Paul, P.C.; Mondal, P.; Bhattacharjee, C. R.; J. Mol. Struct. 2015, 1100 496.

[42] Kursunlu, A. N.; Guler, E.; Sevgi, F.; Ozkalp, B.; J. Mol. Struct. 2013, 1048, 476.

[43] Bertha, O.; Park, S. M.; Bull. Korean. Chem. Soc. 2000, 21, 405.

[44] Sabaté, F.; Gavara, R.; Giannicchi, I.; Bosque, R.; Dalla Cort, A.; Rodríguez, L.; New J. Chem, 2016, 40, 5714.

[45] Akhtar, M. N.; AlDamen, M. A.; Bikas, R.; Shaghaghi, Z.; Jafari, S.; Ibragimov A. B.; Int. J. Hydrog. Energy, 2024, 51, 383-394.

Communications In Catalysis
Vol. 2, No. 2, 2024, pp. 22-43
DOI: 10.22049/CIC.2024.29487.1036
Azarbaijan Shahid Madani University

Porous Covalent Triazine-Based Frameworks: Synthesis and Applications in Adsorption and Catalysis

Somayeh Nasrian [1], Massoumeh Bagheri [2*]

[1,2] Chemistry Department, Faculty of Science, Azarbaijan Shahid Madani University, Tabriz, Iran

E-mail: massomehbagheri@yahoo.com

Received: 2024-02-28, Accepted: 2024-05-03

Abstract

In recent years, porous organic polymers (POPs) have received much attention due to their porous nature and high surface area, and have found wide applications in many fields. An important class of POPs are porous covalent triazine frameworks (CTFs). CTFs have several advantages including high thermal and chemical stability, rich nitrogen contents and tunable porosities. Their structure consists of light elements (C, N, H) and they consist of strong aromatic C=N linkage. These unique properties endow CTFs with great prospects in various applications such as separation and storage of gases, energy storage, adsorption of pollutants, photocatalysis and heterogeneous catalysis. A series of synthetic strategies have been developed, i.e., ionothermal synthesis, superacid-catalyzed method, phosphorus pentoxide- catalyzed method, amidine-aldehyde condensation method, Friedel–Crafts and Schiff-Base reaction methods. Our aim in this review is to take a short look at different synthetic methods of CTFs, and some of their applications.

Keywords: Porous organic polymers, Covalent triazine frameworks, Timerization, Catalysis, Adsorption

Introduction

Porous organic polymers (POPs) are new types of porous materials that have been discovered in recent years [1]. POPs have been used in many applications, including drug delivery, adsorption, separation, and catalysis [2-9]. Porous materials are divided into three classes based on the size of their pores by IUPAC. Microspores have a diameter of less than 2 nm, mesoporous between 2 and 50 nm, and pore sizes above 50 nm are classified as macrospores.

POPs can be divided into several representative groups, for example conjugated microporous polymers (CMPs), covalent organic frameworks (COFs), porous aromatic frameworks (PAFs), hyper-cross-linked polymers (HCPs), and polymer of intrinsic micro polymers porosity (PIMs).

Among these compounds, COFs are a group of crystalline porous materials that are made of molecular organic structural units composed of light elements and connected by covalent bonds. These porous solids were first synthesized by Yaghi et.al in 2005 [10]. Covalent organic frameworks are of various class based on the type of bond, including: boronate ester-linked COFs [11], covalent triazine-based frameworks (CTFs) [12], and imine and hydrazone-linked COFs [13].

Covalent triazine frameworks (CTFs) are an emerging type of porous organic polymers that have recently attracted much attention due to their unique properties. In general, CTFs are extensive porous frameworks containing triazine units connected by covalent bonds (C=N), which have higher stability compared to many COFs that include weak bonds such as imines, boronate esters, borazines, hydrazones, etc. [14].

In 2008, Cohen and co-workers reported for the first time the synthesis of CTF-1 with a surface area of about 1000 $m^2 g^{-1}$ and a hexagonal structure via trimerization of 1,4-dicyanobenzene at 400 °C [15]. This synthesis method is performed at a high temperature, usually above 400 °C and in a sealed ampoule tube. These very harsh conditions do not allow large-scale synthesis. And since then, attempts to synthesize CTFs with new methods have been made by researchers.

The recyclability and reusability of CTFs make them potential candidates for industrial applications such as batteries [16-18], supercapacitor [19, 20], catalyst and photocatalysts [21-23], gas separation [24, 25], removal of pollutants [26], sensors and many other applications.

In this review, we discuss recent developments in the synthetic methods of CTFs and their applications in different fields.

Advantages of nitrogen-rich polymer

CTFs have been investigated due to their conjugated structure, high chemical and thermal stability, as well as high nitrogen content, along with the ability to adjust the structure in various fields of application.

It has been found that nitrogen-rich polymers can be suitable for increasing CO_2 gas adsorption and selectivity towards nitrogen and methane. Their selective adsorption of CO_2 can be due to intermolecular

interactions, guest and polymer, through hydrogen bonding or dipole-quadrupole interactions, and the introduction of heteroatoms, especially nitrogen, into the polymer structure that provides more polar surfaces and increases the selectivity towards CO_2 [27, 28]. In general, the CTFs are a promising prospect for sustainable and green development for various applications, including gas storage and separation, pollutant removal, and catalysis due to their high stability.

CTFs synthesis methods

The triazine ring is the main part of CTFs that contributes to the properties and diverse applications of CTFs. On the other hand, the CTF synthesis methods are classified into two categories based on how the triazine unit is introduced:

The first method is through the synthesis of triazine units by the trimerization reaction and the second method, the synthesis of CTFs, directly introducing the triazine unit through the monomer. The structure of CTFs is highly dependent on the synthesis process, the type of monomer and the type of bond between monomers. Therefore, it is very important to use the appropriate monomer as well as carefully examine the conditions of CTFs synthesis in adjusting the structure of CTFs.

Herein, we aim to explain some synthetic methods for synthesizing CTFs. Various methods have been developed for the synthesis of CTFs, which include ionothermal methods, polycondensation methods, and methods based on superacids.

Synthesis of CTFs by trimerization reaction

Ionothermal synthesis

It was in 2008 that Kuhn et.al [15] synthesized the first CTFs using ionothermal synthesis. In this work CTF-1 using 1-4, dicyanobenzene was synthesized in the presence of zinc chloride as a solvent and catalyst in a sealed glass at 400 °C (Figure 1).

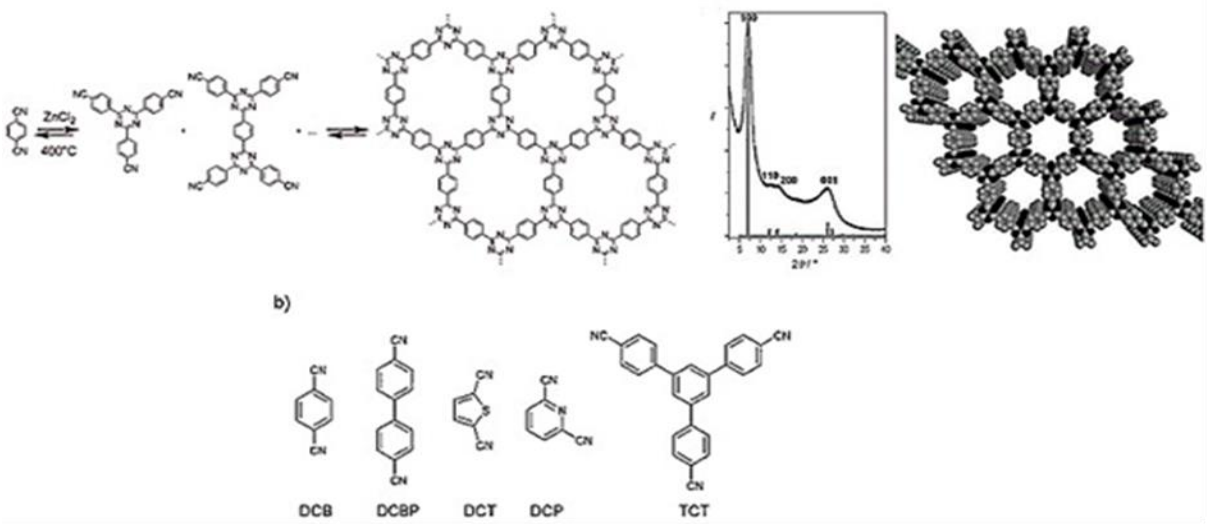

Figure 1. Ionothermal synthesis of polytriazine networks b) Nitrile monomers used in the ionothermal synthesis of triazine frameworks [15].

These synthesized triazine frameworks have high specific surface area, high porosity, and also showed excellent chemical and thermal stability. Temperature had a significant effect on the process of this reaction, because high temperatures cause destruction and carbonization of the structure of the resulting polymers.

The reaction was reversible at a temperature of 400 °C, but a reaction temperature higher than 400 °C would cause irreversible side reactions, because the thermal decomposition of simple aromatic compounds is carried out through the carbonization process and C-C bonds are formed by activating the C-H bond with the successive evolution of H_2.

Also, zinc chloride used in this reaction is molten at temperatures between 300 and 700 °C and boils at 730 °C. The maximum temperature evaluated in order to keep the salt in the liquid state was 700 °C. $ZnCl_2$ at a temperature of 400 °C can be useful for the preparation of crystalline and porous polytriazines. First, because $ZnCl_2$ melts at high temperature and the aromatic nitrile monomers are completely dissolved in this ionic melt with strong Lewis's acid-base interactions and form a clear solution in this molten salt.

Second, $ZnCl_2$ is a Lewis acid, and it can play a catalytic role in the conversion of nitriles to triazines, and facilitate the trimerization reaction, as well as act as a porous catalyst.

These triazine networks were found to be useful for H_2 adsorption. For example, the 4,4′-biphenylcarbonitrile (DCBP) network (1.55 wt% H_2 at 1.00 bar and 77 K) is comparable to metal organic frameworks (MOFs), mesoporous carbon materials, and zeolites, and can provide high thermal, chemical, and mechanical stability and formability of a thermoset polymer material.

Then, in 2010, the same research group synthesized a second member of the family of covalent triazine frameworks, CTF-2, by ionothermal condensation of 2, 6-naphthalenedinitrileat 400 °C for 40 h (Figure 2). CTF-2 showed a relatively smaller surface area than CTF-1.

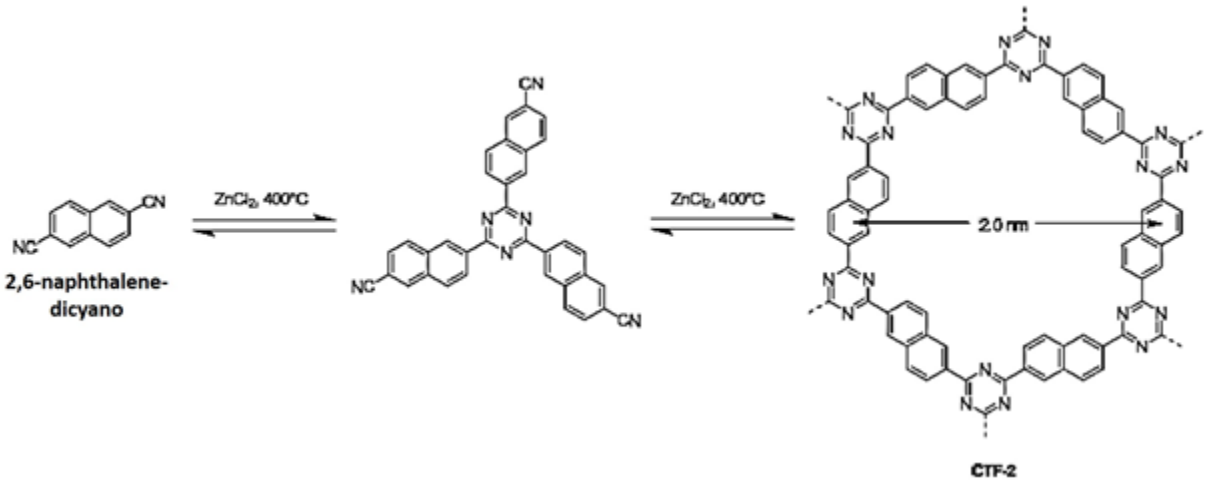

Figure 2. 2,6-Dicyanonaphthalene trimerization reaction to prepare CTF-2 [29].

Adsorption and desorption isotherms of CTF-2 showed the surface area of about 90 m^2 g^{-1} and a pore size of microspores. Indicating that the bulk of micropore content cannot be addressed due to an eclipsed conformation of sheets [29].

Subsequently, in 2013, Thomas' and co-workers synthesized CTF-0 using 1, 3, 5-tricyanobenzene (TCB) monomer by ionothermal method (Figure 3). They found that the reversible trimerization of this monomer leads to a framework that has a smaller pore size than CTF-1 and CTF-2, that's why they named the new framework CTF-0 [30].

This framework showed a high percentage of nitrogen atoms (19.3% by weight) in its structure and showed exceptional CO_2 adsorption due to its high nitrogen content and high surface area. Additionally, CTF-0 has been a suitable metal-free catalyst for the formation of cyclic carbonates from the reaction between CO2 and epoxides (Figure 4). Investigation of the thermal stability of CTF-0 showed that it is even more stable than CTF-1 and is stable in oxygen atmosphere up to 600 ^oC.

CTFs-0 were prepared under different conditions including temperature, time and molar ratio of Zncl2 to monomer, and their names were used in the same order. For example, CTF-0-400-40-1.5 was a framework that was prepared at a temperature of 400 $^{\circ}C$ and within 40 hours and a molar ratio of 1.5, $Zncl_2$ to monomers. The catalytic efficiency of CTFs-0 (prepared under different conditions) and CTF-1 in the preparation of cyclic carbonates using epoxides and carbon dioxide was investigated. All CTFs-0 catalyzed the formation of cyclic carbonates under mild and solvent-free conditions and increased the reaction efficiency compared to non-catalyzed conditions (2.3% efficiency). So that CTF-0-400/600-20/20-5 increased the efficiency to 100% but CTF-0-400-40-1, CTF-0-400-40-1.5 showed less activity, which the authors stated that here the pore size is the controlling factor.

Small micropores accommodate CO_2, but epichlorohydrin cannot fit inside the pores because it is larger, and for this reason, the catalytic activity of CTF-0-400/600-20/20-5 increases with the increase of the surface area and the size of pores increases and reaches 100% [30].

Also, various other monomers have been used to make triazine frameworks with the aim of introducing functional groups into the frameworks (e. g. hetercycle monomers) and also increasing the nitrogen content in the frameworks (e. g. pyridine and pyrimidine monomers) [31-35].

In general, ionothermal synthesis has some limitations along with its advantages. First, because of the high reaction temperature, the monomer must be stable up to at least 400 $^{\circ}C$ in molten $ZnCl_2$. However, aromatic nitriles are mostly stable at high temperatures and decompose above of 400 $^{\circ}C$. Second, increasing the reaction temperature or increasing the ratio of $ZnCl_2$ to monomer leads to the synthesis of amorphous triazine polymers, because the high reaction temperature causes carbonization. However, the effect of temperature and carbonization has been investigated by several groups [36].

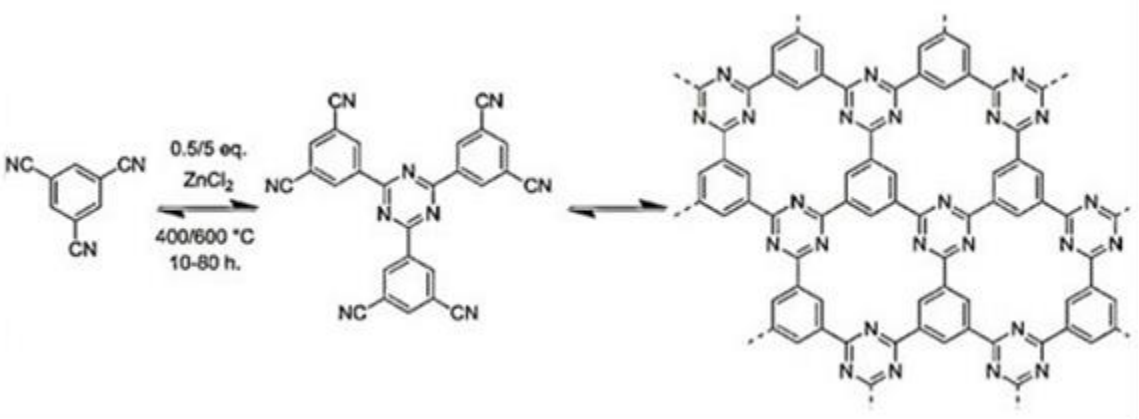

Figure 3. Ionothermal trimerization of 1,3,5-tricyanobenzene [30].

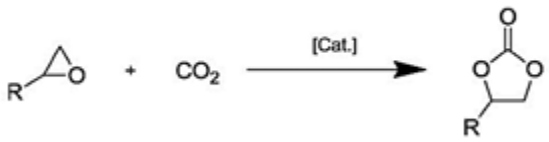

Figure 4. Synthesis of cyclic carbonates in the presence of triazine organic frameworks as catalysts [30]

Superacid- catalyzed synthesis

Despite the success of the ionothermal method for the synthesis of CTfs, due to the long reaction time and high reaction temperature, this method has limitations for some applications. For example, many monomers are not stable under these temperature conditions. The formation of amorphous CTFs as well as the carbonization of materials, the enlargement of pores and the occurrence of some side reactions can occur at high temperatures and long reaction times.

Superacids are a group of highly reactive media with greater potential than pure sulfuric acid. Trifluoromethanesulfuric acid (TFMS) and fluorosulfonic acid are examples of superacids. The catalytic role of superacids in the formation of triazine polymers has already been stablished. In 2012, Cooper et al. [37] used superacids as catalysts in the synthesis of CTFs, and the successful trimmization of aromatic nitriles was achieved with this method both in room temperature and under microwave conditions (Figure 5).

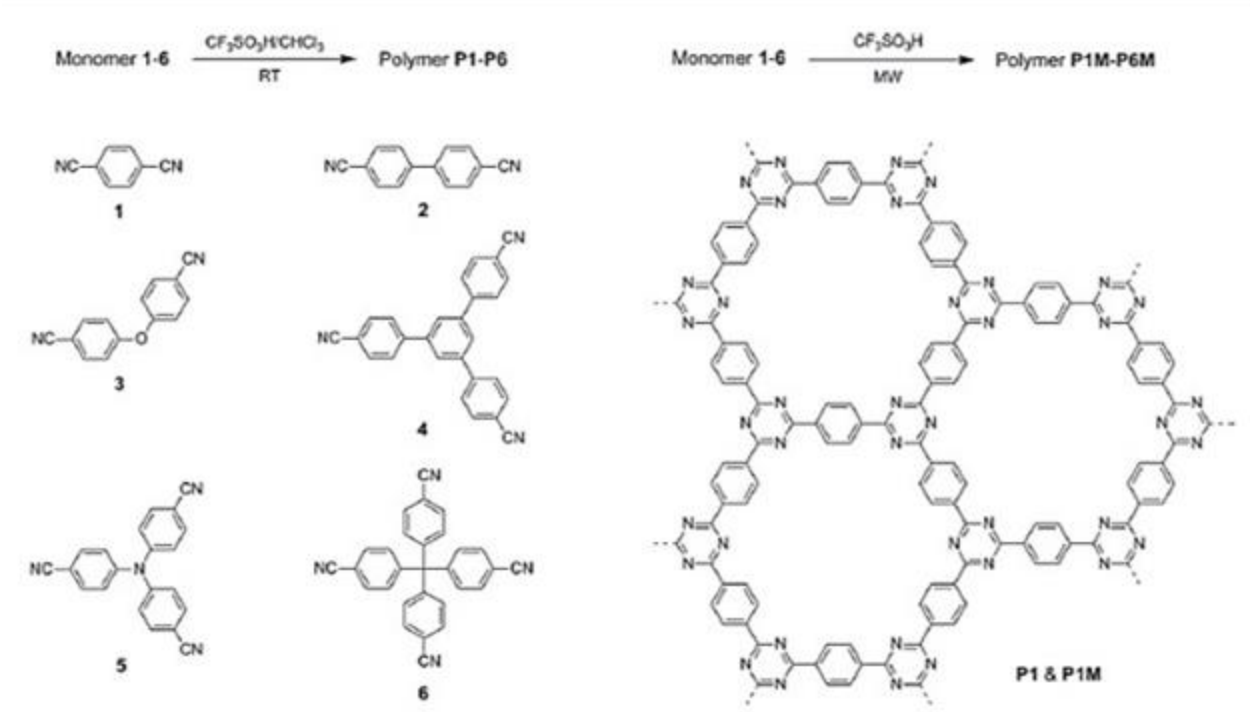

Figure 5. Synthesis of CTF polymers with super acid catalyst at room temperature and under microwave conditions [37].

They emphasized that the much lower temperature used in this method provides a significant advantage and prevents many condensations and side decomposition reactions. Using both of these methods, the infrared spectrum of these polymers showed a significant decrease in the intense nitrile carbon band, along with the appearance of strong triazine bands around 1500, 1360, 800 cm-1 indicating a high degree of polymerization. The obtained frameworks were amorphous at room temperature, while in the microwave assisted method some products showed limited regular structure.

Compared to the ionothermal $ZnCl_2$ catalyzed synthesis, the polymers synthesized via TFMS-catalyzed method show nitrogen contents that are closer to the expected values, suggesting fewer overall defects. The color of CTFs prepared by superacid catalyzed synthesis ranges from pale yellow to brown, and unlike $ZnCl_2$, the CTFs prepared are not black.

In general, this method is a milder method, without carbonization, with easy washing of the products and the obtained frameworks are free of any $ZnCl_2$ residues. The resulting frameworks were evaluated for carbon dioxide adsorption at a pressure of 1 bar at 273 K and the highest adsorption value (4.17 mmol g^{-1}) was obtained,

In the same year, Dai's research team applied this approach to produce triazine-framework-based porous membranes (TFMs) due to milder synthesis conditions [38]. which was one of the highest values obtained in the organic polymer network under these conditions. The resulting membranes also

showed permanent pores, which enabled efficient CO_2/N_2 separation (Figure 6).

Using the Brønsted acid method, only a few semi-crystalline CTFs were produced, only under microwave-assisted conditions, in general, this method was unable to produce large crystalline structures. The polymers obtained from this method were porous, but lacked the long-range order required by crystalline frameworks. Also, the prepared CTFs did not have a layered structure, and acid-sensitive building blocks cannot be used in this method.

In the next step, in order to prepare crystalline CTFs, Dai's research team used a two-step method in which trifluoromethane sulfonic acid played a catalytic role [39]. In order to investigate the synthesis of crystalline CTFs, the temperature of 250 °C was chosen for the first stage of the reaction, which was above the melting temperature of terephthalonitrile but lower than the carbonization temperature of triazine frameworks.

Terephthalonitrile and sulfuric acid were reacted after being placed inside the ampoule and degassing in a sealed system for 12 hours, and after purifying the precipitates, orange-colored products were obtained. Unlike the ionothermal method, the products were black powder.

In the second step, in order to completely remove the residual trifluoromethane sulfonic acid that was physically absorbed in the frame skeleton, the orange powder obtained in this step was subjected to heat treatment in an inert atmosphere at 350 °C, CTF-1-AB obtained in the first stage had a small surface area (22 m^2g^{-1}), while after heat treatment, obtained CTF-1-AA showed a significant increase in surface area (646 m^2g^{-1}).

In the Paxred pattern, after heat treatment, two additional peaks were observed at 12.61° and 14. 38°.This pattern was consistent with the AA-stacking model and indicated that after the he stacking mode had changed from staggered AB to eclipsed AA stacking. In the treatment and complete removal of CF_3SO_3H, the stacking mode has changed from staggered AB to eclipsed AA stacking.

After 2 hours it turned green. The change in texture characteristics after step 2 was complete (Figure 7). Investigations showed that after heat treatment, the stacking mode changed from stepped AB mode to radial AA stacking.

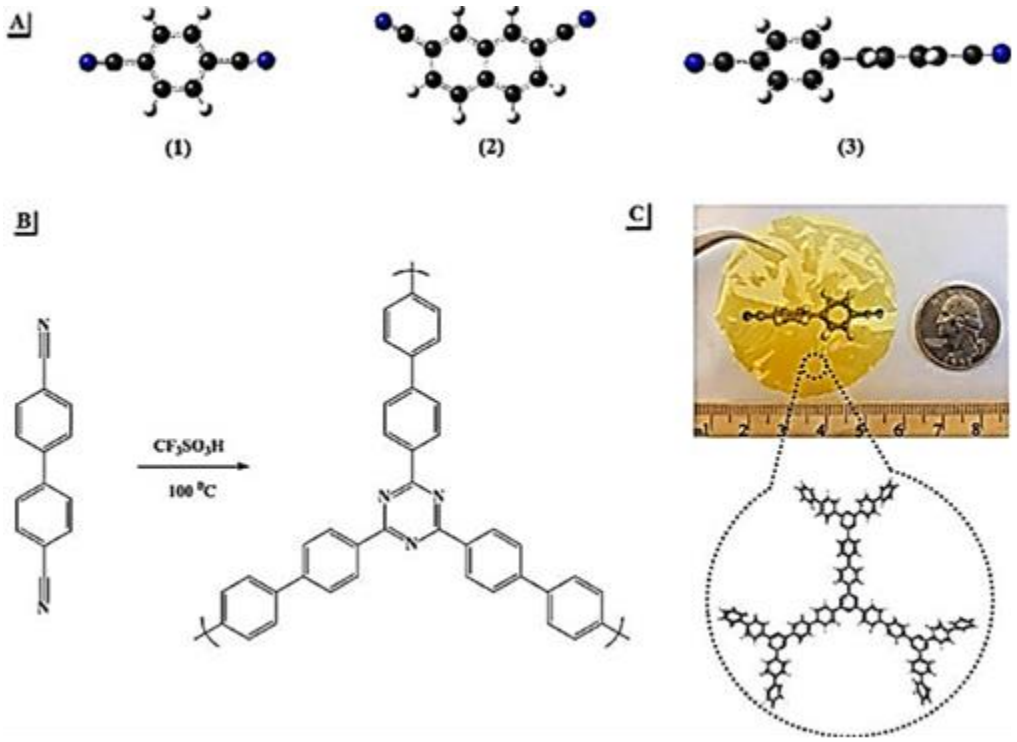

Figure 6. (A) Density functional theory (DFT)-optimized structures of the nitrile monomers used for the membrane synthesis. (B) Trimerization reaction of 4,4-biphenyldicarbonitrile in CF_3SO_3H at 100 °C. (C) Photograph of a directly synthesized sample of the transparent and flexible triazine-framework-based membrane TFMS [38].

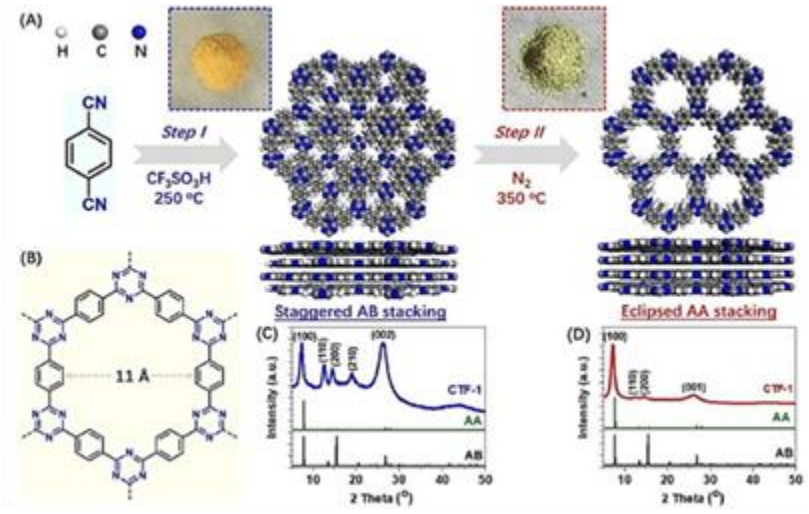

Figure 7. (A) Two-step synthesis of CTF-1 (B) Structure of one triazine unit cell in CTF-1 [39].

Phosphorus pentoxide-catalyzed synthesis

Phosphorus pentoxide (P_2O_5) is one of the known catalysts for dehydrating amides and converting them to nitriles, and it is also a catalyst that is used for the trimerization of nitriles.

In 2018, Beck et al. presented another synthetic strategy using phosphorus pentoxide and aromatic amides. P_2O_5 was used as a catalyst to first convert primary aromatic amides into nitriles and then by applying heat, nitriles were converted into s-triazines rings (Figure 8) [40].

This method is more environmentally friendly compared to CTF synthesis using metal catalysts or acid method. The CTF prepared by this method has high specific surface area, good stability and high crystallinity. The CTFs synthesized by Beck's group showed good crystallinity and relatively high porosity. As a result, due to both the high surface area (2034.1 m^2g^{-1}) and suitable micropores, it showed a high efficiency as a gas absorber.

Amidine−aldehyde condensation

In 2017, Kapur and Tan [41] developed a strategy to prepare ordered crystalline CTFs via in situ oxidation of alcohols followed by polyamidine-aldehyde, which pointed out that the low nucleation concentration and slow nucleation process cause crystallinity (Figure 9).

Compared with ionothermal polymerization or superacid catalyst, this method enables the use of a wide range of monomers for the synthesis of CTFs, and eliminate the contamination of $ZnCl_2$ present in ionothermal polymerization. However, the decomposition of frameworks cannot be avoided due to the high temperature.
In this method, to reduce the rate of nucleation, first the alcohols are slowly oxidized to aldehydes in situ, then the subsequent polymerization starts when the temperature reaches 180 ^oC.

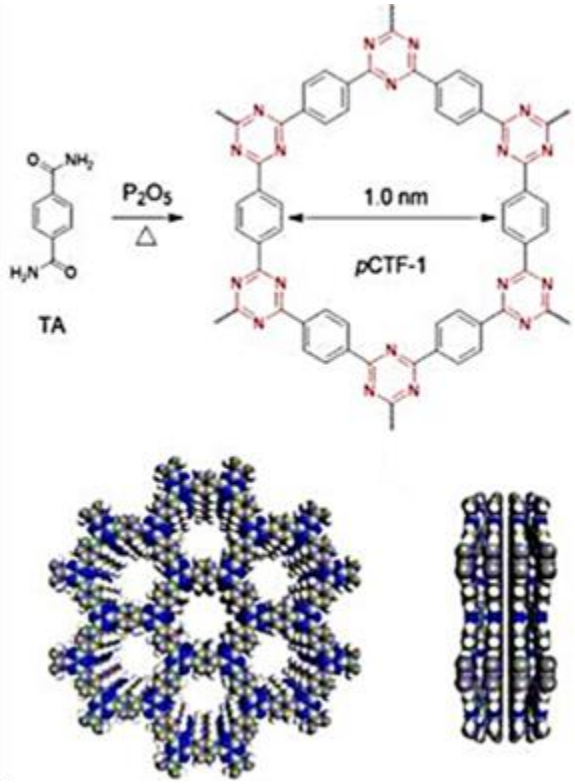

Figure 8. Synthesis of pCTF-1 in the presence of P2O5 [40].

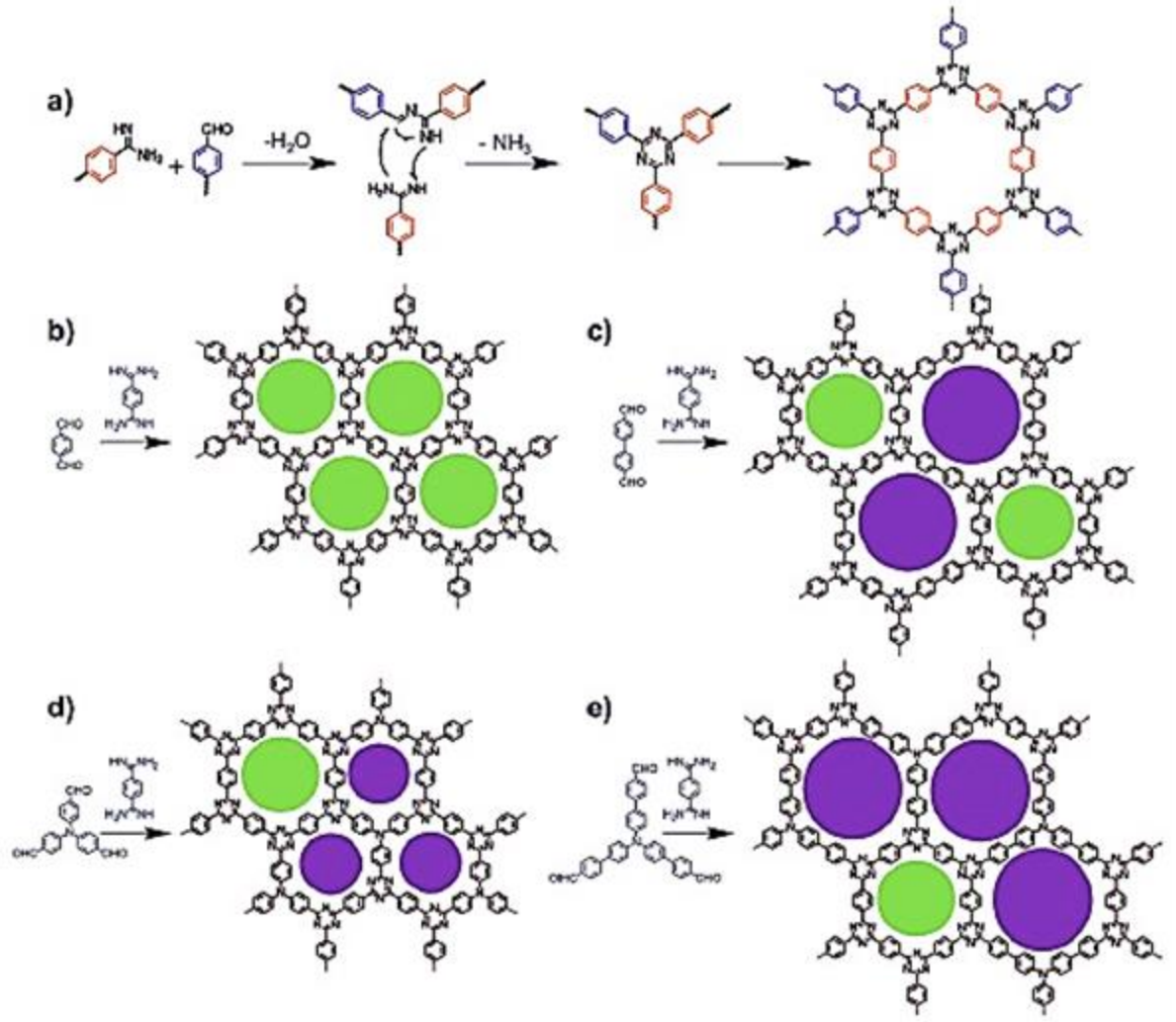

Figure 9. Synthesis of CTF-HUST, based on amidine-aldehyde condensation P2O5 [41].

Polymerization at high temperature increases crystallization. Indeed, the slow production of aldehyde slows down the overall reaction rate and controls the rate of nucleation, enabling the formation of crystalline CTF.

The CTFs prepared by this method had a layered structure and a high surface area (663 to 807 $m^2 g^{-1}$). One of the advantages of this method is the mild synthesis process (temperature of 120 ^oC, and no acid) and CTFs can be prepared up to several grams using this method. These CTFs were promising for use in the field of energy storage and photocatalyst. So that the adsorption of CO_2 for these CTFs was higher than other nitrogen-rich porous organic frameworks.

The formation of CTFs in this method is the condensation between aldehyde and dihydrochloride of amidine, which was initially formed by Schiff base and then increased by Michael. And sodium carbonate was used as base, DMSO as solvent, and 120 ^oC as the optimal condition.

They stated that this method is scalable due to one-pot polymerization, low temperature,

reaction conditions carried out at ambient pressure and an open system**.**

Synthesis of CTFs by direct triazine ring insertion

In this method, monomers that have triazine units are used for the synthesis of triazine polymers. In this section, Friedel-Crafts and Schiff-Base reactions are discussed.

Friedel–Crafts reaction

Another method for the synthesis of CTFs is the Friedel-Crafts reaction. In the Friedel-Crafts reaction, alkyl groups are attached to the aromatic ring.

Cyanuric chloride is reacted with aromatic compounds to synthesis triazine frameworks using Frederic-Crafts method. There are two synthetic routes for this reaction.

Cyanuric chloride is the starting material for the synthesis of triazine compounds. Any of the chlorine groups can be substituted by reacting cyanuric chloride with nucleophiles such as amines, alcohols and thiols. Also, due to electron deficiency, carbons can combine with aromatic compounds under the electrophilic substitution reaction and accordingly, cyanuric chloride is used as an electron-deficient monomer in the Friedel-Crafts reaction.

Different monomers have been used for this reaction (Figure10), which can be performed with two different methods: Methane sulfonic acid (CH_3SO_3H) or anhydrous aluminum chloride ($AlCl_3$) is used as a catalyst in this reaction.

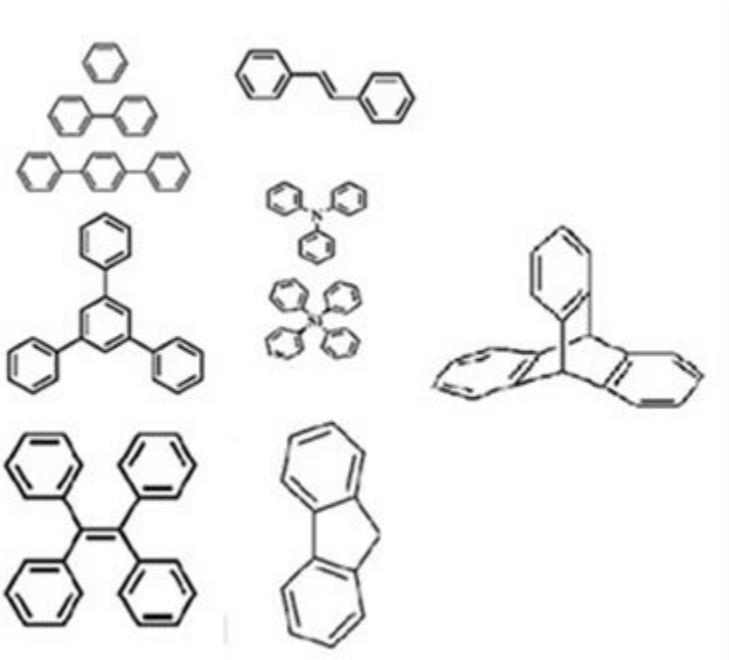

Figure 10. Some monomers used for the synthesis of CTFs in the Friedel-Crafts method.

In the first method, dry aluminum chloride without water is used as a catalyst: In the method, dry aluminum chloride was used as a catalyst, and three triazine compounds were synthesized from the reaction of 2,4,6-trichloro-1,3,5-triazine with benzene, biphenyl, and terphenyl in dichloromethane in the presence of aluminum chloride under reflux for 24 hours [42], respectively (Figure 11).

They reported that the Brunauer-Emmett-Teller (BET) surface area of the resulting polymers depended on the length of the aromatic linker and ranged from 558 to 1266 m2 g-1, although the BET surface area for the benzene-derived polymer from the N2 adsorption isotherm at 77 K was almost zero, which could be because the polymer has very small pores in which N_2 cannot diffuse.

However, when CO_2 was used at 195 K, a BET surface area of 558 m^2 g^{-1} was obtained, which is probably due to the smaller kinetic diameter of CO_2 (3.30 Å) than that of N_2 (3.64 Å).

The use of these polymers in adsorption of gases was investigated and the results showed that the polymers have a high capacity to absorb CO_2 at ambient pressure and temperature.

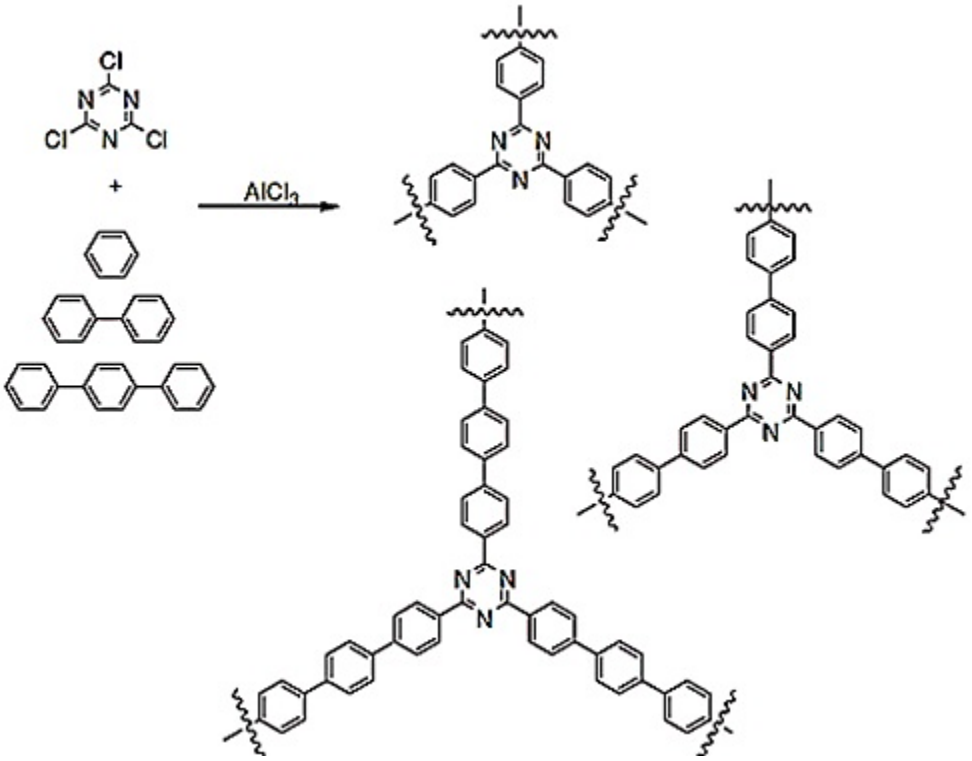

Figure 11. Synthesis of triazine frameworks by Friedel-Crafts method with AlCl3 catalyst [42].

In the second way, methane sulfonic acid is used as a catalyst.

Another group of triazine polymers were synthesized through the Friedel-Crafts reaction and using CH_3SO_3H as a catalyst (Figure 12), cyanuric chloride (as the triazine part), triphenylamine (NOP1-NOP3) and triphenylsilane (NOP4-NOP6). They also investigated the effect of raw material concentration on surface area and pore size. To study the effect of concentration on porosity and surface area, NOPs (NOP-1~3, NOP-4~6) were prepared with different concentrations of CC ($molL^{-1}$) (0.025, 0.050 and 0.100 $molL^{-1}$).

The results showed that high reaction concentration is suitable to increase the pore parameters to some extent, because the properties of pores depend on the degree of polymerization. The degree of polymerization also depends on the concentration of the system (Table 1). Also, the resulting polymers showed a high adsorption capacity for CO_2.

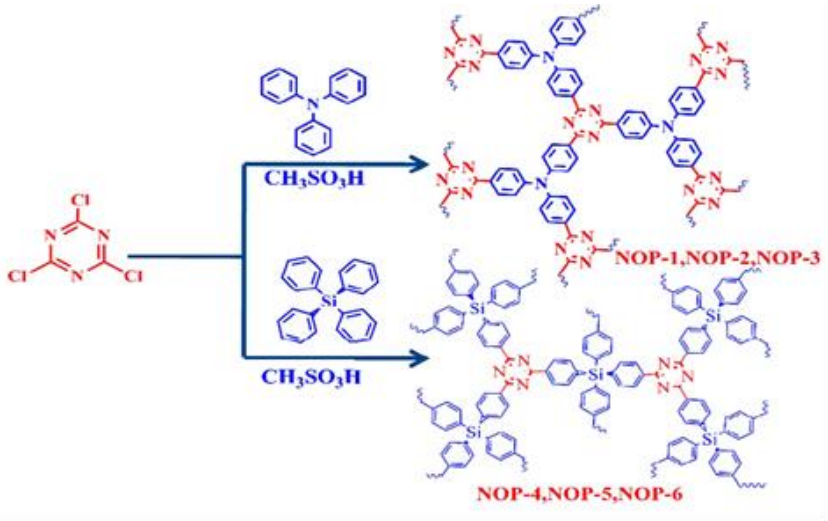

Figure 12. Synthesis of triazine frameworks by Friedel-Crafts method with CH_3SO_3H catalyst [43].

Table 1. Pore parameters of NOPs [43]

Polymer	C_{CC}	SA_{BET}	SA_{LAN}	V_{Total}	V_{Micro}
	mol/l	m^2g	m^2/g	cm^3/g	cm^3/g
NOP-1	0.025	749	978	0.41	0.23
NOP-2	0.050	803	1055	0.44	0.25
NOP-3	0.100	894	1198	0.54	0.25
NOP-4	0.025	428	635	0.67	0.08
NOP-5	0.050	613	913	0.71	0.12
NOP-6	0.100	720	1130	1.44	0.03

NOPs were useful in the field of adsorption and storage, so that NOP-3 hydrogen storage (1.14% by weight) was observed at 77 K (1 bar) and carbon dioxide adsorption 11.03 wt% at 273 K and 6.20 wt% at 298 K (1 bar) which was comparable to many reported organic materials [43].

Schiff-Base reaction

The Schiff-base reaction was discovered in 1864 by Hugo Schiff and has been one of the most important reactions in organic chemistry ever since. The Schiff-base mechanism involves several reversible steps. The reversibility and dynamic nature of imine bonds can be used to create complex crystal structures. As a result, the Schiff-base reaction can be used for the synthesis of triazine-based polymers. In 2009, Mullen et al. [44] using the Schiff-base reaction, succeeded in synthesizing triazine-based polymer networks (Figure 13).

By heating the monomers at a temperature of 180 oC in an inert environment, Schiff-base networks (SNW) were obtained with relatively good efficiency. The resulting networks were stable under humidity and in acidic/alkaline environments, and the thermogravimetric analysis of these materials showed the high thermal stability of these materials (above 400 ^{o}C).

In this method, melamine is used as an amine component, which, in addition to being a cheap industrial material, leads to the production of materials that contain of up to 40% by weight nitrogen content, which has not been achieved before for a microporous material [44].

In a similar research work done in 2013 by Bu and co-workers, a series of new nitrogen-rich aminal-linked porous organic polymers (APOPs) were synthesized from the condensation reaction between diaminotriazines and various benzaldehydes (Figure 14). They showed a surface area in the range of 1402-724 m2g-1. The APOPs exhibit good thermal stability with onset of decomposition above 400 oC as proven by thermogravimetric analysis [45].

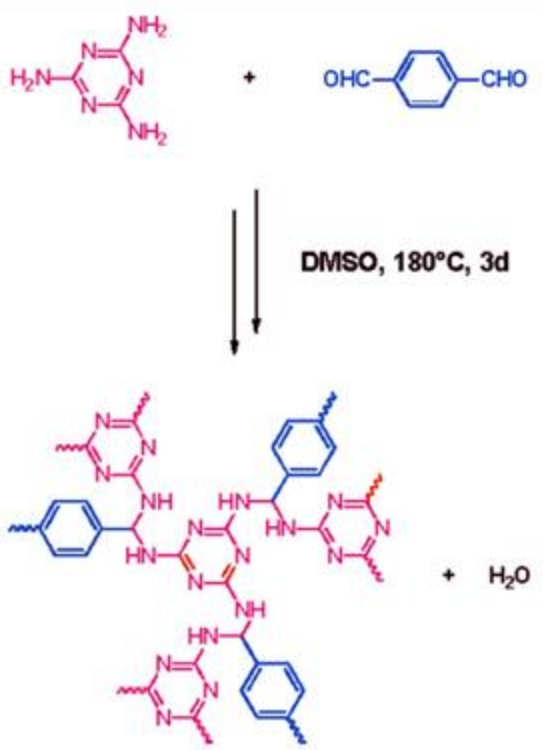

Figure 13. Synthesis route of triazine networks by Schiff-Bass reaction [44].

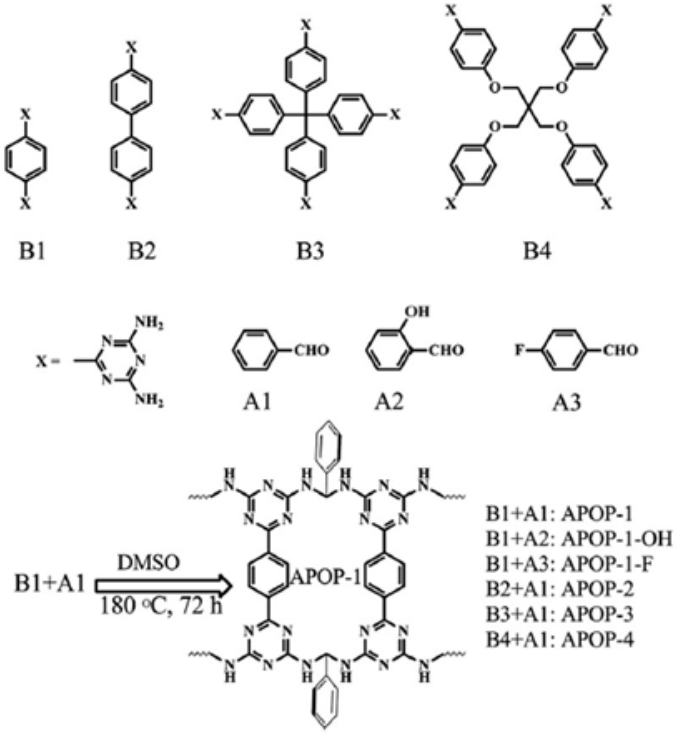

Figure 14. Synthesis of the APOPs [45].

Subsequently, a ferrocene-based nanoporous organic polymer (FNOPs-1) aimed at clean energy applications was synthesized by Zhoua et.al by coupling 1,1'-ferrocene-carboxaldehyde with melamine (Figure 15). FNOPs-1 had a surface area of $752.4 m^2 g^{-1}$ and showed good physico-chemical stability. Also, due to the withdrawing electron nature of ferrocene, it had a high capacity for gas adsorption [46].

Applications of CTFs

Adsorption and separation of pollutants

Due to their porous and microporous nature, high surface area, as well as the possibility of introducing different functional groups into their structures, CTFs have a promising prospect for the adsorption and separation of various pollutants, including metal ions [32, 47], dyes [48, 49], organic pollutants [50] and especially in the field of CO_2 gas adsorption and separation. With the increase of industrial life, followed by the increase in the production of greenhouse gases, the problem of global warming has become one of the most important challenges, and many researchers are looking for a solution to this problem.

The synthesized FNOPs-1 was insoluble in any common organic solvent such as DMSO, N, N'-dimethylformamide (DMF), and tetrahydrofuran (THF), as well as in diluted HCl solution (~10 wt%).

CO_2 gas is one of these gases that plays a role in the problem of pollution and global warming. On the other hand, it has been proven that CTFs are useful in adsorption and separation of CO_2 gas due to their rich nitrogen content and micro and ultra-microporous pores.

In 2012, Cooper's group synthesized a series of CTFs using Brønsted acid as a catalyst [37], and used it to separation of CO_2 gas. These CTFs showed high CO2 adsorption capacity (up to 4.17 mmol g^{-1}). Subsequently, Dai et al. used this approach to produce triazine framework-based porous membranes (TFMs) for CO_2/N_2 separation [38]. The obtained membrane showed a good CO_2 adsorption equal to 1.73 $mmolg^{-1}$ at 273 K and 1 bar pressure, and the membrane showed more selectivity for separation of CO_2 from N_2.

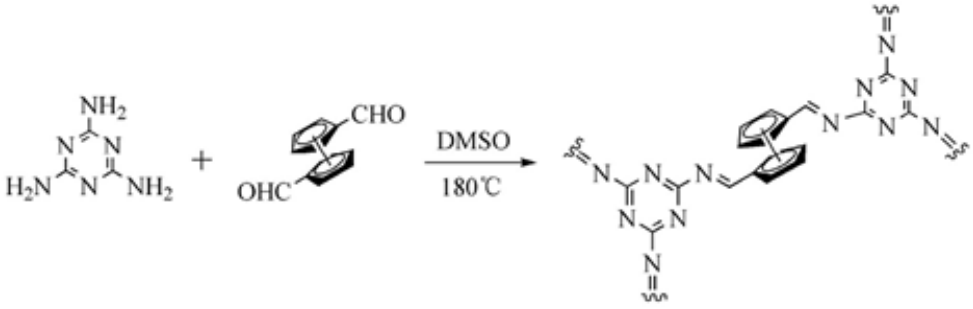

Figure 15. Synthesis of the FNOPs-1 [46].

In 2013, Janiak et al. synthesized a series of adamantane-based CTFs (PCTFs) for CO_2 adsorption, both under Brønsted acid conditions and ionothermal conditions, and proved that the CTFs prepared In 2013, Janiak et al. synthesized a series of adamantane-based CTFs (PCTFs) for CO_2 adsorption, both under Brønsted acid conditions and ionothermal conditions, and proved that the CTFs prepared by the later method showed better adsorption due to their high surface area, porosity, and micropore volume [51]. Also, the results showed that CO_2 adsorption increases with the increase in the number of cyano groups.

On the other hand, introducing CO_2-philic in the structure of CTFs such as oxygen, nitrogen and fluorine increases CO_2 adsorption due to the increase of electrostatic interactions. Accordingly, using the properties of perfluorocarbon compounds, Han's group synthesized a perfluorinated CTF (FCTF) with micro-pores for selective CO2 adsorption. The replacement of H atoms with F atoms improved the surface area and reduced the pore size, which was favorable for the separation of CO_2 from N_2 [52].

Also, recent research showed that the introduction of polar and ionic groups as well as the introduction of heteroatoms in the structure of CTFs improved the CO_2 adsorption in CTFs [53-56].

Catalytic applications

CTFs can be used as catalysts in many organic reactions according to the structure and functional groups in the framework. Also, the ability to adjust the structure (using the synthetic method) and chemical (by choosing the appropriate monomers) allows for a more detailed investigation of the catalytic properties of CTFs. On the other hand, CTFs are suitable catalysts for the synthesis of cyclic carbonates due to their high nitrogen content and good stability in the synthetic conditions of these compounds using epoxides and carbon dioxide.

In 2012, CTF-1 was first used as catalyst for the conversion of carbon dioxide and epoxides to cyclic carbonates, and they catalyzed the conversion of carbon dioxide to cyclic carbonates with very good efficiency and selectivity under solvent-free conditions [57].

In 2013, Thomas' group used CTF-0 as a catalyst in this reaction, and the results showed that CTF-0 showed higher catalytic activity than CTF-1 [30]. Also, other CTF with different functional groups in the framework structure were synthesized and used for this purpose, including imidazolium-based CTFs [58, 59], carbazole-decorated-CTF [60] and pyridine-rich cationic CTFs [61].

Of course, the catalytic role of CTFs is not only limited to cycloaddition reactions, and it can play a good catalytic role in various reactions such as Novenagle reaction [62], oxidation of alcohols [63], also as a photocatalyst [64] in many other reactions [65].

Conclusions

CTFs can be synthesized by various methods, either through trimerization reactions or direct use of monomers containing triazine rings. Many advances have been made in the field of CTFs synthesis. But the synthesis of

CTFs under milder conditions and high scales, as well as the synthesis of CTFs with high crystallinity, is still the goal of many research works.

CTFs can be used in in a broad spectrum of applications including highly efficient and selective adsorption of pollutant, adsorption and storage of gases, metal-free catalysts and photocatalyst, etc. due to structural design capability, high porosity, high nitrogen content, high physicochemical stability and the ability to introduce functional groups into the structure of these compounds.

References

[1] Das, S.; Heasman, P.; Ben, T.; Qiu, S. Chem. Rev. 2017, 1515.

[2] Morris, R. E.; Wheatley, P. S. Angew. Chem. Int. Ed. 2008, 47, 4966.

[3] Bügel, S.; Hähnel, M.; Kunde, T.; de Sousa Amadeu, N.; Sun, Y.; Spieß, A.; Janiak, C. J. Mater. 2022, 15, 2807.

[4] Erdosy, D. P.; Wenny, M. B.; Cho, J.; DelRe, C.; Walter, M. V.; Jiménez-Ángeles, F.; Mason, J. A. Nature. 2022, 608, 712-718.

[5] Bügel, S.; Hähnel, M.; Kunde, T.; de Sousa Amadeu, N.; Sun, Y.; Spieß, A.; Janiak, C. Mater. 2022, 15, 2807.

[6] Yang, J.; Qiu, H.; Huang, L.; Meng, S.; Yang, Y. Chem Plus Chem. 2023, 88, e202300292.

[7] Sayari, A.; Hamoudi, S.; Yang, Y. Chem. Mater. 2005, 17, 212.

[8] Zhang, J.; Chen, J.; Peng, S.; Peng, S.; Zhang, Z.; Tong, Y.; Yan, X. P. Chem. Soc. Rev. 2019, 48, 2566.

[9] Zhao, X. S. J. Mater. Chem. 2006, 16, 623.

[10] Cote, A. P.; Benin, A. I.; Ockwig, N. W.; O'Keeffe, M.; Matzger, A. J.; Yaghi, O. M. Sci. 2005, 310, 1166-1170.

[11] Wan, S.; Gándara, F.; Asano, A.; Furukawa, H.; Saeki, A.; Dey, S. K.; Yaghi, O. M. Chem. Mater. 2011, 23, 4094-4097.

[12] Bojdys, M. J.; Jeromenok, J.; Thomas, A.; Antonietti, M. Adv Mater. 2010, 22, 2202-2205.

[13] Uribe-Romo, F. J.; Hunt, J. R.; Furukawa, H.; Klock, C.; O'Keeffe, M.; Yaghi, O. M. J. Am. Chem. Soc. 2009 131, 4570-4571.

[14] Liu, M.; Guo, L.; Jin, S.; Tan, B. J. Mater. Chem. A 2019, 7, 5153– 5172.

[15] Kuhn, P.; Antonietti, M.; Thomas, A. Porous Angew. Chem., Int. Ed. Engl., 2008, 47, 3450-3453.

[16] Xu, F.; Yang, S.; Jiang, G.; Ye, Q.; Wei, B.; Wang, H. ACS Appl. Mater. Interfaces. 2017, 9, 37731-37738.

[17] Gao, G.; Jia, Y.; Gao, H.; Shi, W.; Yu, J.; Yang, Z.; Zhao, Y. ACS Appl Mater Interfaces. 2021, 13, 50258-50269.

[18] Mahato, M.; Nam, S.; Lee, M. J.; Koratkar, N.; Oh, I. K. Small. 2023, 2301847.

[19] Bhanja, P.; Bhunia, K.; Das, S. K.; Pradhan, D.; Kimura, R.; Hijikata, Y.; Bhaumik, A. ChemSusChem. 2017, 10, 921-929.

[20] Lin, K. Y.; EL-Mahdy, A. F. Mater. Chem. Phys. 2022, 281, 125850

[21] Chan-Thaw, C. E.; Villa, A.; Veith, G. M.; Kailasam, K.; Adamczyk, L. A., Unocic, R. R.; Thomas. Chem. Asian J. 2012, 7, 387-393.

[22] Iemhoff, A.; Vennewald, M.; Palkovits, R. Angew. Chem., Int. Ed. Engl. 2023 62, e202212015.

[23] Qian, Z.; Wang, Z. J.; Zhang, K. A. Chem. Mater. 2021, 33, 1909-1926.

[24] Carta, M.; Malpass-Evans, R.; Croad, M.; Rogan, Y.; Jansen, J. C.; Bernardo, P.; McKeown, N. B. Sci. 2013, 339, 303-307.

[25] Lan, Z. A.; Wu, M., Fang, Z.; Zhang, Y.; Chen, X.; Zhang, G.; Wang, X. Angew. Chem., Int. Ed. Engl. 2022, 61, e202201482.

[26] Liu, J.; Zong, E.; Fu, H.; Zheng, S.; Xu, Z.; Zhu, D. J. Colloid Interface Sci. 2012, 372, 99-107.

[27] Rabbani, M. G.; El-Kaderi, H. M. Chem. Mater. 2011, 23, 1650-1653.

[28] Zheng, B., Bai, J.; Duan, J.; Wojtas, L.; Zaworotko, M. J. J. Am. Chem. Soc. 2011, 133, 748-751.

[29] Bojdys, M. J.; Jeromenok, J.; Thomas, A.; Antonietti, M. Adv Mater. 2010, 22, 2202-2205.

[30] Katekomol, P.; Roeser, J.; Bojdys, M., Weber, J.; Thomas, A. Chem. Mater, 2013, 25, 1542-1548.

[31] Bavykina, A. V.; Olivos-Suarez, A. I., Osadchii, D.; Valecha, R., Franz, R.; Makkee, M.; Gascon, J. ACS Appl. Mater. Interfaces. 2017, 31, 26060-26065.

[32] Farrokhi, H., Bagheri, M. J. Polym. Res. 2023, 30, 45.

[33] Mukherjee, S.; Das, M.; Manna, A., Krishna, R.; Das, S. J. Mater. Chem. A. 2019, 7, 1055-1068.

[34] Jena, H. S.; Krishnaraj, C.; Schmidt, J.; Leus, K.; Van Hecke, K.; Van Der Voort, P. Chem. Eur. J. 2020, 26, 1548-1557.

[35] Park, K.; Lee, K.; Kim, H.; Ganesan, V.; Cho, K.; Jeong, S. K.; Yoon, S. J. Mater. Chem. A. 2017, 5, 8576-8582.

[36] a) Kuhn, P.; Forget, A.; Su, D.;Thomas, A., & Antonietti, M. J. Am. Chem. Soc. 2008, 130, 13333-13337. b) Osadchii, D. Y.; Olivos-Suarez, A. I.; Bavykina, A. V.; Gascon, J. Langmuir 2017, 33, 14278-14285.

[37] Ren, S.; Bojdys, M. J.; Dawson, R., Laybourn, A.; Khimyak, Y. Z.; Adams, D. J.; Cooper, A. I. Adv Mater. 2012, 24, 2357-2361.

[38] Zhu, X.; Tian, C.; Mahurin, S. M.; Chai, S. H., Wang, C., Brown, S.; & Dai, S. J. Am. Chem. Soc. 2012, 134, 25, 10478-10484.

[39] Yang, Z.; Chen, H.; Wang, S.; Guo, W.; Wang, T.; Suo, X.; & Dai, S. J. Am. Chem. Soc. 2020 .142, 6856-6860.

[40] Yu, S. Y.; Mahmood, J.; Noh, H. J.; Seo, J. M.; Jung, S. M.; Shin, S. H.; Baek, J. B. 2018. Angew. Chem., Int. Ed. Engl. 2018, 57, 8438-8442.

[41] Wang, K.; Yang, L. M.; Wang, X.; Guo, L.; Cheng, G.; Zhang, C.; Cooper, A. Angew. Chem., Int. Ed. Engl. 2017, 56, 14149-14153.

[42] Lim, H.; Cha, M. C.; Chang, J. Y. Macromol Chem Phys. 2012, 213, 1385-1390.

[43] Xiong, S.; Fu, X.; Xiang, L.; Yu, G.; Guan, J.; Wang, Z.; Pan, C. Polym. Chem. 2014, 5, 3424-3431.

[44] Schwab, M. G.; Fassbender, B.; Spiess, H. W.; Thomas, A.; Feng, X.; Mullen, K. J. Am. Chem. Soc. 2009, 131, 7216-7217.

[45] Song, W. C.; Xu, X. K.; Chen, Q.; Zhuang, Z. Z.; Bu, X. H. Polym. Chem. 2013, 4, 4690-4696.

[46] Liu, Q.; Tang, Z.; Wu, M.; Liao, B., Zhou, H.; Ou, B.; Li, X. RSC Adv. 2015, 5, 8933-8937.

[47] Chakraborty, A.; Sarkar, S.; Kyarikwal, R.; Nag, P.; Vennapusa, S. R.; Mukhopadhyay, S. ACS Appl. Polym. Mater. 2022, 4, 8118-8126.

[48] Kumar, S.; Kumari, K.; Singh, S. K.; Dholakiya, B. Z.; Jangir, R. New J Chem. 2023, 47, 13676-13686.

[49] Ghanbari, J.; Mobinikhaledi, A. Sci. Rep. 2023, 13, 12962.

[50] Aslam, A. A.; Irshad, A.; Nazir, M. S.; & Atif, M. J. Clean. Prod. 2023, 400, 136737.

[51] Bhunia, A.; Boldog, I.; Möller, A.; Janiak, C. J. Mater. Chem. 2013, 1, 14990-14999

[52] Zhao, Y.; Yao, K. X.; Teng, B.; Zhang, T.; Han, Y. Energy Environ Sci. 2013, 3684-3692.

[53] Xu, G.; Zhang, S.; Xie, W.; Wang, L.; Xue, X.; Qiao, Y.; Su, Z. J. Polym. Res. 2022, 29, 153.

[54] Rangaraj, V. M.; Reddy, K. S. K.; Karanikolos, G. N. J. Chem. Eng. 2022, 429, 132160.

[55] Lin, K. Y.; EL-Mahdy, A. F. Mater. Chem. Phys. 2022, 281, 125850.

[56] Park, K.; Lee, K.; Kim, H.; Ganesan, V.; Cho, K.; Jeong, S. K.; Yoon, S. Mater. Chem. 2017, 5, 8576-8582.

[57] Roeser, J.; Kailasam, K.; Thomas, A. ChemSusChem. 2012, 5, 1793-1799.

[58] Liu, T. T.; Xu, R.; Yi, J. D.; Liang, J.; Wang, X. S.; Shi, P. C.; Cao, R. ChemCatChem. 2018, 10, 2036-2040.

[59] Liu, F.; Duan, X.; Liu, M.; Du, J.; Ma, J.; & Liu, F. Ind. amp; Eng. Chem. Res. 2021, 60, 15027-15036.

[60] Yu, W.; Gu, S.; Fu, Y.; Xiong, S.; Pan, C.; Liu, Y.; & Yu, G. J. Catal. 2018, 362, 1-9.

[61] Zhao, Y.; Huang, H.; Zhu, H.; & Zhong, C. Microporous Mesoporous Mater. 2022, 329, 111526.

[62] M. B. Ansari, M. N. Parvin and S.-E. Park, Res. Chem. Intermed. 2013, 40, 67-75.

[63] Huang, W.; Ma, B. C.; Lu, H.; Li, R.; Wang, L.; Landfester, K.; & Zhang, K. A. ACS Catal. 2017, 7, 5438-5442.

[64] Sun, R.; Tan, B. Chem. Res. Chin. 2022, 38, 310-324.

[65] Iemhoff, A.; Vennewald, M.; Palkovits, R. Angew. Chem., Int. Ed. Engl. 2023. 62, e202212015.

Communications In Catalysis
Vol. 2, No. 2, 2024, pp. 44-55
DOI: 10.22049/CIC.2024.29525.1037
Azarbaijan Shahid Madani University

One- pot facile synthesis of nitrogen doped graphene quantum dots based on N',2-dihydroxyethanimidamide and citric acid

Ebrahim Rezaii[1]*, Mehrdad Mahkam[2], Mohammad Rezaii[3]

[1,2]Chemistry Department, Faculty of Science, Azarbaijan Shahid Madani University, Tabriz, Iran

[3]Educational Sciences Department, Faculty of Science, Farhangian University, Tabriz, Iran

E-mail: *Ebrahimrezayii@gmail.com*

Received: 2024-03-11, Accepted: 2024-05-03

Abstract

Graphene quantum dots (GQDs) are tiny segments of graphene whose electron mobility is confined in all three dimensions. Graphene is a 0-bandgap semiconductor possessing an infinite exciton Bohr diameter. Therefore, quantum confinement is evident in all graphene fragments. The GQDs are usually under 20 nm in dimensions. We report a facile hydrothermal method for synthesis of graphene quantum dots contains nitrogen atoms (N-GQDs). This study shows interaction between citric acid (CA) and N',2-dihydroxyethanimidamide (DHAA) in which N-doped graphene quantum dots were synthesized. Due to use of DHAA that has two active sites, synthesized N-GQDs have special morphology, fluorescence and viscosity. Compared with other nitrogen compounds that is necessary for N-GQDs synthesis, DHAA is much more suitable due to low toxicity and stability. Synthesized N-GQDs were identified by FT-IR, XRD, TGA and fluorescence.

Keywords: N',2-dihydroxyethanimidamide, Nitrogen doped, Graphene quantum dot, One- pot synthesis

Introduction

graphene quantum dots (GQDs) that consist of nanometer-scaled graphene particles with sp^2-sp^2 carbon bonds are expected to show specific properties like size dependent general quantum dots (QDs) [1, 2] or chemically modified quantum dots with sp^2-sp^2 carbon bonds. In contrast to graphene, most applications of GQDs have been focused on the photoluminescence (PL)-related fields since GQDs show a PL. Recent studies clear that, additional properties of GQDs such as high transparency and high surface area have been discussed for energy and display applications [3].

Carbon quantum dots (C-QDs), have received many attentions for exceptional advantages such as low toxicity [4, 5], high chemical stability [6], excellent biocompatibility [7-9], high-fluorescence [10]. Considering these unique physical-chemical characteristics, C-QDs have been applied broadly in fields of catalysis [11], printing ink [12], biological sensors [13-15], bioimaging [16] and drug delivery [17]. Since 2006, Sun et al. found a new fluorescent nanoparticle named as carbon dots, many approaches have been found to prepare C-QDs [18]. Up to now, several methods for obtaining carbon-based materials have been developed, such as chemical oxidation method [19], ultrasonic method [20], hydrothermal synthesis [9, 21-23], solvothermal method [24], microwave method [25] and laser ablation method [18].

There are two main strategies for synthesizing GQDs, i.e., top-down and bottom-up methods. The first approaches involve the exfoliation of graphite into graphene sheets, followed by cutting of graphene sheets into GQDs. Therefore, the top- down method is limited by low product yield and rough conditions because of the use of a toxic organic solvent and strong acid/oxidant [26-28]. However, the bottom-up approaches is based on the construction of GQD from small organic precursor molecules through catalytic or thermal treatment, resulting in the environmentally-friendly production of large scale GQDs with uniform size of distribution and morphology [29, 30].

N-doped into graphene was highly effective in modulating its band gap to achieve new properties for device applications [31, 32]. Due to the considerable quantum

confinement and edge effects of GQDs, direct substitution with nitrogen in GQDs lattice can drastically modulate the chemical and electronic properties and offer more active sites, thus leading to unexpected phenomena which could be extensively applied in various fields. Recently, N-doped GQDs (N-GQDs) have been synthesized through hydrothermal or electrochemical methods which are based on slicing graphene oxide (GO) and its reduction. However, synthesis of GO typically takes several days and requires lots of strong chemical acid and oxidant in a series of chemical treatments of the bulk graphite powder [33, 34].

Chemical doping is one of the important and basic factors in improving the properties of graphene, which has been proved effective in the doping of carbon nanotubes (CNTs) and has extremely broadened their applications [35-39]. When a nitrogen atom is doped into graphene, three common bonding configurations within the carbon lattice, including quaternary N (or graphitic N), pyridinic N, and pyrrolic N are obtained (Figure 1) [40].

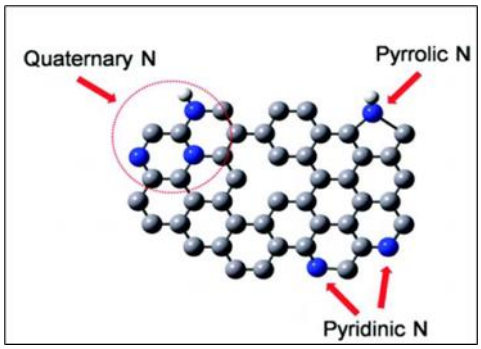

Figure 1: Three common bonding configuration nitrogen-doped graphene

Experimental

Materials

Citric acid and N',2-dihydroxyethanimidamide were purchased from Sigma Aldrich by purity of 99% and NaOH was purchased from Beijing Chemical Works and used directly without further purification.

Synthesis of N-GQDs

The N-GQDs were synthesized by carbonization of citric acid with N',2-dihydroxyethanimidamide through hydrothermal treatment. In brief, CA and DHAA with different molar ratio (1:0.3, 1:1, 1:1.5, 1:3) were transferred

to reaction vessel and heated at 170°C using a heating mantle for 3h under open system. Subsequently, the color of the liquid was changed from colorless to pale yellow, and then orange in 1h, implying the formation of GQDs. Then cooled down to room temperature. After cooling, a suspension of N-GQDs were obtained. If the heating was kept on, the orange liquid would finally turn to black solid in about more than 3h, exits from QDs state.

Characterization

Powder X-ray diffraction (XRD) patterns of the samples were obtained with a Bruker D8 Advance diffractometer using a Cu Kα source (λ= 0.154056 nm). The FT-IR spectra were recorded on a Shimadzu FT-IR-408 spectrophotometer. Fluorescence spectra and intensity measurements were carried out using an FP-6200 spectrofluorometer (JASCO Corporation, Tokyo, Japan). The Thermogravimetric analysis (TGA) of the samples was measured using Mettler Toledo instrument under N_2 with a heating rate of 10 °C min^{-1}.

Result and Discussion

Effectiveness of the N atoms doping of GQDs was evaluated with FT-IR spectra, XRD, TGA and fluorescence.

FT-IR analysis

The Fourier transform infrared (FT-IR) spectra were measured to verify the functional groups. Figure 2 shows the FT-IR spectrums of N-GQDs with various DHAA contents. The spectrum of products was the same, showing a strong OH peak at 3443 cm^{-1}. The peaks related to N-C=O (1633 cm^{-1}) and C=C-H (1361 cm^{-1}) are also clearly observed. Bending peak at 666 cm^{-1} exhibits C-H, N-H. These results confirm the successful introduction of N in N-GQDs and are also consistent with the corresponding FT-IR spectroscopy results.

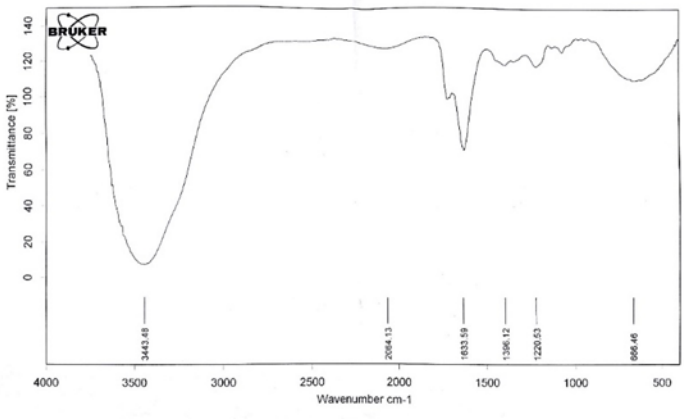

Figure 2: FT-IR spectrum of N-QGDs

XRD analysis

The XRD pattern shown in Figure 3 contains a broad peak centered at 2θ= 21.88° corresponding to an interlayer spacing of the N-GQDs. Such a low diffraction degree suggests a large interlayer spacing, which may be due to the high oxygen content of these N-GQDs, as pointed out by Dong et al [41]. In their study, the interlayer spacing of GQDs increases with the increase in oxygen content.

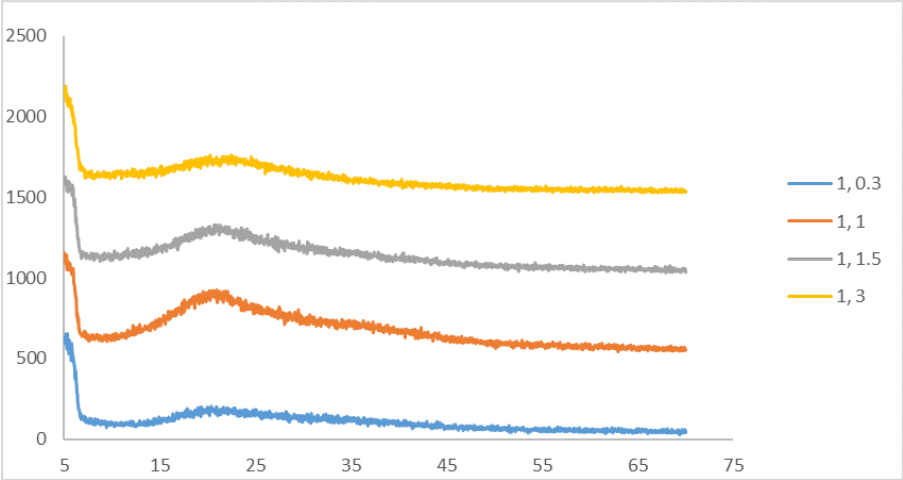

Figure 3: XRD patterns of N-GQDs

TGA

Thermogravimetric analysis (TGA) graphs (Figure. 4) show weight profiles of GQDs variation of temperature (heating rate, 1/min) under N_2 flow. Figure 4a, b (1: 0.3, 1: 1) Weight loss (2.6 wt%) of the GQD up to 100 C could be primarily due to evaporation of water molecules held in the samples [42, 43]. The significant weight loss of 29.59% at 190 °C, presumably due to the loss of those oxygen-containing groups before the complete oxidative decomposition of the GQD over 268-700 °C. Figure 4c (1: 1.5) Weight loss (3.1 wt%) of the GQD up to 100 C could be primarily due to evaporation of water molecules held in the samples.55-56. The significant weight loss of 22.79% at 190 °C, presumably due to the loss of those oxygen-containing groups before the complete oxidative decomposition of the GQD over 258-700 °C. Figure 4d (1: 3) Weight loss (5.4 wt%) of the GQD up to 100 C could be primarily due to evaporation of water molecules held in the samples.55-56. The significant weight loss of 25.15% at 190 °C, presumably due to the loss of those oxygen-containing groups before the complete oxidative decomposition of the GQD over 249-700 °C.

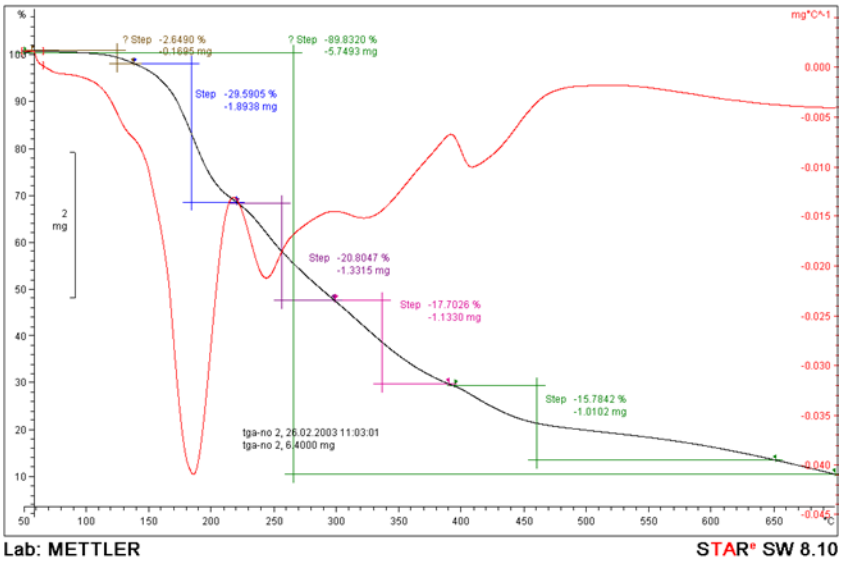
%
mg*C^-1
? Step -2.6490 %
-0.1695 mg
? Step -89.8320 %
-5.7493 mg
Step -29.5905 %
-1.8938 mg
Step -20.8047 %
-1.3315 mg
Step -17.7026 %
-1.1330 mg
Step -15.7842 %
-1.0102 mg
2
mg
tga-no 2, 26.02.2003 11:03:01
tga-no 2, 6.4000 mg
°C
Lab: METTLER
STAR° SW 8.10

(a)

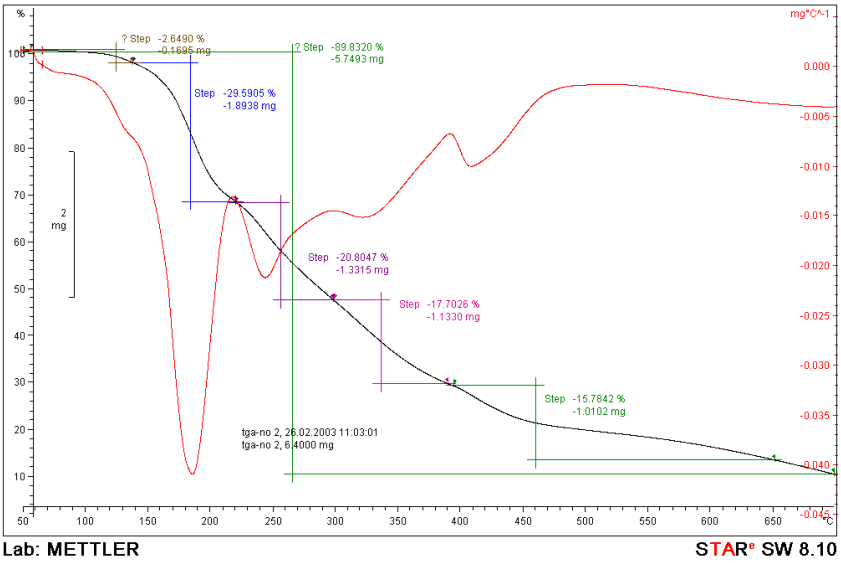
%
mg*C^-1
? Step -2.6490 %
-0.1695 mg
? Step -89.8320 %
-5.7493 mg
Step -29.5905 %
-1.8938 mg
Step -20.8047 %
-1.3315 mg
Step -17.7026 %
-1.1330 mg
Step -15.7842 %
-1.0102 mg
2
mg
tga-no 2, 26.02.2003 11:03:01
tga-no 2, 6.4000 mg
°C
Lab: METTLER
STAR° SW 8.10

(b)

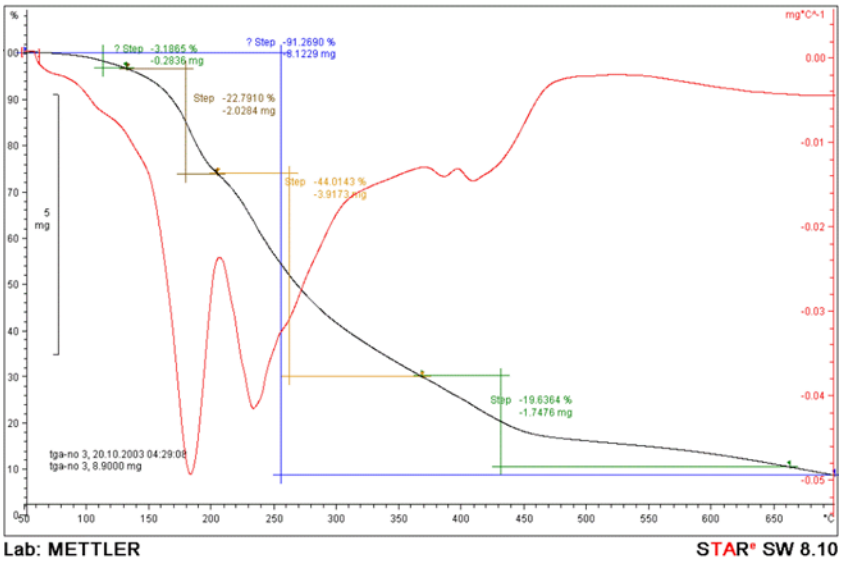

(c)

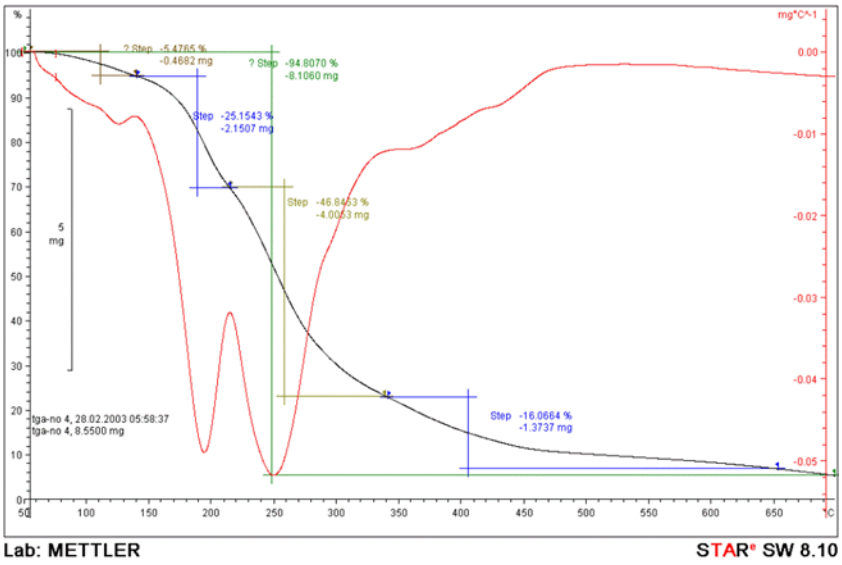

(d)

Figure 4: Thermogravimetric spectrum of GQDs

Photoluminescence analysis

The strong photoluminescence (Fig. 5a) at 383 nm in GQDs is resulted from free zigzag sites with a carbene-like triplet ground state [27]. The initial concentration of DHAA in the hydrothermal treatment can also affect the photoluminescence. By changing the amount of DHAA from ratio of 1: 1 to 1 :3, the intensity of N-GQDs showed drastic decrease, as shown in Fig. 5, indicating the tunable photoluminescence

by the control of N-atom ratio. For a detailed PL study of N-GQDs, we carried out PL measurements by using different excitation wavelengths, as shown in Fig. 5. As the excitation wavelength is changed from 200 to 500 nm, each ratio of N-GQDs showed different peaks in three wavelengths (Fig. 5b-e) in which every four-ratio exhibited peak at 383 nm, that ratio of 1: 1 has the most intensity.

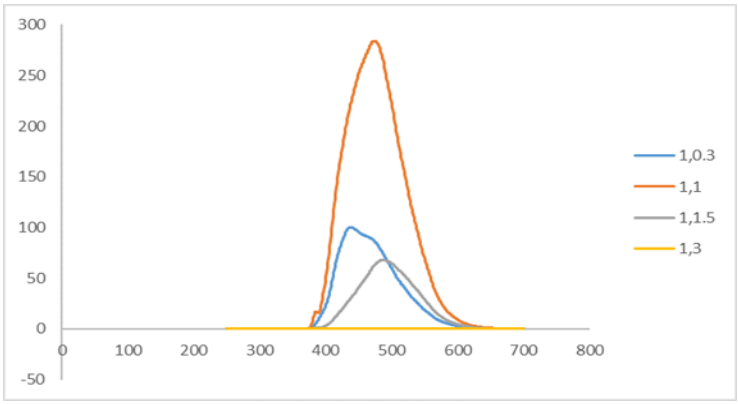

(a)

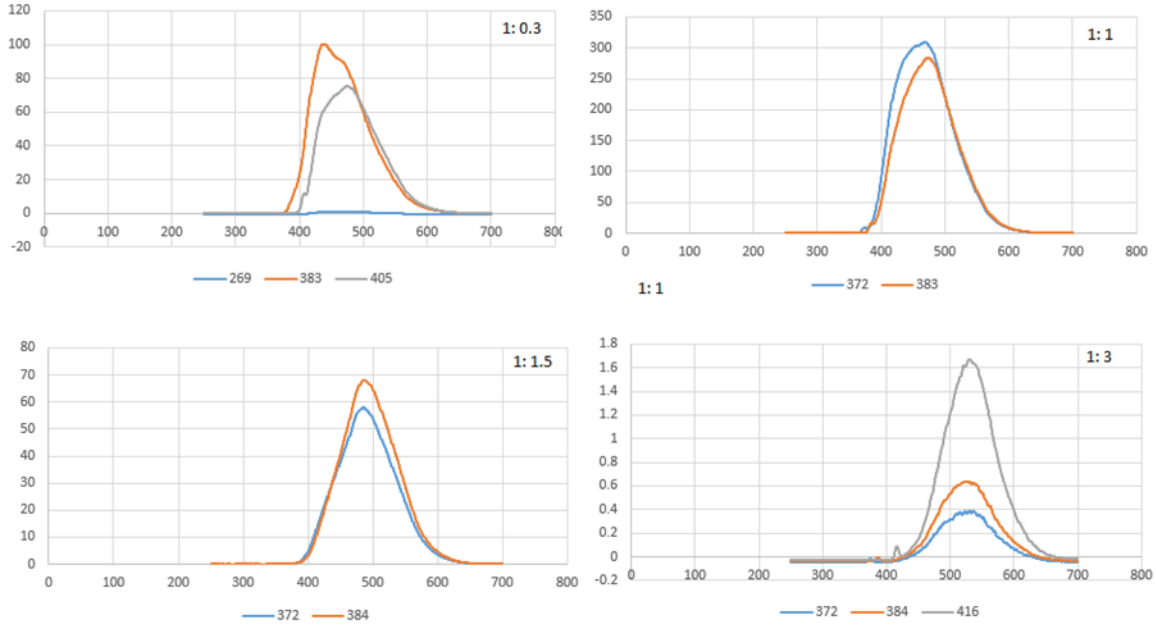

(b)

Figure 5: Fluorescence diagram of N-GQDs

Conclusion

In this study, CA and DHAA with different ratio were reacted together. Considering that DHAA has two active sites, including N and OH, can couple by CA from two positions, this coupling can be occurred as nucleophilic attack of N and water removal by OH groups of two molecules. This process cause's appearance of N-H groups in N-GQDs which effects on fluorescence and morphology of N-GQDs. Furthermore, up to now most of GQDs are synthesized with CA and ammonia [44]. Because ammonia is a volatile compound during working with it, vigorous and closed system is needed. Despite ammonia, DHAA is a stable material which doesn't requires any isolated system.

The fluorescence emission spectra of GQDs were primarily investigated under excitation wavelengths. From the fluorescence spectra (Fig. 5), GQDs have wonderful emission under excitation wavelength from 300 nm to 400 nm that was similar to previous report.(9) This phenomenon is common and contributed to the surface state affecting the band gap of GQDs. The surface state is analogous to a molecular state whereas the size effect is a result of quantum dimensions, both of which contribute to the complexity of the excited states of GQDs [45]. Particularly, the 52% of quantum yield of the GQDs was calculated at 330 nm optimal excitation according to the above comparative equation. This result is higher when compared with previous report [46, 47].

According to above paragraph our products are quantum dot sized. In contrast to other proportion, 1: 1 ratio has the best florescence effect (280 a.u.). Results showed that florescence effect decreased by increase in molar ratio of DHAA which shows a distinct increase N-GQDs size.

Compared with other proportions of N-QGDs, X-ray diffractogram of 1: 1 ratio has the highest intensity (419 a.u.). Increase in molar ratio of DHAA cause's decrease in XRD intensity. Also, by increasing ratio of DHAA, viscosity of N-GQDs decreased, too. So that the 1: 3 proportion has great fluidity. Color of N-GQDs differ from light yellow to dark brown. Darkening procedure is based on increase in DHAA molar ratio (Figure. 6).

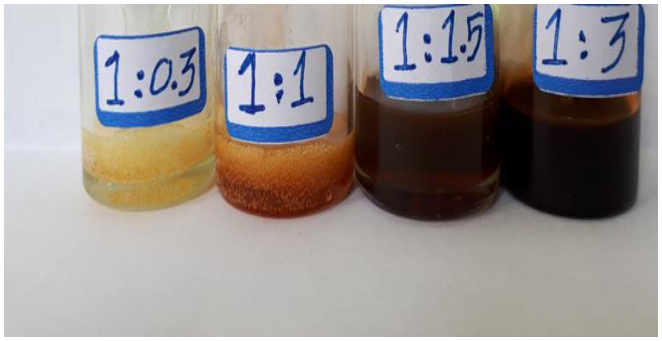

Figure 6: Differing color of N-GQDs

Acknowledgements

This work was supported by the office of the research vice chancellor of Azarbaijan Shahid Madani University.

References

1. Zhang, Z.; Zhang, J.; Chen, N.; Qu, L.; Energy Environ. Sci.. 2012, 5, 8869-90.

2.Shen, J.; Zhu, Y.; Yang, X.; Li, C.; Chem.com. 2012, 48, 3686-99.

3. Liu, WW.; Feng, YQ,; Yan, XB.; Chen, JT.; Xue, QJ.; Adv. Funct. Mater. 2013, 234164.

4. Aillon, KL.; Xie, Y.; El-Gendy, N.; Berkland. CJ.; Forrest, ML.; Adv. Drug Deliv. Rev. 2009, 61, 457-66.

5. Wang, K.; Gao, Z.; Gao, G.; Wo, Y.; Nanoscale Res. Lett. 2013, 8, 122.

6. Zhao, Q-L.; Zhang, Z-L.; Huang, B-H.; Peng, J.; Zhang, M.; Pang, D-W.; Chem.Com. 2008, 41, 5116-8.

7. Zheng, L.; Chi, Y.; Dong, Y.; Lin, J.; Wang, B.; J. Am. Chem. Soc. 2009, 131, 4564-5.

8. Liu, H.; Wang, Q.; Shen, G.; Zhang, C.; Li, C.; Ji, W.; Nanoscale Res. Lett. 2014, 9, 397.

9. Zhu, S.; Meng, Q.; Wang, L.; Zhang, J.; Song, Y.; Jin, H.; Angew. Chem. 2013, 125, 4045-9.

10. Yang, X.; Zhuo, Y.; Zhu, S.; Luo, Y.; Feng, Y.; Dou, Y.; Biosensors and Bioelectronics. 2014, 60, 292-8.

11. Cao, L.; Sahu, S.; Anilkumar, P.; Bunker, CE.; Xu, J.; Fernando, KS.; J. Am. Chem. Soc. 2011, 133, 4754-7.

12. Qu, S.; Wang, X.; Lu, Q.; Liu, X.; Wang, L.; Angew. Chem 2012, 51, 12215-8.

13. Qian, Z.; Ma, J.; Shan, X.; Feng, H.; Shao, L.; Chen, J.; Chem. Eur. J. 2014, 20, 2254-63.

14. Nie, H.; Li, M.; Li, Q.; Liang, S.; Tan, Y.; Sheng, L.; Chem. Mater. 2014, 26, 3104-12.

15. Gude, V.; Beilstein J. Nanotechnol. 2014, 5, 1513.

16. Jiang, C.; Wu, H.; Song, X.; Ma, X.; Wang, J.; Tan, M.; Talanta. 2014, 127, 68-74.
17. Thakur, M.; Pandey ,S.; Mewada, A.; Patil, V.; Khade, M.; Goshi, E.; J. Drug Deliv. 2014.
18. Sun, Y-P.; Zhou, B.; Lin, Y.; Wang, W.; Fernando, KS.; Pathak, P.; J. Am. Chem. Soc.. 2006, 24, 7756-7.
19. Peng, H.; Travas-Sejdic, J.; Chem. Mater. 2009;21, 5563-5.
20. Ma, Z.; Ming, H.; Huang, H.; Liu, Y.; Kang, Z.; New J Chem. 2012, 36, 861-4.
21. Zhang, R.; Chen, W.; Biosensors and Bioelectronics. 2014, 55, 83-90.
22. Guo, Y.; Wang, Z.; Shao, H.; Jiang, X.; Carbon. 2013, 52, 583-9.
23. Fan, R-J.; Sun, Q.; Zhang, L.; Zhang, Y.; Lu, A-H.; Carbon. 2014, 71, 87-93.
24. Zhang, Y-Q.; Ma, D-K.; Zhuang, Y.; Zhang, X.; Chen, W.; Hong, L-L.; J. Mater. Chem. 2012, 22, 16714-8.
25. Liu, Y.; Xiao, N.; Gong, N.; Wang, H.; Shi, X.; Gu, W.; Carbon. 2014,68, 258-64.
26. Shen, J.; Zhu, Y.; Yang, X.; Zong, J.; Zhang, J.; Li, C.; New. J. Chem. 2012, 36, 97-101.
27. Pan, D.; Zhang, J.; Li, Z.; Wu, M.; Adv. mater. 2010, 22, 734-8.
28. Shen, J.; Zhu, Y.; Chen, C.; Yang, X.; Li, C.; Chem. Com. 2011, 47, 2580-2.
29. Yan, X.; Cui, X.; Li, B.; Li, L-s.; Nano let. 2010, 5, 869-73.
30. Liu, R.; Wu, D.; Feng, X.; Müllen, K.; Journal of the American Chemical Society. 2011, 133, 15221-3.
31. Liu, H.; Liu, Y.; Zhu, D.; J. Mater. Chem. 2011, 21, 3335-45.
32. Li, Y.; Zhou, Z.; Shen, P.; Chen, Z.; S Acs Nano. 2009, 3,1952-8.
33. Li, Q.; Zhang, S.; Dai, L.; Li, L-s.; J. Am. Chem. Soc. 2012, 134, 18932-5.
34. Hu, C.; Liu, Y.; Yang, Y.; Cui, J.; Huang, Z.; Wang, Y.; J. Mater. Chem. B. 2013, 1, 39-42.
35. Derycke, V.; Martel, R.; Appenzeller, J.; Avouris, P.; Appl. Phys. Lett. 2002, 80, 2773-5.
36. Gong, K.; Du ,F.; Xia, Z.; Durstock, M.; Dai, L.; Sci. 2009, 323760-4.
37. Wang, S.; Wang, X.; Jiang, SP.; J. A. Sci. 2008, 24, 10505-12.
38. Wang, S.; Yang, F.; Jiang, SP.; Chen, S.; Wang, X.; Electrochem. Com. 2010, 12, 1646-9.
39. Zhou, C.; Kong, J.; Yenilmez, E.; Dai, H.; Sci. 2000, 290, 1552-5.
40. Wang, Y.; Shao, Y.; Matson, DW.; Li, J.; Lin, Y.; ACS nano. 2010, 4, 1790-8.
41. Dong, Y.; Chen, C.; Zheng, X..; Gao, L.; Cui, Z.; Yang, H.; J. Mater. Chem. 2012, 22, 8764-6.

42. Stankovich, S.; Dikin, DA.; Piner, RD.; Kohlhaas, KA.; Kleinhammes, A.; Jia ,Y.; Carbon. 2007, 45, 15, 1558-65.

43. Park, S.; An, J.; Piner, RD.; Jung, I.; Yang, D.; Velamakanni, A.; Chem. mater. 2008, 20, 6592-4.

44. Van Tam, T.; Trung, NB.; Kim, HR.; Chung, JS.; Choi, WM;. Sensors and Actuators B: Chemical. 2014, 202, 568-73.

45. Shang, J.; Ma, L.; Li, J.; Ai, W, Yu. T.; Gurzadyan, GG.; Sci. Rep. 2012, 2, 792.

46. Sun, W.; Du, Y.; Wang, Y.; J. Lumin. 2010, 130, 1463-9.

47. Du, F.; Zeng, F.; Ming, Y.; Wu, S.; Mikrochim. Acta. 2013, 180, 453-60.

Communications In Catalysis
Vol. 2, No. 2, 2024, pp. 56-84
DOI: 10.22049/cic.2024.29549.1038
Azarbaijan Shahid Madani University

A Review on the Methods of Preparing 1,4-dihydropyridine derivatives

Adeleh Moshtaghi Zonouz[1], Saiedeh Abedinpour[2]*

[1,2]Department of Chemistry, Faculty of Basic Sciences, Azarbaijan Shahid Madani University, Tabriz, Iran

**E-mail: saiedeh.abedinpour@gmail.com*

Received: 2024-03-18, Accepted: 2024-05-20

Abstract

1,4-dihydropyridines (1,4-DHPs) are pharmacologically active compounds and are an important class of L-type calcium channel blockers utilized in the treatment of cardiovascular disorders, including hypertension, angina, and other spastic muscle disorders. As a result, 1,4-dihydropyridines (DHPs) serve as privileged pharmacophores and are attractive synthetic targets in organic chemistry. This review aims to describe various methodologies employed in the synthesis of this class of compounds.

Keywords: 1,4-Dihydropyridines, Calcium Channel Blockers, Hantzsch reaction

Introduction

Dihydropyridines (DHPs) are heterocyclic organic compounds based on the pyridine structure. This group of organic compounds can exist in five isomeric forms, and the most common forms are the 1,2-dihydro- and 1,4-dihydropyridine (1,2-DHP, 1,4-DHP) structures (Scheme 1) [1].

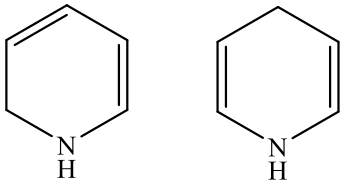

Scheme 1. The structures of the most common isomeric forms of DHPs.

Among compounds with six-membered heterocyclic scaffolds, 1,4-Dihydropyridines (1,4-DHP) are important constituents that are found in biologically active natural products and medicinal compounds [2]. 1,4-DHP derivatives as calcium channel blockers are widely used in treating cardiovascular diseases [3-6]. Apart from their cardiovascular benefits [7], they used anti-convulsant [8,9], anti-inflammatory [10, 11], anti-depressive [12], anti-cancer [13, 14], anti-tubercular [15], antiparasitic and antibacterial [10, 16] and anti-diabetic [17] agents.

Marketed Drugs based on 1,4-Dihydropyridine

Cardiovascular Diseases

An important class of hypertension drugs is the calcium channel blockers (CCBs) or calcium channel antagonists [4, 18]. The currently marketed 1,4-DHP-based drugs as calcium channel antagonists are used for the treatment of hypertension. The early ones include Nifedipine and Nicardipine, known for their rapid action due to limited half-life. The second generation, with improved bioavailability and longer duration of action, has been introduced after over 40 years [19].

The DHP CCBs act as antagonists of the nonindependent, T-type calcium channel [20]. DHP CCBs exhibits pharmacological effects on peripheral, coronary, and cerebral vasodilation; negative inotropic effect; and atrioventricular nodes and inhibition of excitation of sinoatrial [21]. plays a crucial role in their Ca2+ channel-blocking activity. It can be summarized as follows:

C-4 serves as a chiral center in unsymmetrical 1,4-DHPs, with its absolute configuration playing a crucial role in calcium channel modulation. The nature and position of the substituents on the rayl ring at C-4 are vital for optimizing activity. Substitutions at the N-1 position have a deterrent role; they can decrease or abolish activity. The 1,4-DHP is necessary for activity due to its ability to create hydrogen bonding. Substituents in C-3 and C-5 influence activity and tissue selectivity. The DHP receptor can tolerate different changes at the C-2 and C-6 positions [18].

The general structure of these compounds is depicted in Scheme 2.

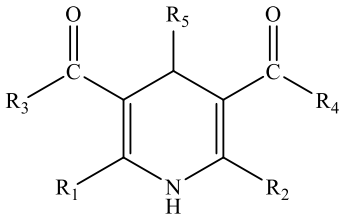

Scheme 2. The general structure of 1,4-DHP marketed calcium channel antagonist drugs.

Infectious Diseases

Tuberculosis is caused by a human pathogen, Mycobacterium tuberculosis, affecting a significant portion of the world's population [22-24]. 1,4-DHP with lipophilic groups exhibit anti-tubercular activity against M. tuberculosis. For example, 4-(4-pyrazol)-1,4-dihydropyridine derivatives [25] and 4-(2-imidazolyl)-1,4-dihydropyridine analogs [26] are anti-tubercular agents. In 2001 and 2002, 4-rayl-2,6-dimethyl-3,5-bis-N(rayl)carbamoyl-1,4-Dihydropyridines were synthesized as anti-tubercular agents (Scheme 3) [27, 28].

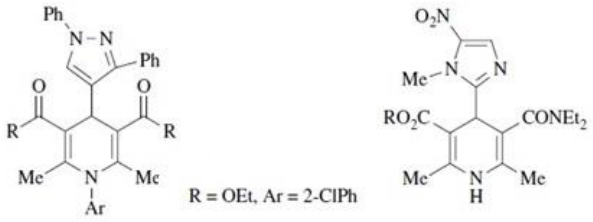

Scheme 3. The structure of 4-(4-pyrazolo)-1,4-dihydropyridine derivatives and 4-(2-imidazolyl)- 1,4-dihydropyridine analogs.

In cancer cells, classical 1,4-DHPs act as inhibitors of the transmembrane efflux pump ABCB1. In 2019, F. Lent, et al. investigated non-classical 1,4-DHP derivatives used to enhance the antituberculotic drug efficacy of the second-line antituberculotic drug clofazimine. Clofazimine is a known substrate of ABCB1, potentially inhibiting a corresponding efflux pump in Mycobacterium tuberculosis (Mt). Discovering new enhancers of clofazimine toxicity may help prevent the development of clofazimine resistance through efflux pump activity (Scheme 4) [29].

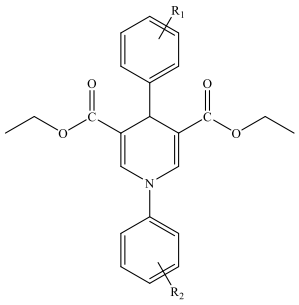

Scheme 4. The structure of nonclassical 1,4-DHPs without a substitution in both the 2 and the 6-position.

In 2012, Y.L.N. Murthy, et al. synthesized thirteen derivatives of 4-aryl-1,4-DHP compounds, and their effectiveness as antibacterials against 27 ESBL isolates of Klebsiella pneumoniae and Escherichia coli were evaluated [30]. The growth inhibition of 1,4-diaryl-1,4-DHP against M. tuberculosis was evaluated in Germany in 2016 (Scheme 5) [31].

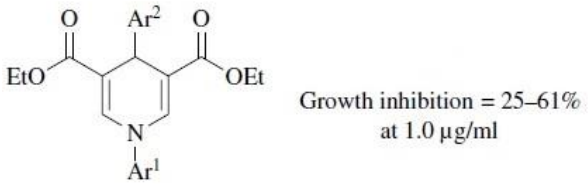

Scheme 5. The structure of 1,4-diaryl-1,4-DHPs.

Inflammatory diseases

Capsaicin is an agonist that transduces painful chemical or thermal stimuli to peripheral nerve endings in skin or deep tissues by activating ion flux

through the TRPV1 channel, a heat and ganglionated cation channel [32, 33]. Researchers from the National Institutes of Diabetes and Digestive and Kidney Diseases have identified 1,4-DHP derivatives as novel "enhancers" of TRPV1 activity. These enhancers have been shown to increase the effect of capsaicin on Ca^{2+} uptake two to threefold compared to when capsaicin is used alone in Scheme 6.

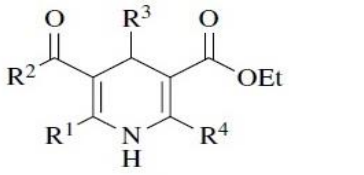

Scheme 6. The structure of novel “enhancers” of TRPV1-based 1,4-DHP derivatives.

2,6-Unsubstituted-1,4-diaryl-1,4-DHPs are selective inhibitors of phosphodiesterase type (PDE4) and could be beneficial in treating inflammatory diseases like asthma and chronic obstructive pulmonary disease (COPD). (Scheme 7) [34, 35].

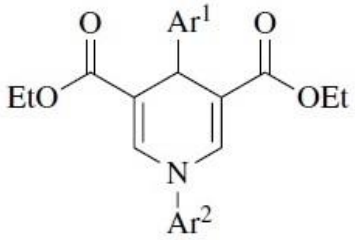

Scheme 7. The structure of 2,6-Unsubstituted-1,4-diaryl-1,4-DHPs.

Mutations in the cystic fibrosis transmembrane conductance regulator (CFTR) gene lead to Cystic fibrosis (CF), an autosomal recessive disease [36]. The deletion of phenylalanine in the CFTR chloride channel is the most common cause of CF. Antihypertensive 1,4-DHPs like Felodipine and Nifedipine inhibit T-type Ca2+ channels and also enhance CFTR gating [37]. Italian researchers have reported that 4-thiophenyl-2′-yl and 4-imidazole-[2,1-b]thiazole-1,4-DHPs act as potentiators of the CFTR chloride channel (Scheme 8) [38, 39].

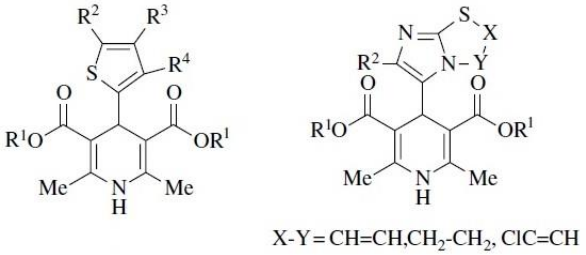

Scheme 8. The structure of 4-thiophenyl-2′-yl- and 4-imidazol[2,1-b]thiazole-1,4-DHPs and as potentiates of the CFTR chloride channel.

Nervous diseases

Alzheimer's disease (AD) is a type of progressive neurodegenerative disorder that can lead to memory loss and dementia in elderly people [40-42]. It is caused by the buildup of abnormal extracellular amyloid-beta peptide (Aβ) deposits, proprotein aggregation, disruptions in biometals like Cu, Fe, and Zn, oxidative stress (OS), intracellular neurofibrillary tangles, widespread neuronal death, and reduced levels of the neurotransmitter acetylcholine (ACh) [43-45]. One approach to treating AD involves boosting ACh levels in the brain, which can be achieved through the use of acetylcholinesterase inhibitors (AChEIs) [46].

The only administered drugs for AD therapy include Donepezil, Rivastigmine, Galantamine, and the N-methyl-D-aspartate receptor antagonist Memantine, all of which act as acetylcholinesterase inhibitors. However, their effectiveness is limited [47].

Tacrine-1,4-DHPs in Spain and (benzylidene-hydrazono)-1,4-DHPs in Germany as AChEis were synthesized (Scheme 9) [48, 49].

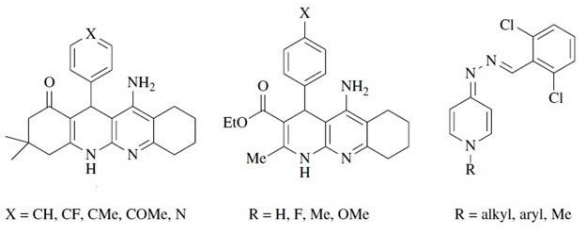

Scheme 9. The structure of Tacrine-1,4-DHPs and (benzylidene-hydrazono)-1,4-DHPs as AChEis.

4,6-Diaryl-1,4-DHPs were synthesized by Spanish researchers. These compounds were found to prevent calcium overload and act as neuroprotective agents (Scheme 10) [50].

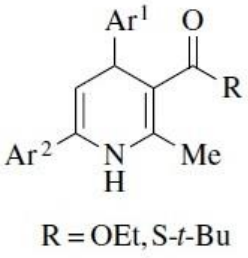

Scheme 10. The structure of 4,6-diaryl-1,4-DHPs.

The multitarget small molecule (MTSM) approach is a novel therapeutic strategy. In this method, drugs are designed to bind simultaneously to various enzymatic systems or receptors involved in AD pathology. R. Malek, et al. synthesized Ca^{+2} channel blockade capacity and investigated the antioxidant power of N3, N5-bis(2-(5-methoxy-1H-indol-3-yl)ethyl)-2,6-dimethyl-4-aryl-1,4-DHP-3,5-dicarboxamides as several new MTSM by using multicomponent reactions (Scheme 11) [51].

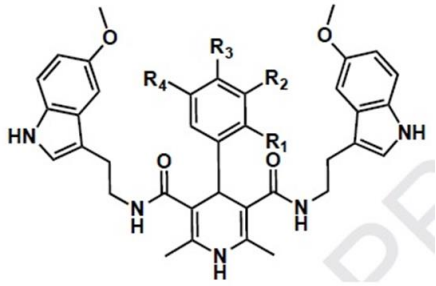

Scheme 11. The structure of N3, N5-bis(2-(5-methoxy-1H-indol-3-yl)ethyl)-2,6-dimethyl-4-aryl-1,4-DHP-3,5-dicarboxamides.

Cancer

Multidrug resistance (MDR) in cancer cells refers to their resistance to multiple classes of chemotherapy drugs, posing a significant challenge in cancer treatment [52]. This resistance is primarily driven by the efflux of drugs through transmembrane activity, leading to insufficient intracellular drug levels for effective therapy. It is commonly associated with the overexpression of various proteins, such as ATP-dependent extrusion pumps like P-glycoprotein (Pgp) and multidrug resistance protein (MRP1), which belongs to the ABC superfamily of transporters [52- 54]. Inhibition of Pgp is an effective method for combating MDR [55,

56]. The cytotoxicity of several compounds of the 1,4-DHP towards cancer cells is more than towards non-cancer cells and they kill cells by inhibiting the P-glycoprotein pump and reversing multidrug resistance [57]. Some 1,4-DHPs which used as inhibitors of Pgp and MRP1 include 3,5-dibenzoyl-1,4-DHPs [58], NArylmethyl-1,4-DHPs [59], 3,5-bis(amido)-1,4-DHPs [60] cage dimeric 1,4-DHPs [61], N-acyloxy-1,4-DHPs [62], 3-pyridin-2-yl methyl 5alkyle 2,6-dimethyl-4-(aryl)-1,4-dihydropyridine-3,5-dicarboxylate [63], VdiE-2N ((isobutyryloxy)methyl 6-chloro-5-formyl-1,4-dihydro-2-methyl-4-(2-nitrophenyl)pyridine-3-carboxylate))(Scheme 12) [64].

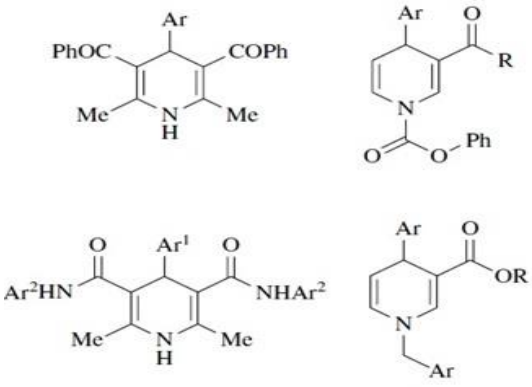

Scheme 12. The structure of some1,4-DHPs which used as inhibitors of Pgp and MRP1.

Synthesis of 1,4-DHPs

For the first time, the synthesis of 1,4- DHP via the condensation of aldehyde, ethyl acetoacetate with ammonia refluxing to 6-72 h in a lower alcohol or acetic acid was reported by Arthur Hantzsch in 1882 (Figure 1) [65]. The reaction time in this procedure is long, and the yields of 1,4-DHP obtained by this method are generally low, especially with aliphatic and unsaturated aldehydes. However, the most common method for the synthesis of a wide variety of 1,4-DHP is the Schantz synthesis. To date, numerous literature citations have reported novel synthetic strategies for improving the classical methods by using alternative catalysts and greener methods [66-72].

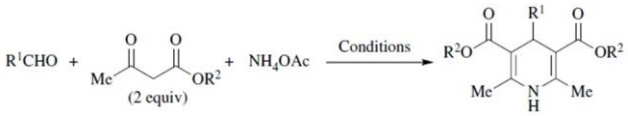

Figure 1. The Hantzsch reaction.

In recent years, various studies have documented different approaches to enhance the Hatzsch reaction, including the use of catalysts [73], fermenting baker's yeast [74], molecular iodine [75], ionic liquids [76], orientalist [77]. However, many of these methods rely on toxic and costly reagents, long reaction times, low yields, strong acidic environments, harsh conditions, and tedious workup, resulting in the production of significant amounts of hazardous waste. Consequently, researchers have endeavored to modify and optimize the Hantzsch reaction to maximize conversion rates, improve efficiency, reduce reaction times, and ensure the high purity of 1,4-DPs. As a result, there is a growing inclination towards adopting environmentally friendly reactions [73].

Up to now, several more environmentally friendly methods have been documented, including solvent-free [78], catalyst-free [79], ultrasound irradiation [80], and aqueous media [81].

Here, we provide a review of various methods for synthesizing 1,4-DHPs. These reactions are categorized into different sections based on the methods used.

Due to issues with the Hantzsch reaction, various effective methods have been devised for the production of 1,4-DHPs.

Using Catalyst

The one-pot multicomponent reactions (MCRs), in which three or more reactants combine in a single process to yield a sole product, are significant in synthetic organic chemistry due to their unique characteristics such as simple procedures, atomic economy, environmental friendliness, straightforward reaction design, high selectivity, and enhancing the yield of a reaction where consecutive chemical reactions are performed on a reactant in a single vessel. Compared to traditional methods for synthesizing complex molecules, MCRs involve two or more synthetic steps. They are conducted without isolating any intermediates, thereby saving time, energy, and raw materials [82-86]. Hantzsch is a notable one-pot MCR that enables the synthesis of a wide range of heterocyclic compounds 1,4-DHPs [65].

One efficient method developed for synthesizing 1,4-DHPs involves the use of catalysts. Catalysts are components that can improve reaction rates and product yield. They hold significant technological importance because of their excellent selectivity and stability [87]. Catalysts are divided into two categories: homogeneous [88-90] and heterogeneous catalysts [91-93].

Molecular iodine is a non-toxic, inexpensive, and readily available catalyst for a variety of organic reactions. It has been utilized as a mild Lewis acid at room temperature, resulting in high yields in the production of symmetrical, unsymmetrical, and N-substituted 1,4-DHPs [75]. See Figure 2, as well as Spiro-dihydropyridine derivatives (Figure 3,4).

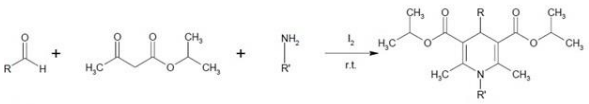

Figure 2. Synthesis of N-substituted 1,4-DHPs.

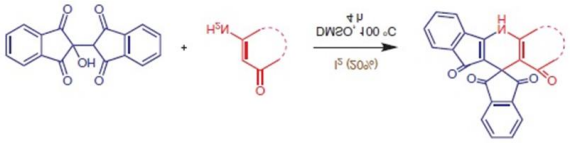

Figure 3. Synthesis spiro-dihydropyridines.

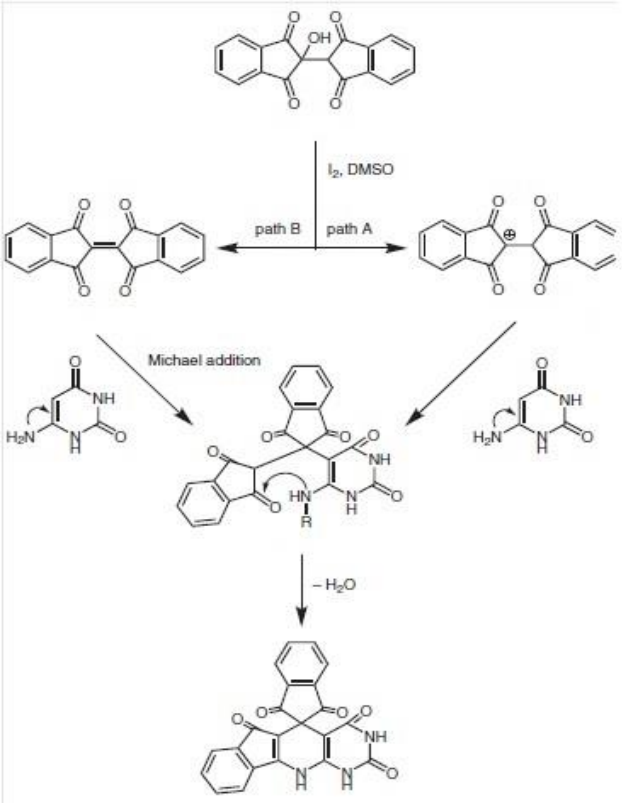

Figure 4. Proposed mechanism of formation of spiro-dihydropyrans.

Graphene oxide nanoparticles were reported as a metal-free heterogeneous catalyst for the synthesis of spirooxindole dihydropyridine derivatives (Figure 5) [95].

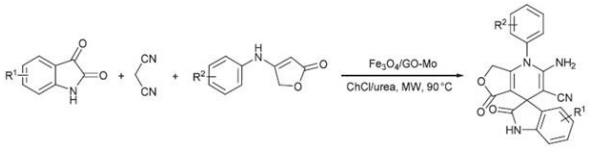

Figure 5. Synthesis of spirooxindole dihydropyridine derivatives.

Today, in organic synthesis, nano-catalysts are highly intriguing due to their large surface area, easy accessibility, cost-effectiveness, ease of product separation, catalyst recovery, high catalytic activity, potential for repeated recycling, and excellent stability. TiCl2/nano-γ-Al2O3, as a novel Lewis acid catalyst, is one such catalyst used in the one-pot synthesis of 1,4-DHPs (Figure 6) [96].

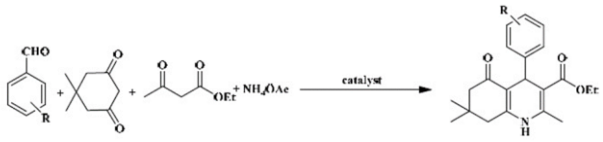

Figure 6. Synthesis of 1,4-DHPs in the presence of $TiCl_2$/Nano-γ-Al_2O_3 as a novel Lewis acid catalyst.

Metal-organic frameworks (MOFs) are hybrid materials combining organic and inorganic components, known for their significant surface area, high porosity, and adjustable chemical properties utilized in heterogeneous catalysis.

Due to the coordinatively unsaturated metal sites and functional groups on the organic linkers, MOFs are well known for their Lewis and Brønsted acidity/basicity [97-100]. The potential of MOFs has been explored as a Lewis acid catalyst in the synthesis of bioactive heterocycles. Functionalized sulfonic acid-containing MOFs are used in heterocycle synthesis, such as pre-sulfonic acid-functionalized MIL-101-SO3H MOF, which serves as a solid Brønsted acid catalyst for the synthesis of 1,4-DHPs (Figure 7) [101].

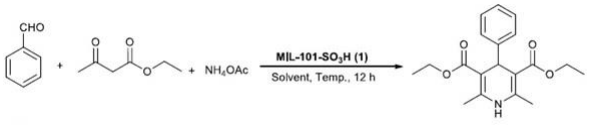

Figure 7. One-Pot Synthesis of 1,4-DHPs in the presence of MIL- 101-SO_3H MOF.

HKUST-1 is another example of MOF which is used as an efficient and reusable heterogeneous catalyst for the synthesis of 1,4-DHPs at room temperature (Figure 8) [102].

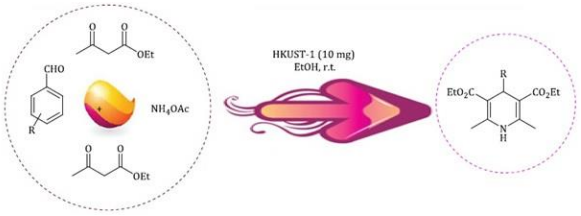

Figure 8. Synthesis of the 1,4-DHPs in the presence of HKUST-1

To enhance the efficiency of Hantzsch DHPs synthesis, various catalysts have been utilized, including Fe3O4 nanoparticles [103], multiwalled carbon nanotubes [104], montmorillonite K10 [105-107], mesoporous vanadium ion doped titania nanoparticles [108, 109], nanomagnetic-supported sulfonic acid [110, 111], silica boron sulfonic acid [112], benzyl trimethylammonium fluoride hydrate (BTMAFH) [113], Fe3O4@silica

sulfonic acid nanocomposite [114], tin dioxide nanoparticles [115, 116], and others.

Green methods

Our environment must be safeguarded from the increasing production of large amounts of waste and toxic by-products, which in turn leads to chemical pollution. Synthetic chemists are therefore working on developing safer technologies that are crucial in the field of green chemistry. Key green principles to be considered in new chemical processes include: the use of eco-friendly mediums, non-toxicity, non-flammability, and the ability to separate and recycle catalysts. As a result, significant efforts have been put into designing and synthesizing environmentally friendly methods that involve reagents, catalysts, and solvents that can easily biodegrade [117, 118].

Hantzsch reaction in water and solvent-free conditions

The advancement of eco-friendly chemical protocols and technologies is a key objective of green chemistry. In green chemistry, significant emphasis is placed on selecting an environmentally friendly solvent [119, 120]. A new trend in organic synthesis has sparked increasing interest in replacing organic reactions in solvent-free conditions or aqueous media [121, 122]. Water, being an affordable, non-toxic, and non-flammable medium, has garnered significant attention as a solvent for organic transformations.

Moshtaghi Zonouz, et al., described the synthesis of 1,4-DHP derivatives through a three-component reaction involving aldehydes, ethyl acetoacetate, and ammonia in refluxing water (Figure 9).

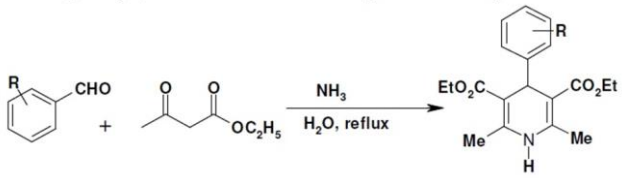

Figure 9. Synthesis of the 1,4-dihydropyridine under aqueous media.

In 2012, they also conducted the MCR between malononitrile, dimedone, aniline, and 3-nitro benzaldehyde in refluxing ethanol but obtained the 4H-chromene derivative instead of quinoline derivative (Figure 10, 11).

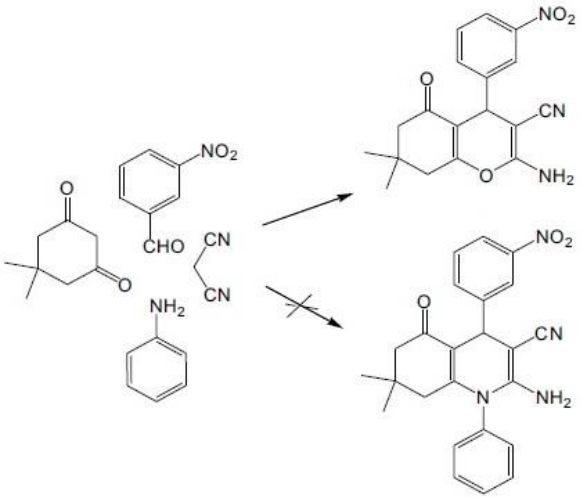

Figure 10. The multicomponent reaction of dimedone, aniline, malononitrile and 3-nitrobenzaldehyde.

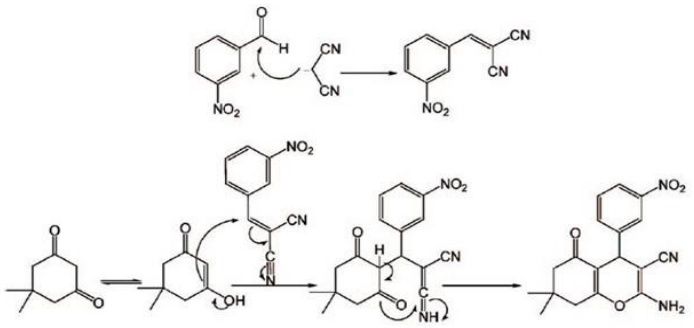

Figure 11. Proposed mechanism for the synthesis of chromene derivative.

So, they employed a one-pot, two-stage approach. By altering the sequence of adding the materials, they managed to synthesize the intended products. Initially, dimedone and aniline were refluxed in ethanol to obtain phenylaminocyclohex-2-enone. Then, arylaldehyde and malononitrile were introduced into the same vessel. The mixture was refluxed until the reaction was complete (2-72 h) (Figure 12). The proposed mechanism is depicted in figure 13 [123].

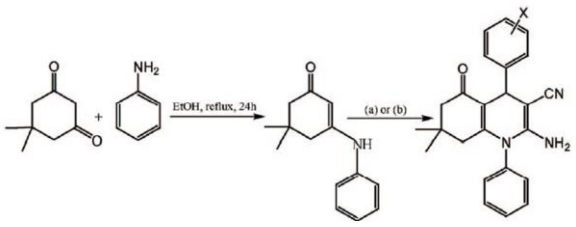

Figure 12. Synthesis of N-arylquinoline derivatives.

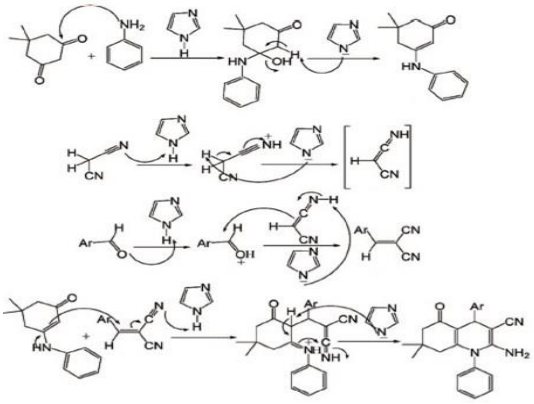

Figure 13. Proposed mechanism for the synthesis of N-arylquinoline derivatives.

Other examples include the synthesis of 4-alkyl/aryl-1,4-DHP through the Hantzsch three-component reaction of an aromatic/aliphatic aldehyde, alkyl acetoacetate, and ammonium carbonate in water (Figure 14) [124, 125].

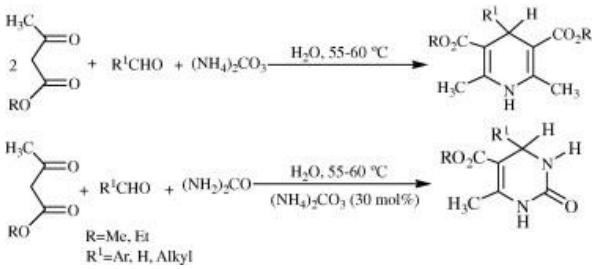

Figure 14. Synthesis of 1,4-dihydropyridines using ammonium carbonate in water.

Yang et al. utilized a sealed system for the Hantzsch reaction, as shown in Figure 15.

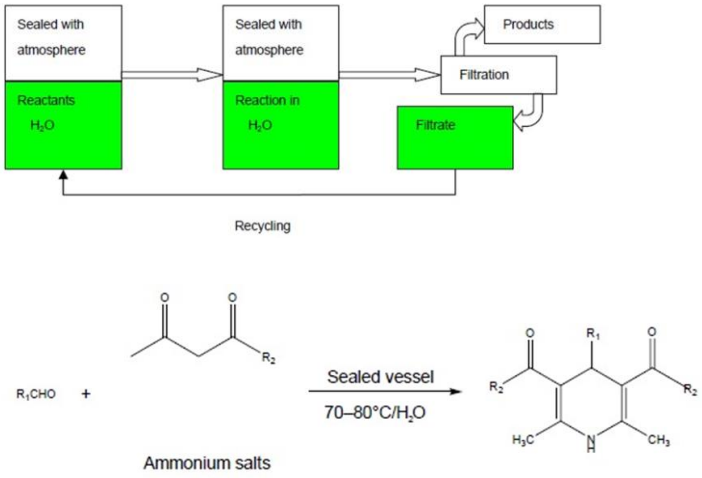

Figure 15. Synthesis of 1,4-DHPs via Hantzsch reaction in water [83].

An important aspect of organic reactions conducted in water is the low solubility of the reactants in aqueous solutions. Consequently, many organic transformations in aqueous environments have limited applicability. To address this issue, micelle-promoted reactions involving surfactants that can be carried out in water have been developed. Heterocyclic compounds such as furans, indoles, pyridines, pyrazolines, dihydropyridines, etc., have been successfully synthesized in aqueous media (Figure 16) [88, 126].

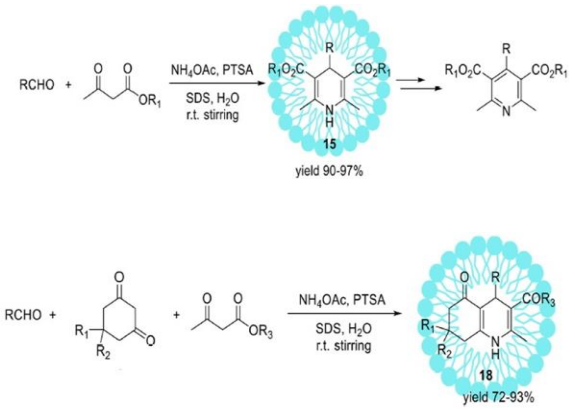

Figure 16. Micelles promoted the synthesis of dihydropyridines and polyhydroquinoline derivatives via the Hantzsch reaction.

Some enhanced techniques for the production of 1,4-DHPs through the Hantzsch reaction involve solvent-free conditions. M. G. Sharma et al. documented the creation of thiophene-based 1,4-DHP derivatives at room temperature and without solvents by employing ceric ammonium nitrate (CAN) as the catalyst, resulting 1,4-DHPs in high yields in short reaction times (Figure 17).

Figure 17. Solvent-free condition for the Hantzsch.

β-Cyclodextrin (β-CD) is an oligomer of D-glucose that can bind with organic molecules through interactions between the charged part of the guest molecule and β-cyclodextrin via van der Waals interaction, hydrophobic interactions, hydrogen bonding, and electrostatic interactions. β-CD is non-toxic to the environment, readily available, and cost-effective compared to other cyclodextrins. It is commonly used as a catalyst under solvent-free conditions in the Hantzsch reaction for the synthesis of 1,4-DHPs (Figure 18, 19) [73].

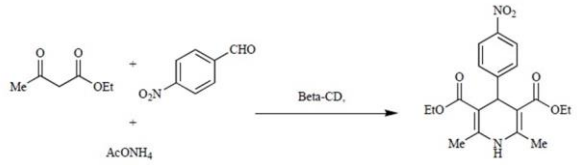

Figure 18. Solvent-free synthesis of the Hantzsch 1,4-DHPs.

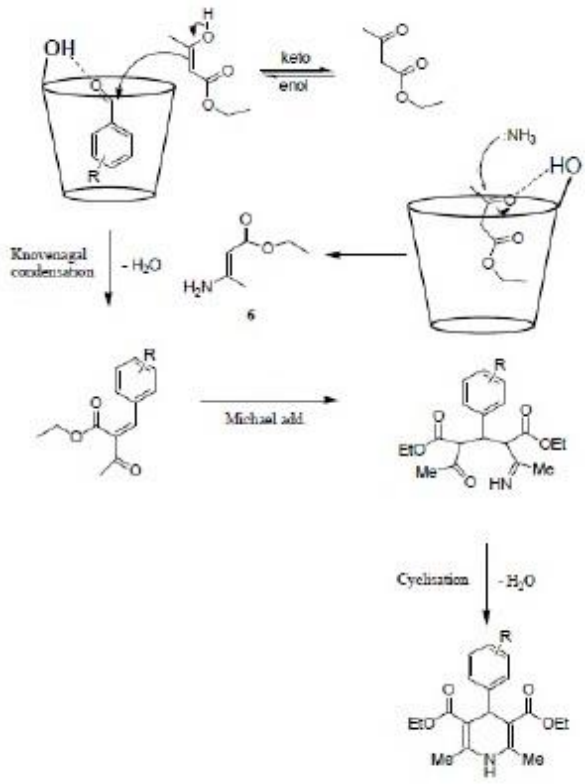

Figure 19. Proposed mechanism for synthesis of 1,4-DHPs.

Pramanik et al. described an ammonium acetate-mediated catalyst-free "on-water"

method for synthesizing the Hantzsch dihydropyridines (Figure 20).

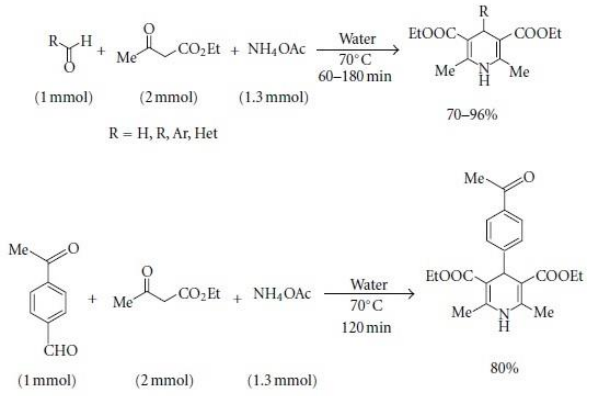

Figure 20. Ammonium acetate-mediated "on-water" synthesis of the Hantzsch 1,4-DHPs.

For the preservation of natural resources for future generations, it is essential to protect our environment. Chemists and chemical engineers are working on developing safe, sustainable, and eco-friendly processes. Among the green aspects of sustainable chemical transformations, such as atom economy, catalysis, and energy efficiency, the reaction media plays a central role. The solvent used in the manufacturing process of the active pharmaceutical ingredient (API) accounts for the maximum amount of total material mass in the process. As a result, major pharmaceutical companies like Pfizer, GSK, and Sanofi have recently created solvent selection guides for chemical processes in drug synthesis [129-133].

The solvent in the reaction plays a crucial role in modifying reactants, facilitating mass and heat transfer phenomena, stabilizing transition states, and influencing catalyst and product reactivity. Solvents are also utilized in various other applications during reactions, such as washing, purification, recrystallization, chromatography, and extraction. Due to their extensive use in multiple steps of the process, solvents have a significant impact on the environmental aspects of the reaction. Typically, solvents are volatile organic compounds (VOCs) with low molecular weight, commonly derived from petrochemicals and alcohols, which possess drawbacks like high flammability, volatility, toxicity, and often non-biodegradability.

Replacing toxic and volatile organic solvents with environmentally friendly alternatives is a key objective of green chemistry. This shift involves utilizing green solvents that are safe, non-toxic, recyclable, and biodegradable. Various alternative solvents, including ionic liquids (ILs), supercritical fluids (such as carbon dioxide and water), perfluorinated compounds, deep eutectic solvents (DESs), glycerol, and other solvents derived from biomass, are being explored.

Ionic liquids (ILs)

In the late 20th century, Ionic liquids (ILs) have established a strong presence in technology and research. Compared to conventional molecular organic solvents (MOSs), the main advantage of ILs is the ability to tailor their structures to specific application requirements [134, 135]. ILs possess unique characteristics like low vapor pressure (eliminating volatility), recyclability, exceptional thermal stability, and effective solvating properties (the capacity to dissolve a wide range of substances) [136].

ILs consist entirely of mobile ions, such as an organic cation (mainly imidazolium, pyrrolidinium, pyridinium, ammonium, or phosphonium) and typically a halide anion (usually Cl^- or Br^-) or a weakly basic non-

coordinating anion like [PF6]−, [BF4]−, or [NTf2]− [136]. These low-temperature molten salts offer a wide range of possible combinations of anions and cations, allowing for adjustable physical and chemical properties. The environmentally friendly nature of this category of compounds makes them suitable as alternative solvents and catalysts in organic synthesis [137-140].

MCRs are conducted in ionic liquid solutions. Ionic environments create internal pressure and facilitate the interaction of reactants in solvent pockets, making them ideal environments for various bond-forming reactions. Due to their high solvating capacity and broad liquid range, they are suitable solvents for multicomponent processes [141]. X. Liu, et al. described a sustainable Hantzsch reaction for producing 1,4-DHPs. They used alcohols instead of aldehydes in the Hantzsch reaction and utilized the brønsted acidic ionic liquid 3-(N,N-dimethyldodecylammonium) propane sulfonic acid hydrogen sulphate ([DDPA][HSO_4]) as a catalyst. This catalyst facilitated the stepwise oxidation of aromatic alcohols with $NaNO_3$, followed by their condensation with a dicarbonyl compound and ammonium acetate. The formation of 1,4-DHP occurred when ethyl acetoacetate and ammonium acetate were introduced into the reaction after the alcohol had been completely oxidized to the aldehyde (Figure 21).

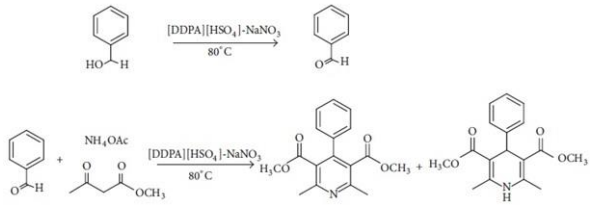

Figure 21. Hantzsch reaction directly from benzyl alcohol in [DDPA][HSO_4].

Different ionic liquids were tested for the same model reaction. In [Hmim]NO3 and [bmin]BF4, the absence of acidic hydrogen in the two ionic liquids led to an unsuccessful reaction. However, when [Hmim][H2PO4] and [DDPA][HSO4] were used, the reaction was successfully completed. The lower yields of the product in [Hmim][H2PO4] can be attributed to the reduced Brønsted acidity associated with [H2PO4]. [DDPA][HSO4] serves a dual purpose as an acid catalyst and a solvent for both the oxidation of alcohol and the subsequent condensation [142].

The sulfamic acid-supported functionalized mesoporous SBA 15/NHSO3H is a heterogeneous catalyst and an ionic liquid type, which can be easily separated from reaction products and recycled. It demonstrates superiority over homogeneous catalysts and was utilized in the synthesis of polyhydroquinolines and dihydropyridines under solvent-free conditions as investigated (Figure 22) [143].

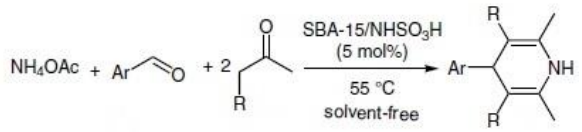

Figure 22. Solvent-Free Synthesis of DHPs Using SBA-15/$NHSO_3H$ Catalyst.

Crown ether complex cation ionic liquids (CECILs) chelated with sodium benzenesulfonates (alkali metal cations) are utilized as a green and environmentally friendly catalyst for the synthesis of 1,4-DHP derivatives. This is achieved through the three-component reaction of aromatic aldehydes and malononitrile with cyclic β-dicarbonyls, or cyclic β-enaminoketone, in H2O/EtOH (1:1) under reflux conditions (Figure 23) [144].

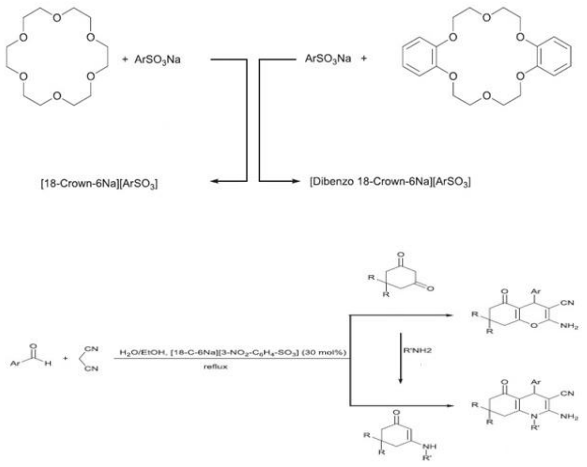

Figure 23. a) Synthesis of CECILs. b) Synthesis of tetrahydro-4H-chromene and 1,4-DHP derivatives.

1-Methyl-3-(2-(sulfooxy)ethyl)-1H-imidazol-3-ium chloride ([MSEI]Cl) is a novel heterogeneous and environmentally friendly acidic ionic liquid catalyst utilized in one-pot multi-component reactions, such as the synthesis of 1,4-DHPs through the one-pot multi-component condensation of 1,3-dicarbonyl compounds (2 equiv.), NH4OAc (1.5 equiv.), and aldehydes (1 equiv.) under solvent-free conditions at a moderate temperature of 90 °C. This catalyst is reusable and unlike other acids, it does not require special precautions for storage and handling. It can be stored on the benchtop for weeks without losing its catalytic activity (Figure 24) [145].

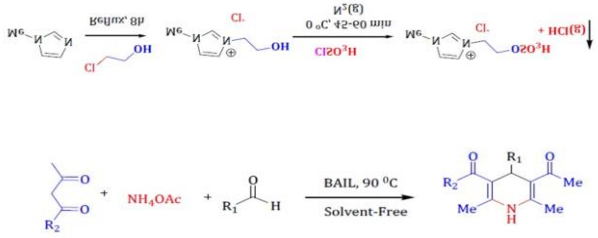

Figure 24. a) Preparation of 1-methyl-3-(2-(sulfooxy)ethyl)-1H-imidazol-3-iumchloride. b) Synthesis of 1,4-DHPs using [MSEI]Cl.

The Dabco-base ILs as highly efficient catalysts used for the synthesis of spiro 1,4-DHP derivatives in moderate to good yields. (Figure 25) [146].

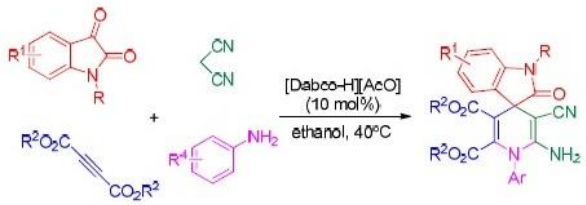

Figure 25. One-pot synthesis of derivatives spiro 1,4-DHPs.

Deep Eutectic Solvents (DESs)

Some significant drawbacks of ILs, such as environmental toxicity [147] and high cost [148], as well as their occasional requirement for high purity that could alter the physical properties of ILs [149], have hindered their widespread industrial use. To address these issues, alternative solvents made from inexpensive, non-toxic, and biodegradable components have been developed. One such alternative to ILs is deep eutectic solvents (DESs), which were first synthesized by

Abbott, et al., based on choline chloride (ChCl) [150]. Other types of DES include low-melting mixtures (LMMs) of sugar, urea, and inorganic salts described by K¨onig and colleagues [151, 152], low-transition temperature mixtures (LTTMs) recommended by Kroon and colleagues [153], natural deep eutectic solvents (NADESs) proposed by Choi and colleagues [154], and deep eutectic ionic liquids (DEILs) described by Hillman's group as low-cost eutectic mixtures with physical properties and phase behavior similar to ILs [155]. These solvents are created from combinations of two or three safe and affordable components (a hydrogen acceptor and a hydrogen-bond donor) that can self-associate through hydrogen bond interactions. Consequently, the charge delocalization is responsible for reducing the melting point of the mixture compared to the melting points of the raw materials [117, 156].

These liquids have melting points below 100 °C, lower than those of their individual components. Due to the special properties of deep eutectic solvents (DES) such as low toxicity, a wide liquid range, low vapor pressure, water compatibility, biodegradability, non-flammability, and cost-effectiveness (cheaper production due to lower raw material costs), they have been utilized in various research fields including biodiesel synthesis, polymerizations, carbon dioxide adsorption, nanotechnology, and organic synthesis [117, 157-160].

DESs are also employed in the Hantzsch reaction. In 2013, Pednekar et al. documented the utilization of ChCl/urea as a deep eutectic solvent in the production of polyhydroacridines (PHA) with outstanding yields (Figure 26) [161].

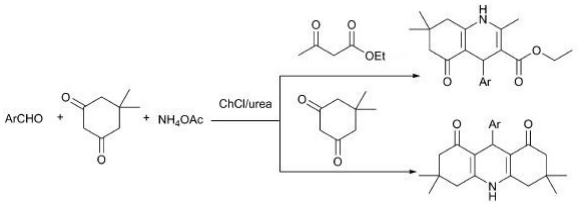

Figure 26. Synthesis of 1,4-DHP derivatives in ChCl/urea.

Wang, et al. have developed an efficient and green procedure for the one-pot synthesis of PHA and PHQ derivatives using ChCl/urea as a reaction medium. This deep eutectic solvent could be recycled and reused for several runs. It was environmentally benign and easily available (Figure 27) [162].

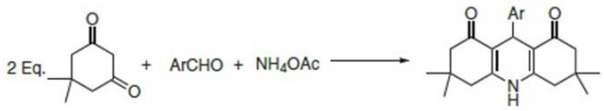

Figure 27. Synthesis of PHA derivatives in ChCl/urea.

Synthesis of 1,4-DHP esters using different low-melting mixtures (LMMs) under catalyst-free conditions was reported in 2016 by J. A. Kumara and colleagues. Various LMMs were prepared by utilizing different hydrogen bond donors (HBD). The use of sugar, urea, and CeCl3 was explored, with the sugar/HBD/CeCl3 ratio fixed at 5:4:1 as a novel solvent medium. They tested 14 aldehydes with five LMMs IA–VA. They achieved moderate to good yields for all desired products (Figure 28) [163].

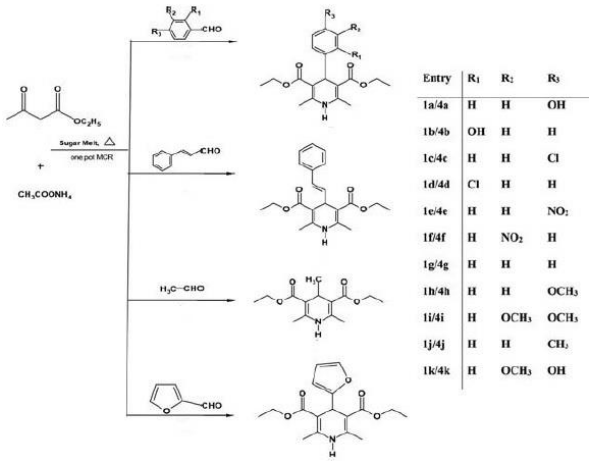

Entry	R_1	R_2	R_3
1a/4a	H	H	OH
1b/4b	OH	H	H
1c/4c	H	H	Cl
1d/4d	Cl	H	H
1e/4e	H	H	NO_2
1f/4f	H	NO_2	H
1g/4g	H	H	H
1h/4h	H	H	OCH_3
1i/4i	H	OCH_3	OCH_3
1j/4j	H	H	CH_3
1k/4k	H	OCH_3	OH

Figure 28. Synthesis of 1,4-DHP esters.

They introduced a more gentle and highly effective protocol that can readily substitute current methods. They utilized DESs, which can be reused without compromising their efficacy for up to 5 cycles, offering a more environmentally friendly option [161].

Ultrasound

One of the most environmentally friendly and efficient methods in producing various bulk and nanomaterials is sonochemistry. When ultrasonic irradiation used in synthesis, the amount of solvents and catalysts is reduced, leading to cost savings. It enables unique pathways for initiating high-energy reactions. Sonochemistry's foundation demonstrates significant potential in accelerating reaction rates, achieved through the mechanical impact of sound waves (for heterogeneous processes) and chemical activation (for homogeneous processes) in an energy-efficient way.

Cavitation is the predominant phenomenon induced by ultrasound in the liquid medium. When a liquid is subjected to a periodic pressure wave, the creation, growth, and then implosion (collapse) of bubbles happens. The result of the implosion of the bubble is the release of a large amount of thermal energy and mechanical energy without any significant change in the whole medium. Therefore, the cavitation bubble collapse is the driving force, which moves the reactions toward completion in a very short time [164, 165]. Due to the unusual properties like simplicity, controllable reaction conditions, rapid reaction rate, enhanced catalyst efficiency, and high purity of the product, this technique has been extensively used [166].

Solvent- and catalyst-free one-pot multicomponent reactions (MCRs) for the synthesis of 1,4-DHPs are the focus of interest for chemists. The synthesis of symmetric 4-(3-bromo-4-hydroxy-5-methoxyphenyl)-2,6-dimethyl-3,5-dicarbethoxy-1,4-DHP (4a) and 4-(3-bromo-4-hydroxy-5-methoxyphenyl)-2,6-dimethyl-3,5-dicarbmethoxy-(4-nitrophenyl)-1,4-DHP (4b) was achieved in high yield using solvent- and catalyst-free microwave-assisted multicomponent Hantzsch reaction by Maru et al. (Figure 29).

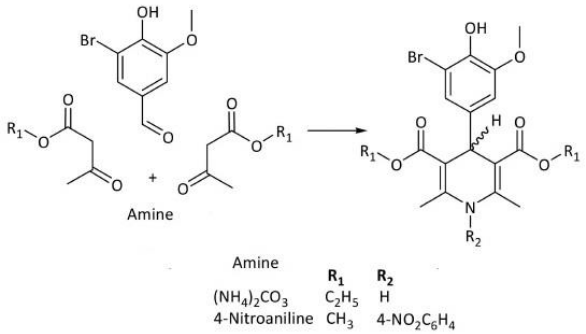

Figure 29. Reaction scheme for the synthesis of compounds (4 a) and (4 b).

The core/shell Fe_3O_4@GA@IG bio nanocatalyst has been prepared and evaluated for the first time in the synthesis of 1,4-DHPs under sonication in ethanol. In this method, ultrasound waves as an alternative green

source of energy have been used. Other advantages of this method are omitting toxic solvents or catalysts, good yields, short reaction times, very simple workup, and magnetically separable, recyclable, and green catalysts obtained from a natural source. This catalyst is recyclable with no significant yield decrease after six runs (Figure 30) [167].

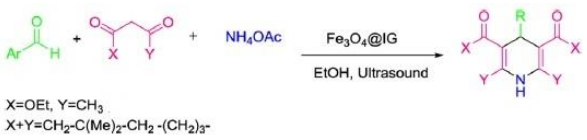

Figure 30. Synthesis of 1,4-DHP derivatives in ethanol under ultrasound irradiation.

the Fe3O4@GA@IG nanocomposite has been compared as a catalyst for the synthesis of 1,4-DHP and polyhydroquinoline derivatives with other catalysts and procedures [168-170].

Moradi et al. presented a novel synthetic method for producing 1,4-DHP derivatives using MWCNTs@meglumine as a highly efficient and recyclable catalyst. The approach followed green chemistry principles to create a practical heterogeneous catalyst by attaching meglumine onto CNT surfaces. The optimal use of ultrasonic irradiation was determined. The reaction was carried out in EtOH with varying power levels. The best yield (95%) was achieved after 15 minutes at 70 W, with no significant impact on reaction time and yield observed at higher power (75 W) (Figure 31) [171].

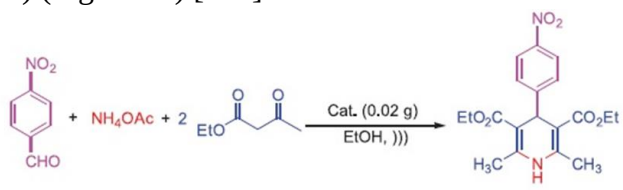

Figure 31. Synthesis of 1,4-DHPs MWCNTs@meglumine as catalyst, under ultrasonic irradiation.

In 2015, Tabassum et al. reported a one-pot four-component cyclocondensation reaction for the synthesis of polysubstituted 1,4-DHPs. The reaction was catalyzed by copper (I) iodide in an aqueous medium under ultrasound irradiation (Figure 32) [172].

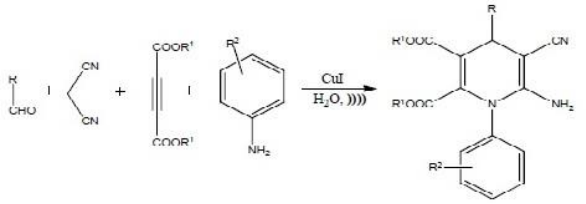

Figure 32. Preparation of polysubstituted 1,4-DHPs.

This experiment was conducted under solvent-free conditions, resulting in a maximum yield (45%) of product. Unsatisfactory yields were obtained under different conditions, even after an extended period. Other examples of ultrasound application in the synthesis of 1,4-DHPs can be found in references [80, 173, 174].

Mechanochemistry

The significance of green chemistry techniques is increasing. Alternative processes can help conserve resources and reduce costs [175]. Mechanochemistry is a method within green chemistry as it allows for solvent-free conditions. Chemical transformations occur through the application of mechanical energy (e.g. compression, shear, or friction). In solvent-free conditions, the reaction rate speeds up due to the absence of solvation phenomena and the high reagent concentrations resulting from the lack of solvents. Reactions involving insoluble

reactants enable efficient solvent-free synthetic procedures with high yields and shorter reaction times, achievable at a rapid pace through mechanochemistry. Mechanochemical reactions involve the direct absorption of mechanical energy, often from grinding or milling processes [176, 177].

A mechanochemical version of the Hantzsch dihydropyridine synthesis was developed by Hunda et al. They ground mixtures of aldehydes, dimedone, acyclic active methylene compounds, and ammonium acetate at room temperature in a mortar in the absence of solvent. When aromatic aldehydes were used, the reaction yielded good to excellent results (Figure 33) [178].

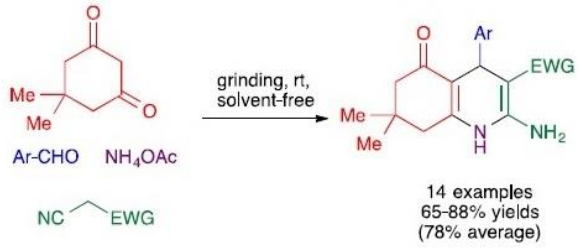

Figure 33. The preparation of polyhydroquinolines under mechanochemical conditions.

Bazgir et al. utilized a reactive cyclic ketone through manual grinding in solvent-free conditions and with toluene sulfonic acid as a catalyst to produce spiro compounds using Hantzsch-like chemistry (Figure 34) [179].

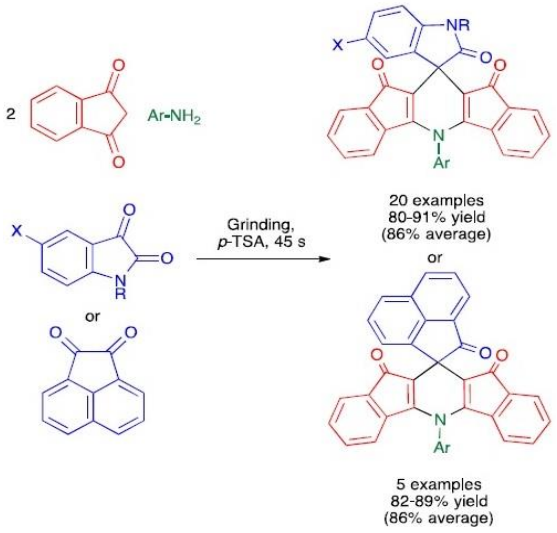

Figure 34. Synthesis of spiro compounds under manual grinding conditions.

Another mechanochemical multicomponent reaction was described by Kamur and Sharma. It involved grinding of aldehydes, amines, diethyl acetylenedicarboxylate (DEAD), and malononitrile/ethyl cyanoacetate in a porcelain mortar for 5-20 minutes to produce the desired compounds (Figure 35) [180].

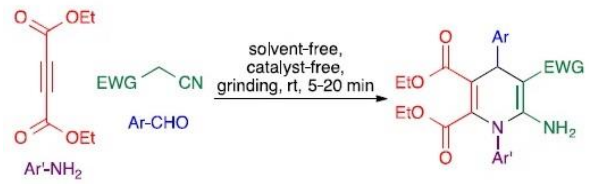

Figure 35. Mechanochemical four-component synthesis of DHPs from an acetylenedicarboxylate.

Synthesis of 1,4-DHP calcium antagonists and their derivatives through a new mechanochemical enzymatic protocol under ball milling conditions was studied by Jiang et al. In mechanochemical reactions, the grinding frequency plays a crucial role. Increasing the grinding frequency from 15 to 25 Hz resulted in a rise in the reaction yield

from 39.7 to 68.8% (Figure 36) [181].

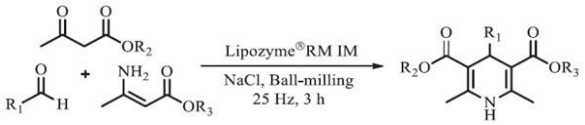

Figure 36. Lipozyme®RMIM-catalyzed rapid synthesis of 1,4-DHP derivatives under ball milling conditions.

In 2016, Moshtaghi Z. et al. reacted aromatic aldehydes, dimedone, and malononitrile with ammonium acetate. Surprisingly, they discovered that tetrahydrobenzo[b]pyrans were formed instead of polyhydroquinolines under both grinding and reflux conditions. The researchers observed that in this transformation, ammonium acetate acts as a catalyst rather than a reactant (Figure 37) [182].

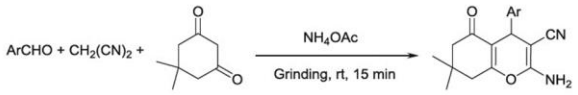

Figure 37. Ammonium acetate-mediated reaction of aromatic aldehydes, dimedone, and malononitrile at room temperature under grinding.

Then, they modified the reaction conditions. The reaction was carried out with the presence of ammonium acetate and imidazole as catalysts. The reaction acceleration and reduction of reaction time occurred upon the addition of either ammonium acetate or imidazole. The two-step synthesis of polyhydroquinoline derivatives in refluxing ethanol was conducted with a catalytic amount of imidazole (20 mol %) and refluxing in ethanol (Figure 38).

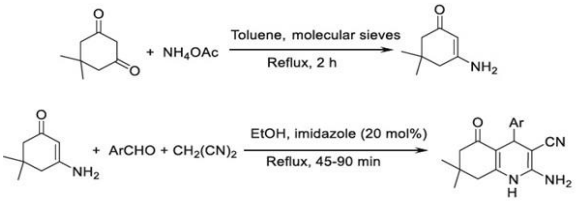

Figure 38. The two-stage synthesis of polyhydroquinoline derivatives in refluxing ethanol in the presence of the catalytic amount of imidazole.

Zhang et al. conducted a mechanochemical reaction by ball milling β-enaminones and chalcones with AlCl3. This method included the in situ formation of enaminones through Michael's addition of anilines to acetylene dicarboxylates (Figure 39) [183].

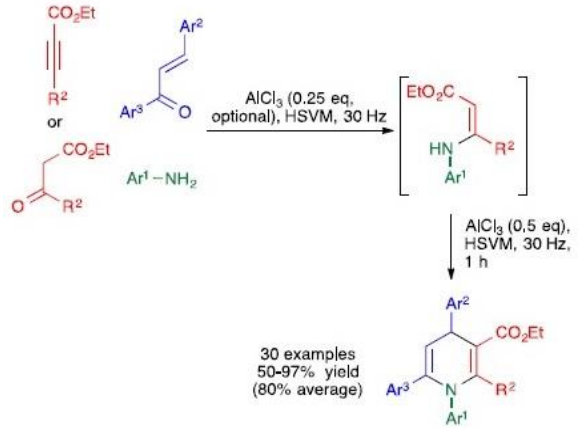

Figure 39. Mechanochemical four-component synthesis of DHPs from chalcones

In a different study, the researchers acquired dihydropyridines through a similar process starting from in situ-generated Knoevenagel adducts. However, they observed that by using 1,3-cyclohexanedione derivatives under the same conditions, instead of the anticipated fused dihydropyridines, they produced fused

pyran derivatives (Figure 40).

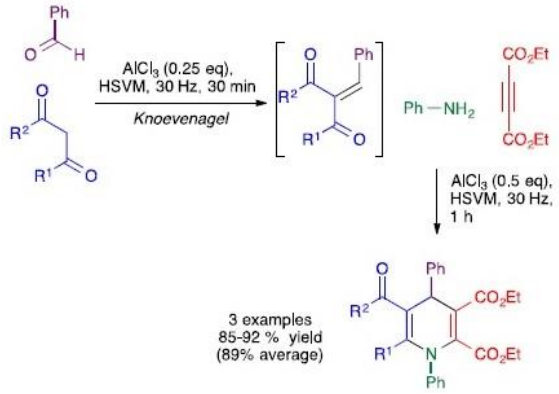

Figure 40. Knoevenagel-initiated mechanochemical four-component synthesis of DHPs.

Stereochemistry investigations (Synthesis of enantiopure 1,4-DHPs)

The Hantzsch procedure is mostly used in the synthesis of the 1,4-DHPs. Although this procedure is simple, and isolation of the product is generally straightforward the yield of the desired products is well for symmetrical dihydropyridines [184]. Later many efforts were made to synthesize the unsymmetrically substituted 1,4-DHP with high efficiency, and in some cases, the crystal structure was investigated [185, 186].

Nifedipine is a symmetrically substituted dihydropyridine, which is an achiral compound. The second-generation such as Amlodipine, Nitrendipine, and Nicardipine, are chiral derivatives and the pharmacological effects of their enantiomers are different from each other. The differences are quantitative in the case of the calcium antagonists. It means that the enantiomers exhibit opposite activities, one of them acting as an agonist, and the other as an antagonist. Moshtaghi et al. reported the synthesis of derivatives of unsymmetrically substituted 1,4-DHP and described the separation of the enantiomers of S-[(6-methyl-3,5-dicarboethoxy-4-(3-nitrophenyl) 1,4- dihydropyridin-2-yl)-methyl]-isothioureas. The C-4 carbon atom of 1,4-DHPs is prochiral (Figure 41) [187].

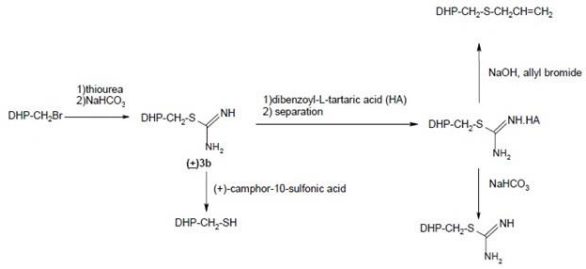

Figure 41. synthesis of DHPs derivatives and separation of the enantiomers of S-[(6-methyl-3,5-dicarboethoxy-4-(3-nitrophenyl) 1,4- dihydropyridin-2-yl)-methyl]-isothiourea.

Auria-Luna et al. used Takemoto's thiourea for the synthesis of 2-oxospiro-[indole-3,4-(1,4-dihydropyridine)] derivatives, which are chiral, and have good reactivity and promising enantioselectivities (Figure 42, route a) [188]. In the next work, they used bis-cinchona derivative as an organocatalyst (Figure 42, route b) [189].

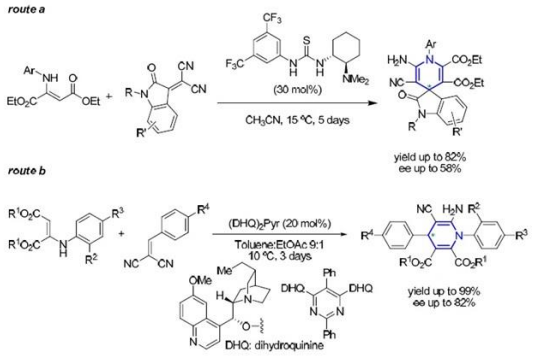

Figure 42. Synthesis of chiral 1,4-DHPs.

In 2018, the first organocatalytic asymmetric synthesis of chiral 1-Benzamido-1,4-dihydropyridine derivatives was investigated by them. In this method, they used chiral

amine-based catalysts, hydrazones, and alkylidenemalononitriles. The catalyst could provide the first asymmetric version of 1,4-DHP derivatives (Figure 43) [77].

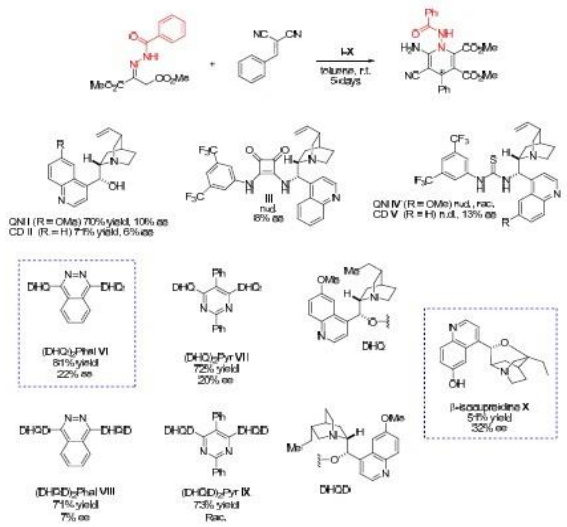

Figure 43. Chiral organocatalyst I-X is used for the synthesis of chiral derivatives of 1,4-DHPs.

For the synthesis of chiral 1-benzamido-1,4-DHP, the solvent, catalyst, and concentration of each reagent were analyzed.

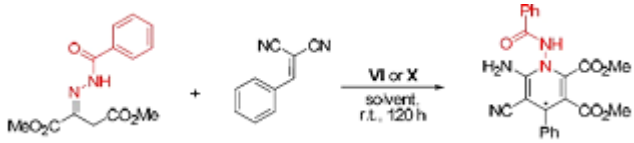

Figure 44. The synthesis of chiral 1-benzamido-1,4-DHP.

Another work in the enantioselective synthesis of 1,4-DHPs was reported, which was catalyzed by chiral brønsted acids (Figure 44) [125].

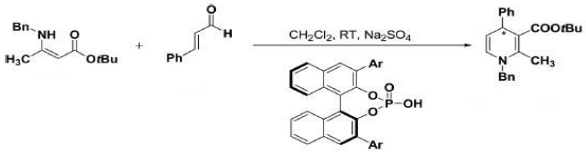

Figure 45. Enantioselective synthesis of 1,4-DHP catalyzed by chiral Brønsted acids.

Using chiral auxiliary for separation of racemic 1,4 DHPs

In this approach for the production of optically active 1,4-DHPs, a chiral auxiliary was utilized. Subsequently, the resulting diastereomeric esters were isolated, and the chiral auxiliary can be selectively removed [125].

Lamm, et al., in the synthesis of pure enantiomers of felodipine, a calcium channel antagonist, utilized a chiral auxiliary (Figure 46) [190].

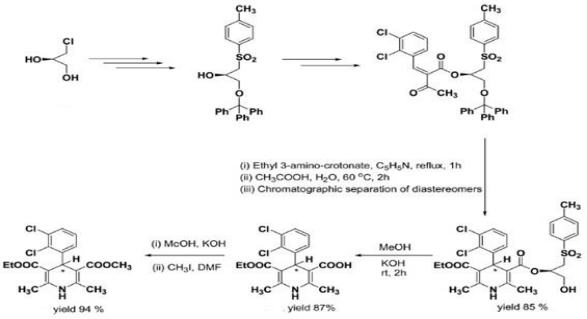

Figure 46. Enantiopure synthesis using chiral auxiliary.

Yamamoto et al. utilized the t-butyl ester of L-valine as a chiral auxiliary in synthesizing asymmetric 1,4-DHP derivatives, achieving a high enantiomeric excess (>95%) in a decent yield. The key aspect of this process is the stereoselective Michael addition (Figure 47) [191].

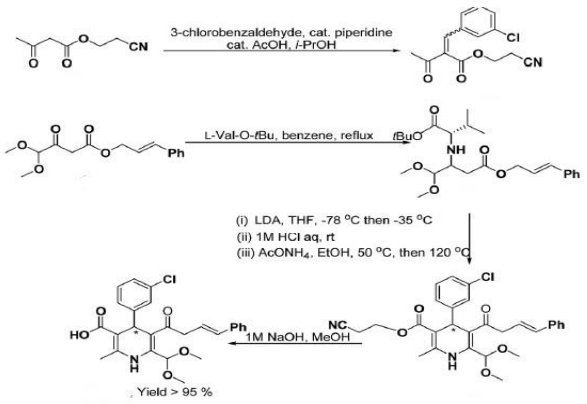

Figure 47. Stereoselective synthesis of 1,4-DHP.

Organocatalytic asymmetric synthesis to form enantiomerically enriched dihydropyridines

Excellent e.e. up to 98% in the asymmetric synthesis of 1,4-DHPs has been achieved in the presence of chiral phosphonic acids (Figure 48) [192].

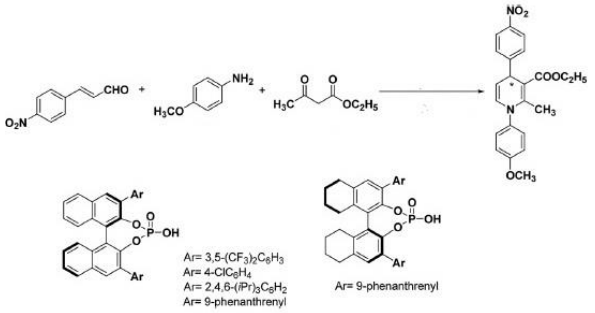

Figure 48. Chiral phosphonic acids catalyzed the synthesis of 1,4-DHP.

Synthesis of enantiomerically pure 1,4-DHPs has been done by utilizing chiral aldehydes. Michael addition of ethyl aminocrotonate to chiral a-acetylacrylates produced enantio-pure 1,4-DHPs (Figure 49) [125].

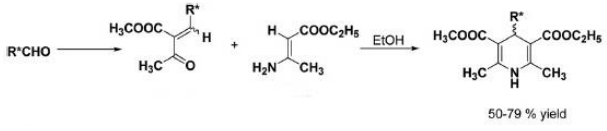

Figure 49. Synthesis of chiral 1,4-DHPs using chiral aldehydes.

Resolution of racemic 1,4-dihydropyridine carboxylic acids via diastereomeric salt formation has been reported [125]. Treating of racemic acid derivative of 1,4-DHP with chiral bases cinchonidine and quinidine, and then recrystallization to form diastereomeric salts. Next, treatment of each diastereomeric salt with hydrochloric acid gave each of enantiomers (Figure 50) [193].

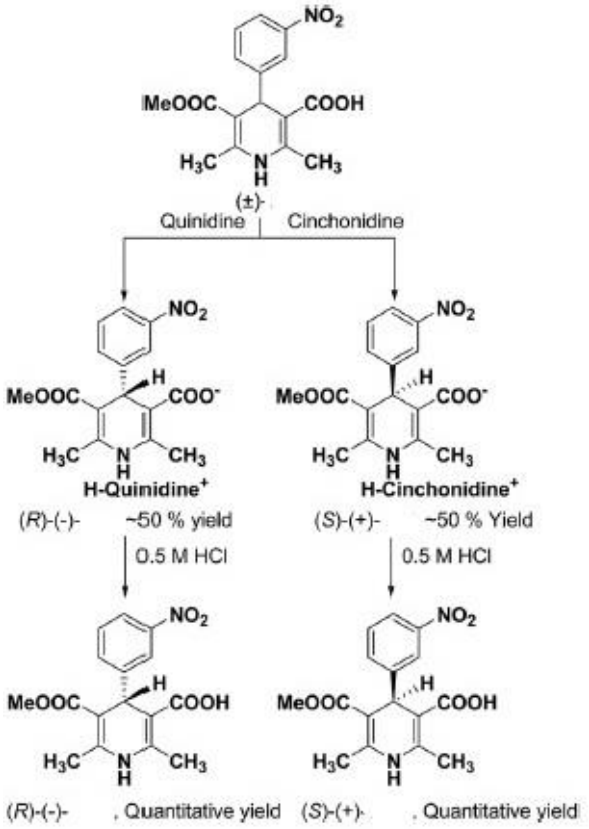

Figure 50. Synthesis of chiral 1,4-DHP *via* diastereomeric salt formation method

Also, R-(+) and S-(-) amlodipine enantiomers have been resolved via diastereomeric salt formation with L- or D-Tartaric acid,

respectively. When L-tartaric acid is used with racemic amlodipine in DMSO, (R)-amlodipine tartrate crystallized out. When the solvent system was switched to DMF/H2O (85:15 ratio), the (S)-(¬-) amlodipine enantiomer crystallized with 99% purity (Figure 51).

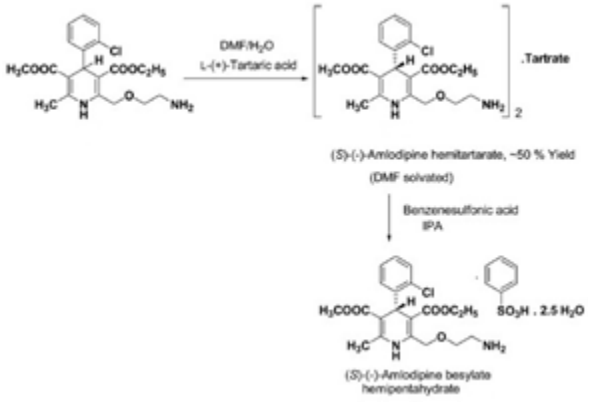

Figure 51. Resolution of R-(+) and S-(-) amlodipine via diastereomeric salt formation with L- or D-tartaric acid, respectively in DMSO.

Conflict of Interest

No conflict of interest was declared by the authors.

References

[1] Eisner, U.; Kuthan, J. Chem. Rev. 1972, 72, 1.

[2] Reddy, BP.; Rajesh, K.; Vijayakumar, V. Arab. J. Chem. 2015, 8, 138.

[3] Navidpour, L.; Shafaroodi, H.;, Miri, R.; Dehpour, A.R.; Shafiee, A. Il Farmaco. 2004, 59, 261.

[4] Triggle, D.J. Cell. Mol. Neurobiol. 2003, 23, 293.

[5] Budriesi, R.; Bisi, A.; Ioan, P.; Rampa, A.; Gobbi, S.; Belluti, F.; et al. Bioorg. Med. chem. 2005, 13, 3423.

[6] Maru, M.S.; Sudhadevi, Antharjanam, P.; Khan, NuH. ChemistrySelect. 2019, 4, 774.

[7] Bisi, A.; Micucci, M.; Gobbi, S.; Belluti, F.; Budriesi, R.; Rampa, A. Molecules. 2018, 23, 3088.

[8] Rasouli, Y.; Davood, A.; Alaee, A.; Dehqani, G.; Shafaroudi, H.; Lotfinia, M.; et al. Iran J Pharm Res. 2017, 16, 893.

[9] Prasanthi, G.; Prasad, K.; Bharathi, K. Eur. J. Med. Chem. 2014, 73, 97.

[10] Niemirowicz-Laskowska, K, Głuszek, K, Piktel, E.; Pajuste, K.; Durnaś, B.; Król, G, et al. Int J Nanomedicine. 2018, 13, 3411.

[11] Khedkar, S. A.; P. B.; Auti. Mini-Rev. Med. Chem. 2014, 14, 282.

[12] Fekri, L.Z. J. Chil. Chem. Soc. 2012, 57, 1415.

[13] Viradiya, D.; Mirza, S.; Shaikh, F.; Kakadiya, R.; Rathod, A.; Jain, N.; et al. Anticancer. Agents. Med. Chem. 2017, 17, 1003.

[14] Mollazadeh, S.; Shamsara, J.; Iman, M.; Hadizadeh, F. Recent. Pat. Anticancer. Drug. Discov. 2017, 12, 174.

[15] Iman, M.; Davood, A.; Lotfinia, M.; Dehqani, G.; Sardari, S.; Azerang, P.; et al. Iran J Pharm Res. 2016, 15, 791.

[16] Van Horn, K.S. 2013.

[17] Praveenkumar, E.; Gurrapu, N.; Kolluri, P.K.; Yerragunta, V.; Kunduru, B.R.; Subhashini, N. Bioorg Chem. 2019, 90, 103056.

[18] Edraki, N.; Mehdipour, A. R.; Khoshneviszadeh, M.; Miri, R. Drug Discov. Today. 2009, 14, 1058.

[19] Arrowsmith, J. E.; Campbell, S. F.; Cross, P. E.; Stubbs, J, K.; Burges, R. A.; Gardiner, D. G.; et al. J. Med. Chem. 1986, 29, 1696.

[20] Triggle, D. J. Drug Dev. Res. 2003, 58, 5.

[21] Vaghy, P. L.; Williams, J. S.; Schwartz, A. A.m J. Cardiol. 1987, 59, A9.
[22] Donald, P. R.; Van Helden, P. D. N. Engl. J. Med. 2009, 360, 2393.
[23] Tripathi, R. P.; Tewari, N.; Dwivedi, N.; Tiwari, V. K. Med. Res. Rev. 2005, 25, 93.
[24] Zhang, Y.; Post-Martens, K.; Denkin, S. Drug. Discov. Today. 2006, 11, 21.
[25] Trivedi, A. R.; Dodiya, D. K.; Dholariya, B. H.; Kataria, V. B.; Bhuva, V. R.; Shah, V. H. Bioorg. Med. Chem. Lett. 2011, 21, 5181.
[26] Khoshneviszadeh, M.; Edraki, N.; Javidnia, K.; Alborzi, A.; Pourabbas, B.; Mardaneh, J.; et al. Bioorg. Med. Chem. 2009, 17, 1579.
[27] Desai, B.; Sureja, D.; Naliapara, Y.; Shah, A.; Saxena, A. K. Bioorg. Med. Chem. 2001, 9, 1993.
[28] Kharkar, P. S.; Desai, B.; Gaveria, H.; Varu, B.; Loriya, R.; Naliapara, Y.; et al. J. Med. Chem. 2002, 45, 4858.
[29] Lentz, F.; Reiling, N.; Spengler, G.; Kincses, A.; Csonka, A.; Molnár, J.; et al. Molecules. 2019, 24, 2873.
[30] Murthy, Y.; Rajack, A.; Ramji, M. T.; Praveen, C.; Lakshmi, K. A. Bioorg. Med. Chem. Lett. 2012, 22, 6016.
[31] Lentz, F.; Hemmer, M.; Reiling, N.; Hilgeroth, A. Bioorg. Med. Chem. Lett. 2016, 26, 5896.
[32] Neubert, J. K.; Karai, L.; Jun, J. H.; Kim, H-S.; Olah, Z.; Iadarola, M. J. Pain. 2003, 104, 219.
[33] Karai, L.; Brown, D. C.; Mannes, A. J.; Connelly, S. T.; Brown, J.; Gandal, M.; et al. The Journal of clinical investigation. 2004, 113, 1344.
[34] Poondra, R. R.; Nallamelli, R. V.; Meda, C. L. T.; Srinivas, B.; Grover, A.; Muttabathula, J.; et al. Bioorg. Med. Chem. Lett. 2013, 23, 1104.
[35] Reddy, T. R.; Reddy, G. R.; Reddy, L. S.; Meda, C. L. T.; Parsa, K. V.; Kumar, K. S.; et al. Eur. J. Med. Chem. 2013, 62, 395.
[36] Revai, T.; Harmos, G. R. Soc. Med. 1999, 92, 23.
[37] Pedemonte, N.; Diena, T.; Caci, E.; Nieddu, E.; Mazzei, M.; Ravazzolo, R.; et al. Mol. Pharmacol. 2005, 68, 1736.
[38] Cateni, F.; Zacchigna, M.; Pedemonte, N.; Galietta, L. J.; Mazzei, M. T.; Fossa, P.; et al. Bioorg. Med. Chem. 2009, 17, 7894.
[39] Budriesi, R.; Ioan, P.; Leoni, A.; Pedemonte, N.; Locatelli, A.; Micucci , M.; et al. J. Med. Chem. 2011, 54, 3885.
[40] Kumar, A.; Singh, A. Pharmacol. Rep. 2015, 67, 195.
[41] Anand, R.; Gill, K. D.; Mahdi, A. A. Neuropharmacol. 2014, 76, 27.
[42] Gauthier, S.; Leuzy, A.; Racine, E.; Rosa-Neto, P. Prog. Neurobiol. 2013, 110, 102.
[43] Schelterns, P.; Feldman, H. The Lancet Neurol. 2003, 2, 539.
[44] Rosini, M.; Simoni, E.; Milelli, A.; Minarini, A.; Melchiorre, C. J. Med. Chem. 2013, 57, 2821.
[45] Bush, A. I. J. Alzheimer's Dis. 2008, 15, 223.
[46] Lahiri, D.; Rogers, J.; Greig, N.; Sambamurti, K. Curr. Pharm. Des. 2004, 10, 3111.
[47] Wilkinson, D.; Wirth, Y.; Goebel, C. Dement. Geriatr. Cogn. Disord. 2014, 37, 71.
[48] León, R.; de los Ríos, C.; Marco-Contelles, J.; Huertas, O.; Barril, X.; Luque, F. J.; et al. Bioorg. Med. Chem. 2008, 16, 7759.

[49] Alptüzün, V.; Prinz, M.; Hörr, V.; Scheiber, J.; Radacki, K.; Fallarero, A.; et al. Bioorg. Med. Chem. 2010, 18, 2049.
[50] Tenti, G.; Egea, J.; Villarroya, M.; León, R.; Fernández, J. C.; Padín, J. F.; et al. Med.Chem. Comm. 2013, 4, 90.
[51] Malek, R.; Maj, M.; Wnorowski, A.; Jóźwiak, K.; Martin, H.; Iriepa, I.; et al. Bioorg. Chem. 2019, 103205.
[52] Teodori, E.; Dei, S.; Scapecchi, S.; Gualtieri, F. Il Farmaco. 2002, 57, 385.
[53] Szabo, D.; Keyzer, H.; Kaiser, H. E.; Molnar, J. Anticancer Res. 2000, 20, 4261.
[54] Dantzig, A.; Law, K.; Cao, J.; Starling, J. Curr. Med. Chem. 2001, 8, 39.
[55] Colabufo, A. N.; Berardi, F.; Grazia Perrone, M.; Capparelli, E.; Cantore, M.; Inglese, C.; et al. Curr. Top. Med. Chem. 2010, 10, 1703.
[56] Baumert, C.; Hilgeroth, A. (Formerly Current Medicinal Chemistry-Anti-Cancer Agents). 2009, 9, 415.
[57] Ranjbar, S.; Firuzi, O.; Edraki, N.; Shahraki, O.; Saso, L.; Khoshneviszadeh, M.; et al. Med. Chem. Comm. 2017, 8, 1919.
[58] Kawase, M.; Shah, A.; Gaveriya, H.; Motohashi, N.; Sakagami, H.; Varga, A.; et al. Bioorg. Med. Chem. 2002, 10, 1051.
[59] Baumert, C.; Günthel, M.; Krawczyk, S.; Hemmer, M.; Wersig, T.; Langner, A.; et al. Bioorg. Med. Chem. 20132, 1, 166.
[60] Sirisha, K.; Shekhar, M. C.; Umasankar, K.; Mahendar, P.; Sadanandam, A.; Achaiah, G.; et al. Bioorg. Med. Chem. 2011, 19, 3249.
[61] Coburger, C.; Wollmann, J.; Krug, M.; Baumert, C.; Seifert, M.; Molnár, J.; et al. Bioorg. Med. Chem. 2010, 18, 4983.
[62] Voigt, B.; Coburger, C.; Monár, J.; Hilgeroth, A. Bioorg. Med. Chem. 2007, 15, 5110.
[63] Nejati, M.; Sadeghpour, H.; Ranjbar, S.; Javidnia, K.; Edraki, N.; Saso, L.; et al. Can. J. Chem. 2019, 1.
[64] Goto, R. N.; Sobral, L. M.; Sousa, L. O.; Garcia, C. B.; Lopes, N. P.; Marín-Prida, J.; et al. Eur. J. Pharmacol. 2018, 819, 198.
[65] Hantzsch, A. Justus Liebigs Ann. Chem. 1882, 215, 1.
[66] Breitenbucher, J. G.; Figliozzi, G. Tetrahedron Lett. 2000, 41, 4311.
[67] Sapkal, S. B.; Shelke, K. F.; Shingate, B. B.; Shingare, M. S. Tetrahedron Lett. 2009, 50, 1754.
[68] Correa, W. H.; Scott, J. L. Green Chem. 2001, 3, 296.
[69] Ghosh, P. P.; Paul, S.; Das A. R. Tetrahedron Lett. 2013, 54, 138.
[70] Baraldi, P. T.; Noel, T.; Wang, Q.; Hessel ,V. Tetrahedron Lett. 2014, 55, 2090.
[71] Khodja, I. A.; Ghalem, W.; Dehimat, Z. I.; Boulcina, R.; Carboni, B.; Debache, A. Synth. Commun. 2014, 44, 959.
[72] Ma, X.; He, Y.; Lu, M. Synth. Commun. 2014, 44, 474.
[73] Patil, R. D.; Dalal, S. D. Lett. Org. Chem. 2011, 8, 477.
[74] Lee, J. H. Tetrahedron Lett. 2005, 46, 7329.
[75] Akbari, J.; Tala, S.; Dhaduk, M.; Joshi, H. Arkivoc. 2008, 12, 126.
[76] Yadav, J.; Reddy, B.; Basak, A.; Narsaiah, A. Green chem. 2003, 5, 60.
[77] Auria-Luna, F.; Marqués-López, E.; Herrera, P. R. Molecules. 2018, 23, 2692.
[78] Kolvari, E.; Zolfigol, M.; Koukabi, N.; Shirmardi-Shaghasemi, B. Chem. Pap. 2011, 65, 898.
[79] Makone, S.; Niwadange, S. Chem Sin. 2012, 3, 1293.

[80] Wang, S-X.; Li, Z-Y.; Zhang, J-C.; Li, J-T. Ultrason. Sonochem. 2008, 15, 677.
[81] Zonouz, A. M.; Sahranavard, N. J. Chem. 2010, 7, S372.
[82] Marques, M. V.; Ruthner, M. M.; Fontoura, L. A.; Russowsky, D. J. Braz. Chem. Soc. 2012, 23, 171.
[83] Yang, J.; Jiang, C.; Yang, J.; Qian, C.; Fang, D. Green chem. lett. rev. 2013, 6, 262.
[84] Hajinasiri, R.; Rezayati, S. Z. fur Naturforsch. 2013, 68, 818.
[85] Shaabani, A.; Maleki, A.; Rezayan, A. H.; Sarvary, A. Mol. Divers. 2011, 15, 41.
[86] Balme, G.; Bossharth, E.; Monteiro, N. Eur. J. Org. Chem. 2003, 2003, 4101.
[87] Polshettiwar, V.; Varma, R. S. Green Chem. 2010, 12, 743.
[88] Kumar, A.; Maurya, R. A. Synlett. 2008, 2008, 883.
[89] Cherkupally, S. R.; Mekala, R.. Chem. Pharm. Bull. 2008, 56, 1002.
[90] Giorgi, G.; Adamo, M. F.; Ponticelli, F.; Ventura, A. Org. Biomol. Chem. 2010, 8, 5339.
[91] Demirci, T.; Çelik, B.; Yıldız, Y.; Eriş, S.; Arslan, M.; Sen, F.; et al. RSC Adv. 2016, 6, 76948.
[92] Tabrizian, E.; Amoozadeh, A. RSC Adv. 2016, 6, 96606.
[93] Chen, W.; Peng, X-w.; Zhong, L-x.; Li, Y.; Sun, R-c. ACS Sustain. Chem. Eng. 2015, 3, 1366.
[94] Moghaddam, F. M.; Saberi, V.; Keshavarz, S. SynOpen. 2018, 2, 0036.
[95] Zhang, M.; Liu, Y-H.; Shang, Z-R.; Hu, H-C.; Zhang, Z-H. Comm. 2017, 88, 39.
[96] Mirjalili, B. B. F.; Bamoniri, A.; Asadollah Salmanpoor, L. J Nanostruct. 2018, 8, 276.
[97] Chughtai, A. H.; Ahmad, N.; Younus, H. A.; Laypkov, A.; Verpoort, F. Chem. Soc. Rev. 2015, 44, 6804.
[98] Devarajan, N.; Karthik, M.; Suresh, P. Org. Biomol. Chem. 2017, 15, 9191.
[99] Jiang, J.; Yaghi, O. M. Chem. Rev. 2015, 115, 6966.
[100] Lin, Y.; Kong, C.; Chen, L. RSC Adv. 2016, 6, 32598.
[101] Devarajan, N.; Suresh, P. New J Chem. 2019, 43, 6806.
[102] Arzehgar, Z.; Sajjadifar, S.; Arandiyan, H. Asian J. Green Chem.2019, 3, 43.
[103] Nasr-Esfahani, M.; Hoseini, S. J.; Montazerozohori, M.; Mehrabi, R.; Nasrabadi, H. J. Mol. Catal. A Chem. 2014, 382, 99.
[104] Mahinpour, R.; Moradi, L.; Zahraei, Z.; Pahlevanzadeh, N. J. Saudi Chem. Soc. 2018, 22, 876.
[105] Liu, Y-p.; Liu, J-m.; Wang, X.; Cheng, T-m.; Li, R-t. Tetrahedron. 2013, 69, 5242.
[106] Zonouz, A. M.; Aras, M. A.; Abuali, N. Transit. Met. Chem. 2013, 38, 335.
[107] Zonouz, A. M.; Hosseini S. B. Synth. Commun. 2008, 38, 290.
[108] Rao, G. D.; Nagakalyan, S.; Prasad, G. RSC Adv. 2017, 7, 3611.
[109] Tajbakhsh, M.; Alinezhad, H.; Norouzi, M.; Baghery, S.; Akbari, M. J. Mol. Liq. 2013, 177, 44.
[110] Otokesh, S.; Koukabi, N.; Kolvari, E.; Amoozadeh, A.; Malmir, M.; Azhari, S. S. Afr. j. chem. 2015, 68, 15.
[111] Davoodnia, A.; Khashi, M.; Tavakoli-Hoseini, N. Chinese. J. Catal. 2013, 34, 1173.
[112] Masoudi, P. J. Sci. I. R. Iran. 2019, 30, 33.
[113] Khaskel, A.; Barman, P. Heteroat. Chem. 2016, 27, 114.

[114] Ghasemzadeh, M. A.; Nasrollahi, S. M. H.; Zolfaghari, M. R. Acta Chim. Slov. 2018, 65, 199.
[115] Mirzaei, H.; Davoodnia, A. Chinese. J. Catal. 2012, 33, 1502.
[116] Vahdat, S. M.; Chekin, F.; Hatami, M.; Khavarpour, M.; Baghery, S.; Roshan-Kouhi, Z. Chinese. J. Catal. 2013, 34, 758.
[117] Liu, P.; Hao, J-W.; Mo, L-P.; Zhang, Z-H. RSC Adv. 2015, 5, 48675.
[118] Irimia-Vladu, M. Chem. Soc. Rev. 2014, 43, 588.
[119] Dallinger, D.; Kappe, C. O. Chem. Rev. 2007, 107, 2563.
[120] Chanda, A.; Fokin, V. V. Chem. Rev. 2009, 109, 725.
[121] Lindström, U. M. Chem. Rev. 2002, 102, 2751.
[122] Wang, Z-X.; Qin, H-L. Green Chem. 2004, 6, 90.
[123] Moshtaghi Zonouz, A.; Raeisolsadati Oskouei, M. J. Chin. Chem. Soc. 2013, 60, 275.
[124] Tamaddon, F.; Razmi, Z.; Jafari, A. A. Tetrahedron Lett. 2010, 51, 1187.
[125] Sharma, V. K.; Singh, S. K. RSC Adv. 2017, 7, 2682.
[126] Ostaszewski, R.; Paprocki, D.; Madej, A.; Koszelewski, D.; Brodzka, A. Front. Chem. 2018, 6, 502.
[127] Sharma, M.; Rajani, D.; Patel, H. Royal Society open science. 2017, 4, 170006.
[128] Pramanik, A.; Saha, M.; Bhar, S. ISRN Org. Chem. 2012, 2012.
[129] Longo, Jr L. S.; Craveiro, M. V. J. Braz. Chem. Soc. 2018, 29, 1999.
[130] Constable, D. J.; Jimenez-Gonzalez, C.; Henderson, R. K. Org. Process Res. Dev. 2007, 11, 133.
[131] Alfonsi, K.; Colberg, J.; Dunn, P. J.; Fevig, T.; Jennings, S.; Johnson, T. A.; et al. Green Chem. 2008, 10, 31.
[132] Henderson, R. K.; Jiménez-González, C.; Constable, D. J.; Alston, S. R.; Inglis, G. G.; Fisher, G.; et al. Green Chem. 2011, 13, 854.
[133] Prat, D.; Pardigon, O.; Flemming, H-W.; Letestu, S.; Ducandas, Vr.; Isnard, P.; et al. Org. Process Res. Dev. 2013, 17, 1517.
[134] Hallett, J. P.; Welton, T. Chem. Rev. 2011, 111, 3508.
[135] Olivier-Bourbigou, H.; Magna, L.; Morvan, D. Appl. Catal. A Gen. 2010, 373, 1.
[136] Wasserscheid, P.; Welton, T. John Wiley & Sons; 2008.
[137] Deetlefs, M.; Seddon, K. R. Green Chemistry. 2010, 12, 17.
[138] Rogers, R. D.; Seddon, K. R. Sci. 2003, 302, 792.
[139] Ghandi, K. Curr. Opin. Green Sustain. Chem. 2014, 4, 44.
[140] Cole, A. C.; Jensen, J. L.; Ntai, I.; Tran, K. L. T.; Weaver, K. J.; Forbes, D. C.; et al. J. Am. Chem. Soc. 2002, 124, 5962.
[141] Isambert, N.; Duque, Md. M. S.; Plaquevent, J-C.; Genisson, Y.; Rodriguez, J.; Constantieux, T. Chem. Soc. Rev. 2011, 40, 1347.
[142] Liu, X.; Liu, B. J. Chem. 2017, 2017.
[143] Rostamnia, S.; Hassankhani, A. Synlett. 2014, 25, 2753.
[144] Abaszadeh, M.; Seifi, M. J. Sulphur Chem. 2017, 38, 440.
[145] Sajjadifar, S.; Mohammadi-Aghdam, S. Asian J. Green Chem. 2017, 1, 1.
[146] Liu, T.; Lai, Y-H.; Yu, Y-Q.; Xu, D-Z. New J Chem. 2018, 42, 1046.

[147] Gericke, M.; Fardim, P.; Heinze, T. Molecules. 2012, 17, 7458.
[148] Perozo, E.; Rees, D.C. Curr. Opin. Struct. Biol. 2003, 13, 432.
[149] Rani, M.; Brant, A.; Crowhurst, L.; Dolan, A.; Lui, M.; Hassan, N. H.; et al. Phys. Chem. Chem. 2011, 13, 16831.
[150] Abbott, A. P.; Capper, G.; Davies, D. L.; Rasheed, R. K.; Tambyrajah, V. Chem. Commun. 2003, 70.
[151] Imperato, G.; Eibler, E.; Niedermaier, J.; König, B. Chem. Commun. 2005, 1170.
[152] Imperato, G.; Höger, S.; Lenoir, D.; König, B. Green Chem. 2006, 8, 1051.
[153] Francisco, M.; van den Bruinhorst, A.; Kroon, M. C. Angew. Chem., Int. Ed. Engl. 2013, 52, 3074.
[154] Dai, Y.; van Spronsen, J.; Witkamp, G-J.; Verpoorte, R.; Choi, YH. Anal. Chim. Acta. 2013, 766, 61.
[155] Skopek, M. A.; Mohamoud, M. A.; Ryde,r K. S.; Hillman, A. R. Chem. Commun. 2009, 935.
[156] Carriazo, D.; Serrano, M. C.; Gutiérrez, M. C.; Ferrer, M. L.; del Monte, F. Chem. Soc. Rev. 2012, 41, 4996.
[157] Zhao, H.; Baker, G. A. J. Chem. Technol. Biotechnol. 2013, 88, 3.
[158] Del Monte, F.; Carriazo, D.; Serrano, M. C.; Gutierrez, M. C.; Ferrer, M. L. ChemSusChem. 2014, 7, 999.
[159] Rodríguez, N. R.; González, A. S.; Tijssen, P. M.; Kroon, M. C. Fluid Ph. Equilibria. 2015, 385, 72.
[160] Abo-Hamad, A.; Hayyan, M.; AlSaadi, M. A.; Hashim, M. A. J. Chem. Eng. 2015, 273, 551.
[161] Pednekar, S.; Bhalerao, R.; Ghadge, N. Chem. Sci. J. 2013, 125, 615.
[162] Wang, L.; Zhu, K-Q.; Chen, Q.; He, M-Y. Green Process. Synth. 2014, 3, 457.
[163] Kumar, J. A.; Shridhar, G.; Ladage, S.; Ravishankar, L. Synth. Commun. 2016, 46, 1989.
[164] Cravotto, G.; Cintas, P. Chem. Soc. Rev. 2006, 35, 180.
[165] Xu, H.; Zeiger, B. W.; Suslick, K. S. Chem. Soc. Rev. 2013, 42, 2555.
[166] Puri, S.; Kaur, B.; Parmar, A.; Kumar, H. Curr. Org. Chem. 2013, 17, 1790.
[167] Pourian, E.; Javanshir, S.; Dolatkhah, Z.; Molaei, S.; Maleki, A. ACS Omega. 2018, 3, 5012.
[168] Kulkarni, P. J. Chil. Chem. Soc. 2014, 59, 2319.
[169] Tekale, S. U.; Pagore, V. P.; Kauthale, S. S.; Pawar, R. P. Chin. Chem. Lett. 2014, 25, 1149.
[170] Yoo, J. S.; Laughlin, T. J.; Krob, J. J.; Mohan, R. S. Tetrahedron Lett. 2015, 56, 4060.
[171] Moradi, L.; Zare, M. Green chem. lett. rev. 2018, 11, 197.
[172] Tabassum, S.; Govindaraju, S.; Pasha, M. RSC Adv. 2016, 6, 29802.
[173] Ozer, E. K.; Gunduz, M. G.; El-Khouly, A.; Sara, Y.; Simsek, R.; Iskit, A. B.; et al. Turk. J. Biochem. 2018, 43, 578.
[174] Abaszadeh, M.; Seifi, M.; Asadipour, A. Res. Chem. Intermed. 2015, 41, 5229.
[175] Zonouz, A. M.; Eskandari, I.; Khavasi, H. R. Tetrahedron Lett. 2012, 53, 5519.
[176] Leonardi, M.; Villacampa, M.; Menéndez, J. C. Chem. Sci. 2018, 9, 2042.
[177] Hernandez, J. G.; Bolm, C. J. Org. Chem. 2017, 82, 4007.
[178] Kumar, S.; Sharma, P.; Kapoor, K. K.; Hundal, M. S. Tetrahedron. 2008, 64, 536.

[179] Ghahremanzadeh, R.; Ahadi, S.; Shakibaei, G. I.; Bazgir, A. Tetrahedron Lett. 2010, 51, 499.
[180] Kumar, A.; Sharma, S. Green Chem. 2011, 13, 2017.
[181] Jiang, L.; Ye, L. D.; Gu, J.; Su, W. k.; Ye, W. t. J. Chem. Technol. Biotechnol. 2019, 94, 2555.
[182] Moshtaghi, Z. A.; Okhravi, S.; Moghani, D. Monatsh. Chem. 2016, 147, 1819.
[183] Zeng, J-C.; Yu, F.; Asiri, A. M.; Marwani, H. M.; Zhang, Z. J. Rev. Comm. Heterocycle. Chem. 2017, 94, 2054.
[184] Moshtaghi, Z. A.; Oskuie, M. R.; Mollazadeh, S. Synth. Commun. 2005, 35, 2895.
[185] Moshtaghi, Z. A.; Sadr, M. H.; Oskuie, M. R.; Bachechi, F. J. Chin. Chem. Soc. 2010, 57, 1081.
[186] Rastgar Mirzaei, Y.; Moshtaghi Zonouz, A. Iran. J. Chem. Chem. Eng. 1997, 16, 29.
[187] Moshtaghi, Z.; Raisossadat, O.; Sadeghi, S. Q. Arkivoc. 2006, 15.
[188] Auria-Luna, F.; Marqués-López, E.; Mohammadi, S.; Heiran, R.; Herrera, R. Molecules. 2015, 20, 15807.
[189] Auria-Luna, F.; Marqués-López, E.; Gimeno, M. Cn.; Heiran, R.; Mohammadi, S.; Herrera, R. P. J. Org. Chem. 2017, 82, 5516.
[190] Lamm, B.; Simonsson, R.; Sundell, S. Tetrahedron Lett. 1989, 30, 6423.
[191] Yamamoto, T.; Ohno, S.; Niwa, S.; Tokumasu, M.; Hagihara, M.; Koganei, H, et al. Bioorg. Med. Chem. Lett. 2011, 21, 3317.
[192] Jiang, J.; Yu, J.; Sun, X. X.; Rao, Q. Q.; Gong, L. Z. Angew. Chem. Int. Ed. 2008, 47, 2458.
[193] He, W.; Shi, X.; Huan, M; Huang, Q-j.; Zhou, S-y. Bioorg. Med. Chem. Lett. 2010, 20, 805.
[194] Gotrane, D. M.; Deshmukh, R. D.; Ranade, P. V.; Sonawane, S. P.; Bhawal, B. M.; Gharpure, M. M.; et al. Org. Process Res. Dev. 2010, 14, 640.

Communications In Catalysis
Vol. 2, No. 2, 2024, pp. 85-91
DOI: 10.22049/CIC.2024.29630.1039
Azarbaijan Shahid Madani University

Effect of the alkyl chain length of Hydrogen bond donor on the intermolecular interaction in eutectic solvents

Samaneh Barani Pour [1*], Haleh Vakili [2], Jaber Jahanbin Sardroodi [3*]

[1,2] Molecular Science and Engineering Research Group (MSERG), Molecular Simulation Lab, Azarbaijan Shahid Madani University, Tabriz, Iran

[3]Molecular Science and Engineering Research Group (MSERG), Department of Chemistry, Molecular Simulation Lab, Azarbaijan Shahid Madani University, Tabriz, Iran

**Corresponding Author E-mail: samaneh.baranipour@gmail.com*

**Corresponding Author E-mail: jsardroodi@azaruniv.ac.ir*

Received: 2024-04-03, Accepted: 2024-05-20

Abstract

The binary mixtures of L-menthol and a series of fatty acids such as Acetic acid (C2), Butyric acid and (C4), and Decanoic acid (C10) have been prepared. The structural properties of the deep eutectic solvents were investigated using radial distribution functions (RDF), combined distribution functions, and hydrogen bond networks. The results proved dipole strong intermolecular dipole-dipole interaction and hydrogen bond network in the deep eutectic solvents.

Keywords: L-menthol, Molecular dynamics simulations, Deep eutectic solvents, Structural properties, Dipole-dipole interaction

Introduction

Deep eutectic solvents are defined as mixtures with a low melting point compared to the two pure components [1]. DESs are created by combining a salt with a molecular hydrogen bond donor (HBD) which has a clear liquid phase. These novel solvents are sometimes created as a result of a hydrogen bond interaction between two components. DESs frequently exhibit non-flammability, great thermal stability, and low volatility [1] . L-menthol is a common ingredient in flavoring, foods, and medications [2]. This compound has become interesting as a hydrogen bond donor (HBD) and hydrogen bond acceptor (HBA) in the design of hydrophobic deep eutectic solvents. The saturated fatty acids are obtained from meat fats and plant oils such as coconut oil and palm kernel oil [3]. The fatty acids are important compounds that can have wide applications in the chemical as solvents [4]. The study of the interaction between fatty acids and L-menthol is expected to provide valuable information regarding the interaction between different alkyl chains. Furthermore, fatty acids are found in biodiesel fuels of plant origin that have been considered fossil fuels. It is very difficult to separate fatty acids from the mixtures because these compounds undergo thermal decomposition easily. The fatty acids and terpenes mixture was proposed as a hydrophobic DES able to extract Metal ions and biomolecules from aqueous solutions. The examination of the distribution syntactic of solvent molecules using radial and spatial distribution functions, along with the justification of observed trends, might yield important insights into thermophysical properties. Therefore, one other theme of this study is investigating the possible effect of intermolecular interactions on the structural properties of deep eutectic solvents based on L-menthol and fatty acid. The results proved dipole strong intermolecular dipole-dipole interaction and hydrogen bond network in the deep eutectic solvents.

Simulation Details

The binary mixtures of FAs and L-MEN were prepared using the PACKMOL package. All MD simulations were performed using the NAMD 2.14 software package [5]. The simulation studies of binary mixtures were performed with the CHARMM force fields. The partial charges for L-menthol and Fatty acid (e.g., acetic acid, butyric acid and Lauric acid) species were calculated at the MP2/6-31G* level by fitting the RESP (restricted electrostatic potential). The systems were then allowed to stabilize for 50 ns in an

isothermal-isobaric (NPT) ensemble at a temperature of 298.15 K and a pressure of 1 atm. The desired temperature was maintained using the Langevin dynamics method. Finally, intermolecular interactions were investigated in a menthol-based eutectic solvent.

Results and discussion

Hydrogen bond networks

The significant variation in the observed melting point of L-menthol is correlated readily with the strength and number of hydrogen bonds between HBA and HBD. In this work, the importance of intramolecular hydrogen bonding in the orientation of molecules was discussed. The hydrogen bond plugin in VMD was used to obtain the number of Hydrogen bonds [6]**.** Gaussian functions fitted to the number of H-bond data were used to determine the average number of H-bonds (Eq.1).

$$F(X) = \frac{a}{\sigma\sqrt{2\pi}} exp^{\frac{-(X-\bar{X})^2}{2\sigma^2}} \qquad (1)$$

, where $\bar{X}$ is the mean of the distribution, σ is the standard deviation[7]. The average numbers of H-bonds are clearly seen in Figure 1 (a). It is found that the carboxyl group (-COOH) of FAs and hydroxyl group (—OH) of L-menthol plays a key role in the formation of hydrogen bonds between two components. The L-MEN···DEC hydrogen bond with a value of 4 is again shorter than the L-MEN···BUA hydrogen bond with an average value of 4.25 (for each molecule). The hydrogen bonds occupancy analysis shows that the H-bond between decanoic acid and L-menthol molecules is much stronger than acid and makes a stable interaction in the mixture (see Figure1)

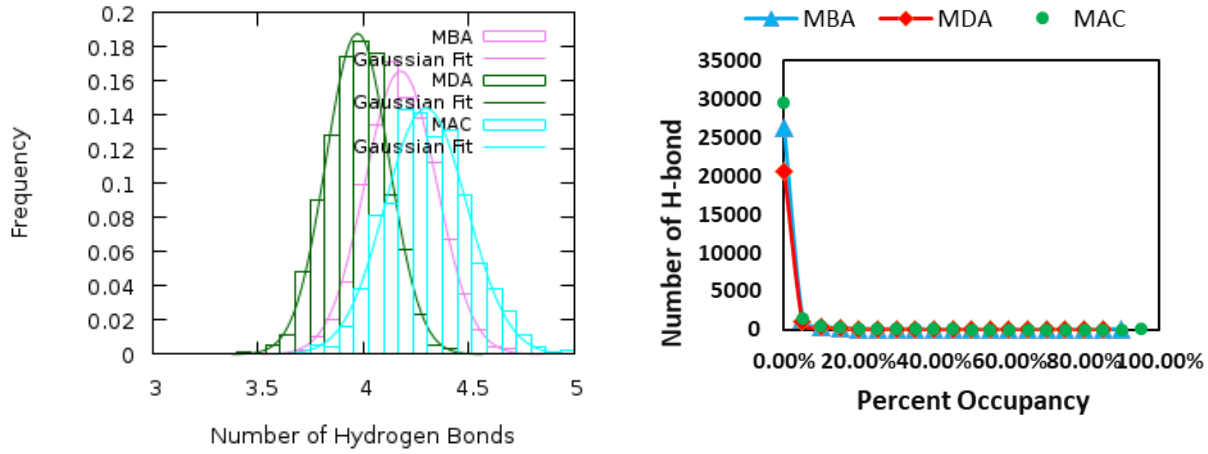

(a) (b)

Figure 1. Number of hydrogen bonds (a) and the distribution of the hydrogen bond between the FAs and L-MEN, (b) Hydrogen bond percent occupancies between the FAs and L-MEN

Dipole-dipole interaction energies

The obtained results put in evidence the importance of hydrogen bonding formed between the HBA and HBD in DES synthesis, they are nevertheless key contributors to the overall strengths of HBA–HBD interactions. Therefore, the dipole-dipole interaction energies were obtained using Eq.2:

$$\langle V(r)\rangle = \frac{-1}{3}\frac{\mu_A^2\mu_B^2}{(4\pi k\varepsilon_0)^2}\frac{1}{r^6}\frac{1}{k_B T} \quad (2)$$

where T, r, and μ are temperature, distance, and dipole moment. The j, k_B, and ε_0 are the relative permittivity of the medium, permittivity of free space, and Boltzmann constant. The energy of dipole-dipole interactions is the source of van der Waals interactions. It is often possible to characterize the well-known Keesom energy as a function of intermolecular distance (r) (see Eq. 2).

The electrons may be asymmetrically distributed at a given moment, therefore, the value of dipole moment assigned to a molecule is usually a time average. The average values of the dipole moments of solvent components were obtained by fitting the Gaussian Eq. (1). The normalized-Gaussian distribution has a mean of 2.693 Debye for the L-menthol in the deep eutectic solvent based on acetic acid, while the mean value is 2.7850 Debye in the Decanoic acid-based DES with the longer chain. As can be seen, the dipole moment for the L-menthol molecule in the system containing DEC is

greater than that of the mixture MAC, and this can be attributed to the presence of more hydrogen bonds between the L-menthol and Decanoic acid. Also, a negligible difference can be seen for the corresponding average values of the dipole moments of L-MEN in the mixtures MAC and MBA (liquid phase). The dipole-dipole interaction energies are reported in Table 1. The energy of the dipole-dipole interactions between menthol molecules and acid species follows the order [MEN] [ACE] < [MEN] [BUA] < [MEN] [DEC]. In the system containing Ace, the energy of ion-dipole interaction in the case of the acid molecule, is slightly more than the system containing butyric acid, and this is due to the lower electronegativity of this Ace, compared to BUA. It should be noted that the dipole – dipole interaction occurs when the angles between the dipole moment vector of L-MEN and the dipole moment vector of DEC are 80 degrees (see Figure 2).

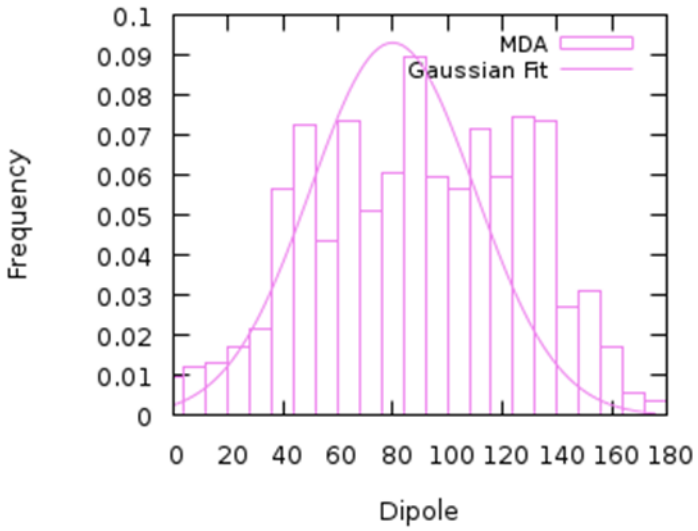

Figure 2. The obtained dipole moment distribution between Decanoic acid and L-menthol molecules at 298.15 K.

Table. 1. Calculated dipole moment of species (in Debye) in the liquid phase.

Interaction	**MAC**	**MBA**	**MDA**
ACE _ MEN	54.4177		
MEN _ MEN	52.5699		
BUA _ MEN		56.2903	
MEN _ MEN		60.1626	
DEC _ MEN			56.4539
MEN _ MEN			60.1726

Tracking the Bridge Species Using the Respective CDFs

For the binary mixtures, the corresponding distance/distance CDFs of the three neighboring species (L-MEN⋯FAs⋯L-MEN) are computed to track the bridging role of species in solutions. The TRAVIS package was used to draw the CDFs. As seen in Fig.3, we looked into the possibility of connecting two [FAs] molecules as the H-bond donors by a one [MEN] bridge in the binary mixture. As shown in the CDFs, one of the axes of CDF represents the distance between the hydrogen of the Decanoic acid bridge, H1, and hydroxyl oxygen of one neighbor DEC, O2, and the other axis belongs to the distance between the O1 atom of the acid bridge and H1 atom of another menthol (see Figure 3). An intense probability region for the two distances of L-menthol - Decanoic acid neighbors (O1-H1) and (O2−H1) is apparent at about 2 Å /2 Å. Since the color spectrum of the CDF graphic for L-MEN - DEC interaction is slightly larger than that of L-MEN - BUA, the average value of the distribution function of the H-bond of L-MEN -DEC molecules surrounding menthol has more numerical values.

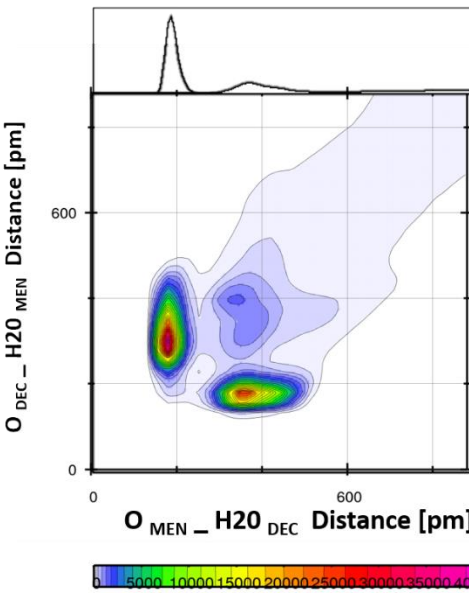

(a)

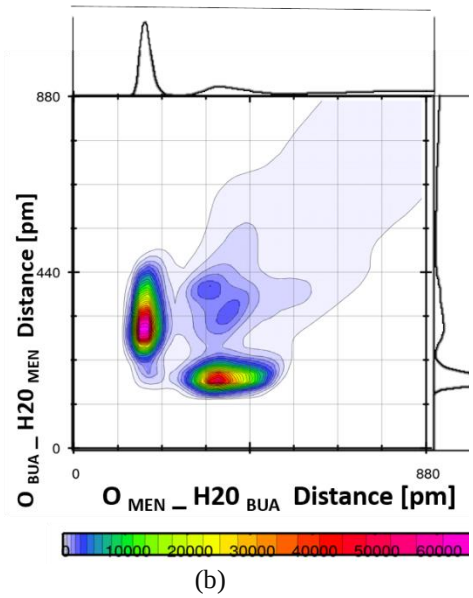

(b)

Figure 3. CDFs showing one [FAs]− bridge between two [MEN] molecule

Conclusions

In this work, the structural properties of four Eutectic Solvents based on L-menthol and fatty acids (L-MEN: ACE, L-MEN: BUA, and L-MEN: DEC) have been investigated using MD simulations. Based on the findings of structural investigations, it is likely that the hydrogen bonds that form between HBD and HBA are what cause the menthol molecules in the mixtures to lose their aggregation. In addition, Dipole-dipole interaction energy was increased with the increase of alkyl chain length.

References

[1] Smith, E.L.; Abbott, A.P.; Ryder, K.S.; Chem. rev. 2014, 114, 11060-82.
[2] Oshima, T.; Ito, M.; J. nat. med. 2021, 75, 319-25.
[3] O'Connor, S.; Rudkowska, I.; Adv. Food Nutr. Res. 2019, 87, 43-146.
[4] Aouf, C.; Durand, E.; Lecomte, J.; Figueroa-Espinoza, M.-C.; Green Chem. 2014, 16, 1740-54.
[5] Barhaghi, M.S.; Crawford, B.; Schwing, G.; Hardy, D.J.; Stone, J.E.; Schwiebert, L.; J. Chem. Theory. Comput. 2022, 18, 4983-94.
[6] Balabin, I.A.; Hu, X.; Beratan, D.N.;. J. Comput. Chem. 2012, 33, 906-10.
[7] Pour, S.B.; Sardroodi, J.J.; Ebrahimzadeh, A.R; Fluid Phase Equilibria. 2022, 552, 113241.